Neutronic simulation of a European Pressurised Reactor

OE Montwedi

18010210

Dissertation submitted in partial fulfilment of the requirements for the degree *Master of Engineering* at the Potchefstroom Campus of the North-West University

Supervisor: Dr. V Naicker

September 2014

NORTH-WEST UNIVERSITY
UNIBESITI YA BOKONE-BOPHIRIMA
NOORDWES-UNIVERSITEIT
POTCHEFSTROOMKAMPUS

Abstract

The South African government's integrated resource plan for electricity IRP2010 states that the country plans to have an additional 9.6 GW of nuclear power on the national electricity grid by 2030. In support of this, the NRF-funded SARChI Research Chair in Nuclear Engineering within the School of Mechanical and Nuclear Engineering at the North-West University recently initiated research studies focused on Light Water Reactor (LWR) systems. These studies inter alia involve coupled neutronic and thermal hydraulic analyses of selected LWR systems.

This study focuses on the steady state neutronic analysis of the European Pressurised Reactor (EPR) using Monte-Carlo N-Particle (MCNP5). The neutronic model will in due course be coupled to a thermal hydraulic model forming part of a broader study of the system. The Monte Carlo neutron transport code MCNP5 has been widely used since the 1950s for analysis of existing and future reactor systems due to its ability to simulate complex fuel assemblies without making any significant approximations. The primary aim of the study was to develop an input model for a representative fresh fuel assembly of the US EPR reactor core from which the fluxes and fission power of the reactor can be obtained. There after a 3D model of full EPR core developed by the school of mechanical and nuclear engineering based on findings of this work is also tested. The results are compared to those in the US EPR Final Safety Analysis Report.

Agreement in major core operational parameters including the k_{eff} eigenvalue, axial and radial power profiles and control rod worth are evaluated, from which consistency of the model and results will be confirmed. Further convergence of the model within a reasonable time is assessed.

Keywords:

Nuclear, Neutronics, MCNP, EPR, Power profile, Flux, Convergence, Rods worth

Declaration

I, the undersigned, hereby declare that the work contained in this project is my own original work.

Ontlametse Emmanuel Montwedi

Date: 02 September 2014

Potchefstroom

Acknowledgements

I would like to firstly give thanks to the God all mighty for giving me the strength and persistence throughout my studies.

I would also like to give special thanks to my family and friends for the endless support throughout my entire studies to date.

Special thanks go to Dr Vishnu Naicker for his support, motivation and guidance throughout out the project life. His expertise and inputs made everything achievable even in the most difficult stages of the study.

Special thanks also go to the staff of the school of mechanical and nuclear engineering for the support and teaching during my stay at the North-West University.

I would also like to give special thanks to M-Tech Industrial for their assistance with equipment that helped reduce the CPU time required for MCNP runs.

The financial assistance of the National Research Foundation (NRF) towards this research is hereby acknowledged. Opinions expressed and conclusions arrived at, are those of the author and are not necessarily to be attributed to the NRF.

Table of Contents

List of figures

List of tables

List of abbreviations

Abbreviation	**Definition**
EPR	European Pressurised Reactor
SAR	Safety Analysis Report
NRC	Nuclear Regulatory Commission
LWR	Light Water Reactor
PWR	Pressurised Water Reactor
BOL	Beginning of Life
DOE	Department of Energy
GWt	Giga watt thermal
MW	Mega watt
eV	Electron volts
KeV	Kilo electron volts
MeV	Mega electron volts
MCNP 5/MCNP	Monte-Carlo N-Particle
GWe	Giga watt electric
MWt	Megawatt thermal
EOL	End of life
RCCA	Rod control cluster assembly
Gd_2O_3	Gadolinium Oxide
UO_2	Uranium Oxide

1. Introduction

1.1 Overview and background

There are currently about 437 nuclear power reactors in operation in the world and about 68 new reactors under construction. The global nuclear power generating capacity reached 372.5 GWe at the end of 2012. Despite public scepticism and fears following the Fukushima Daiichi nuclear accident, nuclear power demand continues to grow steadily, even if at a slower rate two years later (IAEA, 2013). A number of countries such as South Africa continue to press for addition of nuclear power into their energy mix despite the Fukushima Daiichi nuclear accident, because the need for nuclear power still exists.

Safety analysis of nuclear reactor systems remains an important issue to reassure the public of the safety and reliability of nuclear power plants. Safety analysis is also critical in aiding countries to make decisions on the type of reactor systems to build and also to incorporate the lessons learned from nuclear accidents into safety analysis for added safety assurance.

I. Motivation for research

The South African government's integrated resource plan for electricity IRP2010 states that the country plans to have an additional 9.6 GW of nuclear power on the national electricity grid by 2030 (DOE, 2011). In support of this, the NRF-funded SARChI Research Chair in Nuclear Engineering within the School of Mechanical and Nuclear Engineering at the North-West University initiated research studies focused on Light Water Reactor (LWR) systems. These studies inter alia involve coupled neutronic and thermal hydraulic analyses of selected LWR systems.

This study forms part of a broader study which is the safety analysis of the EPR. Safety analysis consists of steady state analysis, transient analysis and accident analysis. The neutronic analysis needs to be performed at a steady state, and then coupled to a thermal hydraulic study done by the school. The two analyses coupled will then form a coupled steady state neutronic-thermal hydraulic analysis of the EPR from which transient and safety analysis will follow see (Figure 1:1 below).

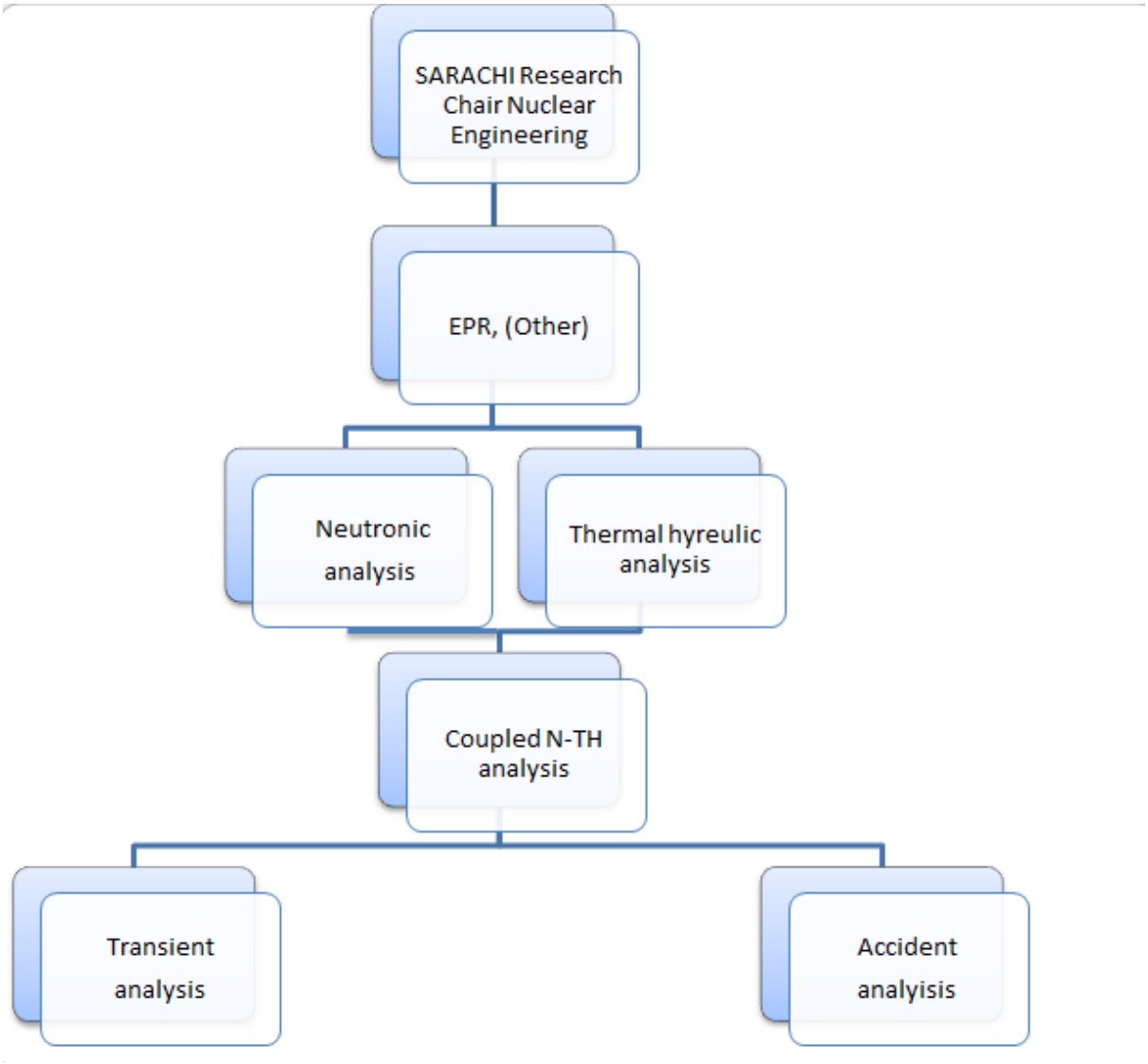

Figure 1:1 Flow chart of the system analysis research

II. European Pressurised Reactor overview

This section intends to introduce a brief overview of the EPR. The EPR has been chosen because its specifications best match those proposed by the South African government for the nuclear new build programme. The EPR is a generation III+ evolutionary four-loop Pressurised Water Reactor (PWR) designed by AREVA NP. The EPR main components of design, loop configurations and primary system design are very similar to those of operating PWR power plants around the world, which implies that the design is based on proven technology (AREVA, 2012). The following EPR projects are in progress around the world; Finland (Olkiluoto), France (Flamanville), China (2 Units Taishan), and two are going through certification - one in the USA and one in the UK (AREVA, 2012). The US-EPR is discussed in more detail in section 2.7

III. Research methodology overview

The methodology to be followed is presented in a form of a flow chart to give a brief description of how the study was done (see Figure 1:2 below).

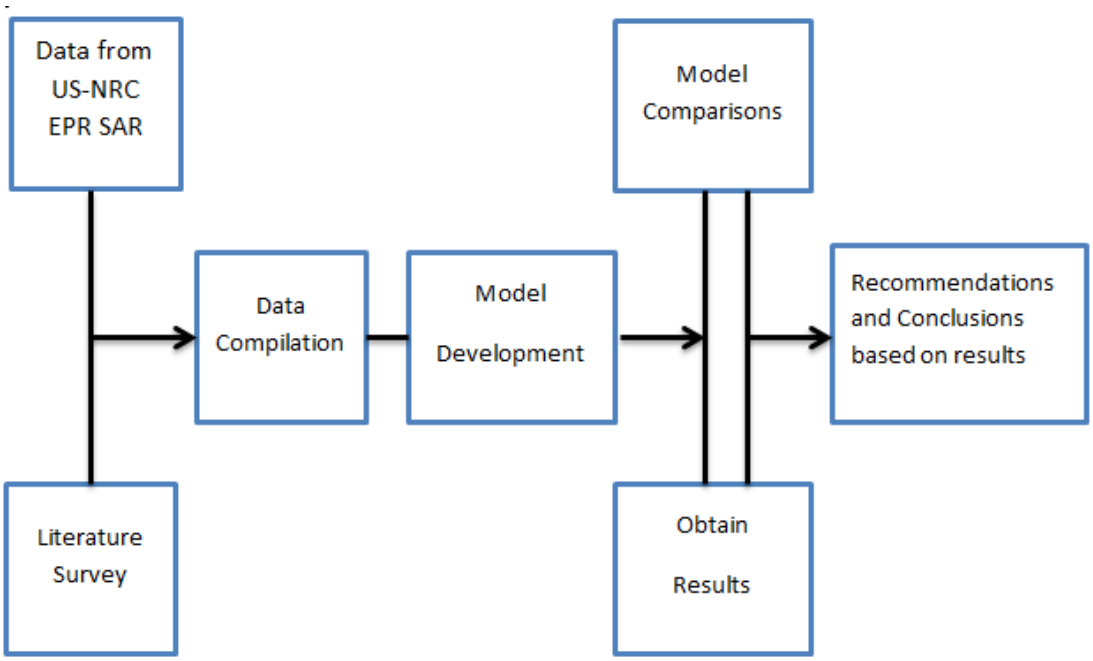

Figure 1:2 Quantitative research methodology with model development

Data for model development were obtained from the United States Nuclear Regulatory Commission (US-NRC) EPR final safety analysis report (AREVA, 2012). The report was submitted by AREVA to the NRC for licensing of the US-EPR. The US-EPR-SAR contains most of the technical and design information required to model the EPR reactor core in computational codes for analysis. A literature survey was performed to determine which methodology was best to follow in order to develop the US-EPR MCNP model and to also obtain the relevant theory on the methodology followed. Data compilation then followed which included conversion of design measurements from American units to SI units and calculations of material concentrations for EPR modelling in MCNP. Modelling of the reactor system components (i.e. fuel assembly) followed. This was done on an MCNP5 input file which was written manually and then later on a FORTRAN program was used to produce the input file in order to reduce human error. The manual model results were compared to results from another MCNP5 model developed by the school using an approach different to

the one used in this study. Results were also obtained and compared to EPR-SAR results. Conclusions followed and recommendations were made based on the results obtained. The chapters that follow discuss the methodology in more detail.

1.2 Problem statement

The North-West University initiated research studies focused on Light Water Reactor (LWR) systems. These studies inter alia involve coupled neutronic and thermal hydraulic analyses of selected LWR systems.

This study focuses on the steady state neutronic analysis of the European Pressurised Reactor (EPR) using MCNP5. The neutronic model will in due course be coupled to a thermal hydraulic model forming part of a broader study of the system.

1.3 Aims and objectives of the study

a. Develop an input model for a representative fresh fuel assembly
b. Test the input script that is used to create the input for both the fresh fuel assembly calculations and fresh full core calculations
c. Determine how economical it is to use MCNP for calculations
d. Determine the path to convergence.

1.4 Layout of dissertation

This dissertation is presented in five chapters

Chapter 2: Provides a review of the theory and literature relevant to this study. The theory covered is on transport theory Monte Carlo methods and the theory relevant to MCNP. Literature covered is that which is relevant to this study and similar work that has been done by other researchers.

Chapter 3: Provides details of what MCNP is and how it works. Detailed descriptions of all the models used in this study are also presented. The homogeneous fuel assembly model, the heterogeneous fuel assembly model and the full core models are discussed.

Chapter 4: Presents results and discussion of these results. Comparison of some of the results to EPR SAR is presented as a form of verification.

Chapter 5: Presents conclusions and recommendations that arise from this work.

2. Theory and literature survey

2.1 Introduction

This chapter introduces the theory relevant to Monte Carlo techniques and neutron transport. The chapter also covers the motivation for using MCNP and similar work done by other researchers to perform neutronic analysis of rectors. The chapter also provides a general description of the EPR and a detailed description of the EPR nuclear design.

2.2 Neutron transport theory

The behaviour of nuclear reactors is governed by the distributions of neutrons in space, angle, energy and time in a reactor system and one common difficulty of reactor theory is to predict this distribution. In principle, the prediction of the distribution of neutrons can be done by solving the neutron transport equation. The prediction can be done using numerical methods to model the neutron behaviour based on a selected method (i.e. deterministic methods: finite difference, discrete ordinate; stochastic methods: Monte Carlo). The methods can then be used to calculate quantities of interest from the neutron behaviour in the system modelled. The quantities may include but not limited to, neutron flux, reaction rate, power and reactor system criticality. The general form of the neutron transport equation may be written as (Stacey, 2007):

$$\frac{\partial N}{\partial t}(\boldsymbol{r},\boldsymbol{\Omega},t)d\boldsymbol{r}d\boldsymbol{\Omega}$$

$$= v\big(N(\boldsymbol{r},\boldsymbol{\Omega},t)\big) - \big(N(\boldsymbol{r}+\boldsymbol{\Omega}dl,\boldsymbol{\Omega},t)\big)dAd\boldsymbol{\Omega}$$

$$+\int_0^{4\pi} d'\Omega \sum_s(\boldsymbol{r},'\Omega\rightarrow\boldsymbol{\Omega})vN\,(\boldsymbol{r},'\Omega,t)d\boldsymbol{r}d'\Omega\; +\frac{1}{4\pi}\int_0^{4\pi} d'\Omega v\sum_f r\, vN(\boldsymbol{r},'\Omega,t)d\boldsymbol{r}d\boldsymbol{\Omega} +$$
$$S_{ex}(\boldsymbol{r},\Omega)d\boldsymbol{r}d\Omega - (\sum_a(\boldsymbol{r})+\sum_s(\boldsymbol{r}))vN(\boldsymbol{r},\boldsymbol{\Omega},t)d\boldsymbol{r}d\boldsymbol{\Omega} \qquad (2.1)$$

where:

$\boldsymbol{r}$ = position vector.

v = neutron velocity.

$'\Omega$ = characterises the direction of motion.

t = time.

N = number of delayed neutron precursors.

$\frac{\partial N}{\partial t}(\boldsymbol{r}, \boldsymbol{\Omega}, t) d\boldsymbol{r} d\boldsymbol{\Omega}$ = rate at which neutrons are flowing into the volume element.

$N(\boldsymbol{r}, \boldsymbol{\Omega}, t)$ = number of neutrons in volume element $d\boldsymbol{r}$ at position $\boldsymbol{r}$ moving in cone direction $d\boldsymbol{\Omega}$ about direction $\boldsymbol{\Omega}$.

$\big(N(\boldsymbol{r} + \boldsymbol{\Omega} dl, \boldsymbol{\Omega}, t)\big) dA d\boldsymbol{\Omega}$ = is the rate at which neutrons are flowing out of the volume element.

$\int_0^{4\pi} d'\Omega \sum_s (\boldsymbol{r}, '\Omega \rightarrow \boldsymbol{\Omega}) vN\,(\boldsymbol{r}, '\Omega, t) d\boldsymbol{r} d'\Omega$ = rate at which neutrons travelling in direction $\boldsymbol{\Omega}$ are being introduced into the volume element by scattering of neutrons within the volume element from a different direction $'\Omega$.

$\frac{1}{4\pi} \int_0^{4\pi} d'\Omega v \sum_f r\, vN(\boldsymbol{r}, '\Omega, t) d\boldsymbol{r} d\boldsymbol{\Omega}$ = rate at which neutrons are being introduced into the system volume by fission.

$S_{ex}(\boldsymbol{r}, \Omega) d\boldsymbol{r} d\Omega$= rate at which neutrons are produced into the system by an external source

$(\sum_a (\boldsymbol{r}) + \sum_s (\boldsymbol{r})) vN(\boldsymbol{r}, \boldsymbol{\Omega}, t) d\boldsymbol{r} d\boldsymbol{\Omega}$ = rate at which neutrons are being absorbed or scattered into a different direction $'\Omega$.

The neutron transport equation holds under some strict assumptions such as (Miller & Lewis, 1993):

- The particles may be considered as points.
- Particles travel in straight lines between points.
- Particle-particle interactions may be neglected.
- Collisions may be considered instantaneous.
- The material properties are assumed to be isotopic.
- The properties of nuclei and the composition of the material under consideration are assumed to be known and time-dependent unless explicitly stated otherwise.
- Only the expected or mean value of particle density distribution is considered.

2.3 Methods used to solve or simulate neutron transport

A literature review of available codes for use in LWR's analysis was performed to investigate their capabilities for the US EPR applications. In order to identify a code type for modelling the EPR, different types of methods applied to neutronic codes need to be discussed.

2.3.1 Deterministic methods

Deterministic methods basically solve the neutron transport equation for the average particle behaviour.

I. Diffusion methods

Diffusion theory, with flux reconstruction, is the present state of the art for reactor physics analysis and design. The diffusion theory method based codes solve the neutron diffusion equation to obtain the neutron flux, from which the power profile is determined. They use macroscopic cross-section data from two or more energy groups for neutron particles. Diffusion codes have been used to study reactors with appropriately homogenised fuel, moderator and absorbing material distribution. However for a very heterogeneous system like the EPR fuel assembly and core the simplified model will require a lot of homogenisation techniques and calculations. Examples of diffusion codes are given as follows.

DYN3D is a neutron kinetic code used for calculation of transients in LWR cores (Kotlyar, et al., 2011). PANBOX is a multidimensional neutron kinetics code developed to perform safety and transient analysis of PWR (Sanchez, et al., 2002).

II. Other methods

Only discrete ordinate methods are discussed in this section because it is the most common. The discrete ordinate method sees the geometry or phase space to be divided into many volumes and angles. The neutron transport equation is then solved in terms of the volumes and discrete angles. If this method is used to model the EPR core, the moderator, fuel rods, guide tubes and instrumentation tubes will be homogenised for each volume and angle to be able to solve the transport equation.

Examples of these codes are DORT, TORT and DORT-TD

DORT is a two-dimensional (X-Y and R-Z) code while TORT is a three-dimensional discrete transport code (Pautz, et al., 2005) and DORT-TD is a transient neutron transport code (Waata, 2006).

2.3.2 Stochastic methods

Stochastic methods or Monte Carlo do not solve the transport equation like the deterministic method based codes mentioned above, but rather simulates particle transport for each particle by tracking the path of each individual particle throughout its life time and records (tallies) the average behaviour of these particles. Monte Carlo codes use given libraries e.g. ENDF cross-section data of continuous energy. Monte Carlo codes are used because of their ability to model complex geometries and the accuracy of solutions produced with the ENDF continuous energy cross-section data. Hence the reason MCNP5 was chosen to be used for this study despite the MCNP5 drawbacks such as extensive calculation time and computational memory required per calculation. However, it should be noted that this does not imply that MCNP is better than other methods, but rather why MCNP was been chosen.

Monte Carlo based computer codes include Monte Carlo N-Particle (MCNP). This is a general-purpose, continuous-energy, generalised-geometry, coupled neutron/photon/electron transport code (X-5 Monte Carlo team, 2003). However it should be noted that energy group collapsed cross-section data can also be used in MCNP. Section 2.4 further discusses the Monte Carlo technique and MCNP 5 to justify its use in the study.

2.4 Monte Carlo Technique

A Monte Carlo based code MCNP5 is used to calculate neutron flux, fission energy and heating energy deposition in the fuel assemblies from fission. It should be noted that non local gamma heating is not taken into account in this work. The F7 tally includes only local gamma-ray heating. This fission energy and heating energy corresponds to the power distribution in the fuel assemblies. The power distribution is obtained as a function of axial height and radial distance. The power distribution physics of MCNP is described in detail in reference (X-5 Monte Carlo team, 2003). In this section a brief introduction of the Monte Carlo technique is provided to allow a good understanding of the modelling.

The fundamental idea of Monte Carlo is to create a series of histories of particle life (neutrons) by using statistical sampling techniques to sample the probability laws that describe the behaviour of neutrons and trace the particle events steps by step till the death of the particle. Monte Carlo techniques are based on statistical concepts; this implies that the result given is an estimate and should lie on some confidence interval about the true answer. The statistical error or rather the uncertainty associated with the result and the confidence interval is a function of the number of particle histories simulated. The more histories run the

smaller the confidence interval about the true behaviour of the particles. According to the central limit theorem the estimated quality will improve with increase in sample size. (See section 2.4.3-V). For example, a Monte Carlo simulation outputs successive independent scores, x_1, x_2 ...x_n of a random variable x. Then the sample mean ($\bar{x}$) is formed where *N* is the total number of histories.

$$\bar{x} = \frac{1}{N}\sum_{i=1}^{N} x_i \qquad (2.2)$$

The law of large number states the sample mean with a probability that approaches 1 as $N \to \infty$ approaches the population mean or true mean. In this case x may represent the neutron flux, heating energy deposition, fission energy deposition, k_{eff} etc.

I. Analogue of Monte Carlo sampling

Neutrons are born/ produced randomly in Monte Carlo except for the first cycle of a Monte Carlo calculation, in which case they are born according to the user-specifications (e.g. geometry, direction energy, etc.). Energy and direction are sampled randomly from their distribution functions. Neutron path lengths between collisions depend on the total macroscopic cross-section Σ. The neutron leakage or collision at the end of its path is determined by the geometry. Types of collisions are selected randomly according to the relevant reaction cross-sections. Different scattering events change the direction and energy of the neutron while it is transported in the system. Fission, capture or leakage terminate the history and initiate the start of the next neutron history.

2.4.1 MCNP tallies

Note that a tally refers to counts that are kept by MCNP. In MCNP there are seven types of tallies present. They include six standard neutron tallies, six standard photon tallies and four standard electron tallies (X-5 Monte Carlo team, 2003). The standard tallies can be modified by the user in many ways. All the tallies are normalised to be per starting particle except for the KCODE criticality problems, which are normalised to be per fission.

For this study only neutron tallies are used, so only neutron tallies will be discussed. These tallies are the F4: N tally which is the track length estimate of cell flux and F7: N which is the track length estimate of the fission energy deposition.

2.4.2 Neutron flux and power distribution

MCNP is used in this study to simulate average behaviour of neutron particles in the material contained in the geometry cells. These neutrons are tracked with ENDF/B (evaluated cross section data files); however, it is important to note that the ENDF/B is not the only cross-section library used in MCNP. Other data libraries that might be used in MCNP are the European JEF-2.2 library, the Japanese Atomic Energy Institute's JENDL library, the Chinese Data Center's CENDL library and the Russian BOFOD library. The neutron tracks recorded represent the neutron flux distribution and are multiplied with reaction cross-sections track by track and with fission functions to obtain an estimate of the fission energy, which corresponds to power distribution. The quantity F7 which represents fission energy in MCNP is defined as: (X-5 Monte Carlo team, 2003)

$$F7 = WT_l\sigma_f(E)Q\frac{\rho_a}{m} \tag{2.3}$$

where:

W = particle weight

T_l = track length (cm)

$\sigma_f(E)$ = microscopic fission cross section (barns)

Q = fission heating Q-value (MeV)

ρ_a = atom density (atoms/barn-cm)

m = cell mass (g)

It is important to note that the F7 is a volume tally which gives the average fission energy deposited in a volume cell of a fuel rod.

The microscopic fission cross-section is given as the probability of a fission reaction taking place between a neutron and a nucleus of a material. Its units are those of area or square centimetres. The fission heating Q-value and the fission cross-section are stored in an MCNP cross-section library. Equation (2.3) can be expressed in terms of particle flux and fission heating function as shown below:

The integrated particle flux φ in a cell volume (V) as a function of position $\vec{r}$, energy E and time t is defined in MCNP as: (X-5 Monte Carlo team, 2003)

$$F4 = \frac{1}{V}\int dE \int dt \int dV \int d\Omega\varphi\left(\vec{r},\widehat{\Omega},E,t\right) = \frac{W_t T_l}{V} \quad (2.4)$$

The particle flux is defined as the path length traversed by all particles passing through a volume per unit volume per unit time (Stacey, 2007)

$$\varphi = nv \quad (2.5)$$

where:

φ = is the neutron flux (neutrons/cm^2-s)

n = is the neutron density (neutrons/cm^2)

v = is the neutron velocity (neutrons/sec)

The microscopic fission cross-section multiplied by the fission heating in equation 2.3 gives the fission heating Q summed over nuclides in a material. The fission energy is therefore defined by particle flux as a function of time, position in the volume and heating function as:

$$F7 = \frac{\rho_a}{m} Q \int dE \int dt \int dv \int d\Omega\sigma_f(E)H(E)\varphi\left(\vec{r},\widehat{\Omega},E,t\right) \quad (2.6)$$

The unit for the fission energy deposition F7 is MeV/g (million electron-volts/ gram)

(Note: for more detailed derivation of quantities F4 and F7 refer to (X-5 Monte Carlo team, 2003) section 2-80 to 81.)

2.4.3 Estimation of Monte Carlo precision

Monte Carlo results are an average of contributions from a lot of histories sampled during the cause of the problem. A quantity equally important as the Monte Carlo result is the error or uncertainty associated with the result. The behaviour of the error versus the number of histories gives insight into the quality of the result and determines whether the tally is statistically well-behaved. If the tally result is not well-behaved its estimated error may not reflect its true confidence interval and the answer could be completely wrong.

A number of quantities are present in MCNP to help assess the quality of the confidence interval of a tally result. These qualities are the estimated mean, relative error, variance of variance and history score probability density

I. Estimated mean

Monte Carlo results are obtained by sampling random walks and assigning a score x_i to each random walk.

Assume *f(x)* is the history score probability density function for selection of a random walk that scores *x* to the tally being estimated. The true mean is the expected value of *x*, *E(x)*, where

$$E(x) = \int x f(x)\, dx = \text{true mean} \tag{2.7}$$

The true mean is then estimated by the sample mean $\bar{x}$ where

$$\bar{x} = \frac{1}{N}\sum_{i=1}^{N} x_i$$

As explained in section 2.4, the quantities *E(x)* and $\bar{x}$ are related by the law of large numbers which states that if *E(x)* is finite, $\bar{x}$ tends to the limit *E(x)* as N approaches infinity (Sheffield, 2011).

Note that for a detailed derivation of the estimated mean the reader may refer to (X-5 Monte Carlo team, 2003) sections 2-108 to 110

II. Relative error

The estimated relative error is defined as the ratio of the estimated standard deviation of the sample mean $S_{\bar{x}}$ and the sample mean $\bar{x}$

$$R \equiv \frac{S_{\bar{x}}}{\bar{x}} \tag{2.8}$$

The relative error can also be expressed as follows for large numbers

$$R = \left[\frac{1}{N}\left(\frac{\overline{x^2}}{\bar{x}^2} - 1\right)\right]^{\frac{1}{2}} = \left[\frac{\sum_{i=1}^{N} x_i^2}{\left(\sum_{i=1}^{N} x_i\right)^2} - \frac{1}{N}\right]^{\frac{1}{2}} \tag{2.9}$$

A detailed derivation of the above equation can be found in (X-5 Monte Carlo team, 2003)

III. Variance of variance

Variance is a measure of a population of points. It is a measure of the spread of these points and it is given by

$$\sigma^2 = \int \big(x - E(x)\big)^2 f(x)\, dx = E(x^2) - \big(E(x)\big)^2 \tag{2.10}$$

The standard deviation in Monte Carlo is defined as the Square root of variance σ for large numbers

$$S^2 = \frac{\sum_{i=1}^{N}(x_i - \bar{x})^2}{N-1} \approx \overline{x^2} - \bar{x}^2 \tag{2.11}$$

and the estimated variance of the mean $\bar{x}$ is then given by

$$S_N^2 = \frac{S^2}{N} \tag{2.12}$$

The variance of variance VOV is given by

$$VOV = \frac{S^2\big(S_{\bar{x}}^2\big)}{S_{\bar{x}}^4} \tag{2.13}$$

where

$S_{\bar{x}}^2$ Is the estimated variance of the $\bar{x}$ and $S^2\big(S_{\bar{x}}^2\big)$ is the estimated variance in$\big(S_{\bar{x}}^2\big)$.Variance of variance gives a measure of the statistical uncertainty in the estimated error R, and hence the importance to Monte Carlo calculations and to tally assessment.

IV. Central limit theorem

In Monte Carlo the central limit theorem is used to define confidence intervals for precision of the results. The central limit theorem of probability can be written as follows:

$$\lim_{N\to\infty} Pr\left[E(x) + \alpha\frac{\sigma}{\sqrt{N}} < \bar{x} < E(x) + \beta\frac{\sigma}{\sqrt{N}}\right] = \frac{1}{\sqrt{2\pi}}\int_{\alpha}^{\beta} e^{\frac{-t^2}{2}}dt \tag{2.14}$$

where α and β are arbitrary values and $Pr[Z]$ is the probability of Z. The equation can be rewritten in terms of estimated standard deviation of $\overline{x}$, $S_{\bar{x}}$ as follows for large *N*:

$$Pr\left(\left[\alpha S_{\bar{x}} < \frac{\bar{x} - E(x)}{\frac{\sigma}{\sqrt{N}}} < \beta S_{\bar{x}}\right] \approx \frac{1}{\sqrt{2\pi}}\int_{\alpha}^{\beta} e^{\frac{-t^2}{2}}dt\right) \tag{2.15}$$

This form of the central limit theorem states that for large values of *N* (i.e. as N approaches infinity) and identically distributed independent random variables x_i with finite means and variances, the distribution of the $\bar{x}$'s approaches a normal distribution.

(Note: for a detailed explanation of equations 2.14 and 2.15 refer to (X-5 Monte Carlo team, 2003).)

V. History score probability density

The history score of a tally bin can be seen as being sampled from an unknown history score PDF *f(x)*, where *x* is a random variable from one complete particle history of a tally bin. The quantity *f(x)* is the probability of scoring between *x* and $x + xdx$ for the tally bin. Each tally bin has its own *f(x)*

The general form of *f(x)* is

$$f(x)dx = f_c(x) + \sum_{i=1}^{n} p_i \delta(x - 0) \quad (2.16)$$

where $f_c(x)$ is the continuous and non-zero part and $\sum_{i=1}^{n} p_i \delta(x - x_i)$ represents *n* different discrete components occurring at x_i with a probability of p_i. The *f(x)* may be composed of either or both parts of the distribution.

The PDF is defined as

$$\int_{-\infty}^{\infty} f(x)dx \equiv 1 \quad (2.17)$$

For a detailed derivation of equations 2.16 and 2.17 refer to the reference (X-5 Monte Carlo team, 2003) section 2-109 to 123.

Using the central limit theorem; when "complete" sampling has occurred the largest values of the sampled *x*'s (i.e. histories) should have reached the upper bound or decrease faster than $\frac{1}{x^3}$ (X-5 Monte Carlo team, 2003) . This is translated as stating that the second moment of *f(x)* exists; i.e. $E(x^2) = \int_{-\infty}^{\infty} x^2 f(x)\, dx$ exists. See the reference (X-5 Monte Carlo team, 2003) page 2-124.

2.4.4 Fission cross-section

By definition fission cross-section σ_f, is a measure of the probability that a neutron and a nucleus interact to form a compound nucleus which then undergoes fission (Stacey, 2007).Total cross-section is defined by neutron interactions scattering σ_{sca} and absorption σ_a

$$\sigma_{TOT} = \sigma_{sca} + \sigma_a \quad (2.17)$$

Scattering can both be sub-divided into further parts

$$\sigma_{sca} = \sigma_{nonelastic} + \sigma_{elastic} \quad (2.18)$$

and

$$\sigma_a = \sigma_f + \sigma_\gamma + \sigma_a^{other} \quad (2.19)$$

Substituting (2.17) and (2.18) into (2.19) and rearranging using gives

$$\sigma_f = \sigma_{TOT} - (\sigma_{sca} + \sigma_\gamma) \quad (2.19)$$

2.4.5 Nuclear cross-section data

Nuclear cross-section data describe the frequency and outcome of interactions between particles (neutrons) and materials through which they are traversing. The type of nuclear data used in MCNP is point-wise cross-section data. Nuclear data in this form are stored at a significantly large number of energy points such that the point-wise data retain the particle energy as a continuous variable. The cross-section data for neutrons interaction is obtained from the evaluated MCNP libraries ENDF/B. The cross-section data provided for MCNP are evaluated at set temperatures.

2.4.6 Treatment of thermal neutrons

A collision interaction between a neutron and an atom is dependent on the thermal motion of the atom and in many instances it is also affected by the presence of other atoms next to it. In MCNP the thermal treatment is based on the free gas approximation to account for the thermal motion. MCNP also has capabilities of using an explicit thermal scattering S(α, β) that accounts for the effect of chemical bonding and crystal structure for incident neutron energies less than 4eV. The shortcoming of the S(α, β) is that data are available for a limited number of materials and temperatures. Because of lack of cross-section data, the free gas model can be used for treatment of the thermal neutrons. With the free gas model MCNP assumes that the hydrogen is a free gas. Since most of the scattering of fast neutrons is due to hydrogen the results should be significantly close.

In the range of atomic weight and neutron energy where thermal effects are significant the elastic scattering cross-section is almost independent of the energy of the neutron and the reaction cross-sections are nearly independent of the temperature.

However it should be noted that since this was the first model the thermal scattering S(α, β) treatment was not used and its recommended that its studied further in section 5.2

The free gas model in MCNP is included by using a temperature card "tmp card" in the input file. The application of free gas model is discussed further in the MCNP manual (X-5 Monte Carlo team, 2003) and by (Mattes & Keinert, 2005).

2.4.7 Neutron multiplication factor

The effective multiplication constant k_{eff} is generally defined as the product of P_{NL} and k_{∞}, which is the total number of fission neutrons, produced on average by one neutron from previous fission events:

$$k_{eff=\eta f \varepsilon \rho P_{NL}} \equiv k_{\infty} P_{NL} \tag{2.20}$$

where:

k_{∞} = k infinity for infinite systems

η = reproduction factor

f = Fuel utilisation factor

ε = Fast fission factor

ρ = Resonance escape probability

P_{NL} = Non leakage probability

Note that the above equation (2.20) is very well explained in literature and nuclear reactor physics books which can be referred to. For a better understanding consult (Stacey, 2007, Knief, 2008 and Lamash & Baratta, 2012).

In MCNP the calculation of the multiplication factor, is obtained by the use of a criticality calculation. The MCNP definition of k_{eff} *is* given as the ratio of neutrons in one generation to the number of neutrons in the previous generation in a system containing fissile material and in the absence of any external source.

A generation is the neutron lifetime from birth in fission to death by leakage, parasitic capture or absorption to fission. In MCNP neutron generations are referred to as cycles.

$$k_{eff} = \frac{fission\ neutrons\ in\ generation\ i+1}{fission\ neurtons\ in\ generattion\ i} \tag{2.21}$$

For critical systems, $k_{eff} = 1$ this implies that the fission reaction will be able to sustain itself. For sub-critical systems, $k_{eff} < 1$ this implies that the fission reaction will not be able to sustain itself. For super-critical systems, $k_{eff} > 1$ this implies that the number of neutrons will increase due to an increase in fission events.

2.5 Convergence

Monte Carlo based calculations such as criticality (k_{eff}) calculations are based on a numerical method called iteration (Brown , 2005). A user specifies the fission source distribution and an estimated value for $k_{eff,}$ random walks of a single-generation of neutrons are carried out for each cycle to estimate the new value of k_{eff} and fission source distribution of the next generation. The iterative process is repeated until both $k_{eff}$and fission source distribution has converged. Results obtained before this point should be discarded (set as inactive). Only after convergence tallies are initiated and the iterations are continued until statistical uncertainties are acceptably small. That is why there is a need to divide the cycles into two, these being the inactive and active cycles. The inactive cycles are before convergence and active cycles are post convergence of the k_{eff} and the fission source distribution (H_{src}) where Monte Carlo tallies are accumulated.

Determination of convergence in Monte Carlo criticality calculations is made difficult by inherent statistical noise of neutron random walks in each generation (Brown, 2006). Historically, convergence in MCNP (MCNP5, 2003) and other codes was determined by performing a preliminary calculation from which post-processing is done to assess trends in k_{eff}. After determining the inactive and active cycles, the calculation is then repeated and results are obtained. This can become a problem because convergence of k_{eff} happens before the fission source distribution converges, so the testing should also include both k_{eff} and the fission source distribution using the Shannon entropy estimation capabilities built in MCNP5. The use of Shannon entropy is further discussed in chapter 3.

2.5.1 Theory of convergence of K_{eff} and the fission source distribution

Although MCNP does not solve the transport equation, the transport equation is used in this section to explain convergence in k_{eff}. From the transport equation k_{eff} can be written in standard form as follows (Brown , 2005):

$$[\Omega \cdot \nabla + \sum_T(\vec{r},\mathrm{E})]\cdot\Psi(\vec{r}\,E,\Omega) = \iint \Psi(\vec{r}\,,E',\Omega')\sum_S(\vec{r}\,,E' \rightarrow E,\Omega\cdot\Omega')d\Omega'\,dE'$$

$$+ \frac{1}{k_{eff}}\frac{X(E)}{4\pi}\iint \nu\ \sum_F(\vec{r}\,E')\Psi(\vec{r},E'\,,\Omega')d\Omega' dE' \qquad (2.22)$$

where:

k_{eff} is eigenvalue for fundamental mode

$\Omega \cdot \nabla\Psi\ ((\vec{r}\,E,\Omega)$ is the loss term, leakage

$\sum_T(\vec{r},\mathrm{E})\ \Psi\ (\vec{r}\,E,\Omega)$ is the loss term, collisions

$\iint \Psi(\vec{r}\,,E',\Omega')\sum_S(\vec{r}\,,E' \rightarrow E,\Omega\cdot\Omega')d\Omega'\,dE'$ is the gain term, scatter from E', Ω' into E, Ω

$+ \frac{1}{k_{eff}}\frac{X(E)}{4\pi}\iint \nu\ \sum_F(\vec{r}\,E')\Psi(\vec{r},E'\,,\Omega')d\Omega' dE'$ is the gain term from fission.

The above equation can be simplified using operator form and written as

$$(\boldsymbol{L}+\boldsymbol{T})\boldsymbol{\Psi} = \boldsymbol{S}\boldsymbol{\Psi} + \frac{\mathbf{1}}{k_{eff}}\boldsymbol{F}\boldsymbol{\Psi} \qquad (2.23)$$

and rearranged to

$$\Psi = \frac{1}{k_{eff}}\left(\boldsymbol{L} + \ \mathbf{T} - \mathbf{S}\right)^{-1}\boldsymbol{M}\Psi = \frac{1}{keff}\boldsymbol{F}\Psi \qquad (2.24)$$

Equation (2.3) can be solved numerically using a standard iteration method as in (Brown , 2005)

$$\Psi^{(n+1)} = \frac{1}{k_{eff}{}^{(n)}}\boldsymbol{F}\boldsymbol{\Psi}^{(\boldsymbol{n})}, \qquad n = 0,1 \qquad \text{given } k_{eff^0}\ \Psi^{(0)} \qquad (2.25)$$

Regarding convergence of k_{eff} and fission source distribution during the power iteration process, if expansion of $\Psi^{(0)}$ is done in terms of the eigenvectors $\vec{u}_j$ as $\Psi = \sum_{j=0} a_j^0\,\vec{u}_j$ and substituted into (2.24) and rearranged algebraically to give

$$\Psi^{(n+1)}(\vec{r}) = \vec{u}_0(\vec{r}) + \frac{a_1}{a_0}\rho^{(n+1)} \cdot \vec{u}_1(\vec{r}) + \cdots \quad (2.26)$$

$$k_{eff}^{(n+1)} = k_0\left[1 - \frac{a_1}{a_0}\rho^n(1-\rho)g_1 + \cdots\right] \quad (2.27)$$

where ρ is the dominance ratio (k_1/k_0), k_0 and $\vec{u}_1$ are the fundamental mode eigenvalue (exact k_{eff}) and eigenfunction, k_1 and $\vec{u}_1$ are the first higher mode eigenvalue and eigenfunction, and a_0, a_1 and g_1 are constants obtained from expansion of the initial fission distribution. Equation (2.26) shows that the higher-mode noise in the fission distribution disappears as $\rho^{(n+1)}$, whilst higher mode noise in k_{eff} disappears as $\rho^n(1-\rho)g_1$. When the dominance ratio approaches 1, k_{eff} converges before fission source distribution because of the extra dumping factor $(1-\rho)$ that is close to Zero (Brown , 2005). Hence the importance of monitoring convergence of both k_{eff} and the fission source distribution, not only that of k_{eff}. More information on convergence of fission source distribution is given below.

2.5.2 Shannon Entropy for the fission source distribution

MCNP5 has capabilities of computing a quantity called the Shannon entropy (H_{src}) which is a well-known concept from information theory that provides a single number for each batch or cycle to assist in characterisation of convergence of the fission source distribution. To compute H_{src} it is essential to superimpose a 3D grid on the geometry defining the problem enclosing all the fissile materials and then tallying the number of fission sites in a batch that belong to each grid box. MCNP5 automatically determines the grid (MCNP5, 2003). The tallies are then used to determine a discretised estimate of the source distribution, (P_J, J= 1, N_S), where N_S is the number of grid boxes in the superimposed mesh, and P = (Number of source sites in J-th grid box)/ (total number of source sites). Then the Shannon entropy of the discretised source distribution for that batch is given by

$$H_{src} = -\sum_{J=1}^{N} P_J \cdot ln_2(P_J) \quad (2.28)$$

H_{src} varies between 0 for point distribution and $ln_2(N_s)$ for a constant distribution. Also it is seen from equation (2.28) that as P_J approaches 0, H_{src} approaches 0.

2.5.3 MCNP5 10 statistical checks for tally convergence

Convergence of the tally of interest is equally as important as the convergence of k_{eff} and the convergence of the fission source distribution H_{src}. The convergence of the tally (i.e. F7) assists in improving the precision of the MCNP5 result. There are 10 tally checks that are analysed by MCNP and presented in table form, these checks do not guarantee the absolute reliability of the tally, but assist in identifications of tallies that where not sampled well.

The 10 statistical checks are presented as follows.

results of 10 statistical checks for the estimated answer for the tally fluctuation chart (tfc) bin of tally 8

tfc bin	--mean--	---------relative error---------			----variance of the variance----			--figure of merit--		-pdf-
behavior	behavior	value	decrease	decrease rate	value	decrease	decrease rate	value	behavior	slope
desired	random	<0.10	yes	1/sqrt(nps)	<0.10	yes	1/nps	constant	random	>3.00
observed	random	0.02	yes	yes	0.00	yes	yes	constant	random	10.00
passed?	yes	yes	yes	yes	yes	yes	yes	yes	yes	yes

Table 2-1 MCNP5 10 statistical checks (X-5 Monte Carlo team, 2003)

The 10 statistical checks are discussed below.

I. Mean behaviour

The first column of Table 2:1 above shows the desired and observed behaviour of the estimated mean defined in section 2.4.3-I. The behaviour of the mean is required to be random because an ideal random quantity should according to the central limit theorem show a normal distribution of values around an average value. MCNP checks whether the mean is not increasing or decreasing for the last half of the problem. If the mean meets the criteria then it passes the test.

II. Relative error(R)

Three tests are done on the relative error.

The first test checks whether the relative error as defined in section 2.4.3-II is below a limit required to give a reliable confidence interval (0.5 for detector tallies and 0.1 for all other tallies). The second test checks whether the relative error is decreasing monotonically during the last half of the calculation. The third test checks the decreasing rate of the relative error as a function of the number of histories (NPS).If the decreasing rate of the relative error is decreasing at the desired rate ($\frac{\sim 1}{\sqrt{NPS}}$) for the last half of the calculation, then the tally passes the test.

III. Variance of variance

Three tests are done on the variance of variance (VOV), and the VOV is defined in section 2.4.3-III.

The first test checks whether the VOV is below the required value 0.1.The second test checks if VOV decreases monotonically for the last half of the calculation. The third test checks whether the rate of the decrease of the VOV is the desired ($\frac{\sim 1}{\sqrt{NPS}}$) for the last half of the calculation.

IV. Figure of merit (FOM)

The figure of merit is defined in MCNP as

$$FOM = \frac{1}{R^2 T} \qquad 2.29$$

where T = computer time used. It is important to note that the relative error $(R^2) \sim \frac{1}{N}$ and the computer time $(T) \sim N$ therefore *FOM* are expected to be approximately a constant in any MCNP run (Brown , 2005). The FOM is also used to compare the effectiveness of different variance reduction techniques.

There are two tests done on the figure of merit.
The first test checks whether the value of the figure of merit is constant for the last half of the calculation. The second test checks whether the figure of merit behaviour is random.

V. Probability density function slope

From section 2.4.3- V the requirement is that at least the second history score moment should exist for all valid MCNP tallies. In MCNP5; this is done by fitting a generalised Pareto function to the largest history scores for each tally bin. When the slope of this function is greater than 3, then the second moment of *f(x)* exists; and *f(x)* is then assumed to be "completely" sampled. See the reference (X-5 Monte Carlo team, 2003) page 2-128 for a more in depth discussion on this.

2.6 Coupled studies

Steady state reactor analysis is divided into two parts, namely neutronics and thermal hydraulics.

Coupling neutronic and thermal hydraulic calculations is necessary because the two are dependent on each other for input. The coupling represents the interface where heat generated in the core from the fuel is removed by the coolant to cool the core.

It is important to couple a neutronic model with a thermal hydraulic model because coupling enables you to perform temperature dependant calculation rather than assuming the temperature to be constant. Coupling provides detailed information on power distribution, temperature distribution, and coolant flow conditions for each fuel assembly.

To perform a coupled study, a neutronic model and a thermal hydraulic model are developed separately. The output of the neutronic calculation such as power or heat from fission serves as an input to the thermal hydraulic code. Similarly the output of a thermal hydraulic calculation such as temperature serves as an input to a neutronic code. Then the two calculations are done with updated input information. This process is repeated until both the results have converged and this is assessed using a convergence criterion.

The interchanging of information between the neutronic and the thermal hydraulic calculation can be automated using a script or software that reads data from both calculations and updates the input file every cycle.

Table 2-1 below shows some work that has been done in coupling MCNP and various thermal hydraulic codes and for more detailed explanation it can be referred to the sources referenced on the table below. The table below serves to show that coupling has been done by other researchers. Similar methodologies may be used for coupling of this model in the future.

Neutronic	Thermal hydraulic	System	Researcher	Cross-section used
MCNP	STAFS (sub channel)	HPLWR	(Waata, 2006)	Pseudo-material at a chosen temperature interval
MCNP	STAR-CD (CFD)	3 x 3 PWR fuel pins	(Seker, et al., 2007)	5K temperature intervals
MCNP	COBRA-TF	PWR FA	(Sanchez & Al-Hamry, 2009)	Pseudo-material at a chosen temperature interval
	SUBCHANFLOW	LWR pin and FA	(Ivanov, et al., 2011)	Pseudo-material at a chosen temperature interval
MCNP	THERMO (sub channel)	1/8 PWR core	(Kotlyar, et al., 2011)	Polynomial expansion

Table 2-1 Recent coupled studies with MCNP and various thermal hydraulic codes

2.7 European pressurised reactor

2.7.1 Design philosophy

The European Pressurised Reactor (EPR) was designed by framatome ANP, Inc., a jointly-owned subsidiary of AREVA and Siemens. The EPR is a four-loop plant with a thermal power rating of 4500 MWt. The primary system design, loop configuration and main components are very similar to those currently operating PWRs, therefore forming a proven foundation for the design.

The EPR is a global reactor with basic set of design features adaptable to the specific regulatory and commercial requirements of each country in which it is offered. The EPR design is based on combined operating and design experience of Framatome ANP and Siemens; French and German utilities and safety authorities; and with roots in the PWRs currently operating in the USA to date.

The EPR design philosophy is based on objectives related to the current generation of PWR such as increased redundancy and separation, reduced core damage frequency, reduced large release frequency, mitigation of severe accidents, protection of critical systems from external events, improved man-machine interface, extended response time for operator actions and improved defence-in-depth which is the cornerstone of EPR design philosophy.

2.7.2 EPR design overview

The EPR consists of a four-loop pressurised water Reactor Cooling System (RCS) composed of a reactor vessel that contains the fuel assemblies, a pressuriser to maintain system pressure, one Reactor Coolant Pump (RCP) per loop, one Steam Generator (SG) per loop, associated piping, and related control and protection systems (Framatome ANP, Inc, 2005) as in Figure 2:1.

The EPR uses normal light water to remove heat produced in the reactor core from nuclear fission. Water is used to slow down neutrons released during the nuclear fission process. Slowing down the neutrons is important to sustain the chain reaction so that the fissile atom nuclei can interact with incident neutrons at a thermal energy. The heat produced in the reactor is then transferred to the secondary system turbines by heat exchangers in the steam generators. Water from the primary system is pumped through the core and the primary side of the steam generators, pumping is done by active motor pumps and each loop has a coolant pump and a steam generator. The reactor operates at a pressure and temperature suitable for

the water not to boil and retain its liquid state, which maintains its cooling efficiency. The pressuriser is connected to the hot leg and controls pressure. The water entering the secondary side of the steam generator exchanges heat with water in the primary side via heat exchanger in the steam generator and produces saturated steam. The steam is then dried in the steam generators and directed to the turbine. The steam is then condensed goes back to the steam generator as feed water as explained in (AREVA, 2012) , the components mentioned in the process above are seen in Figure 2:1 below.

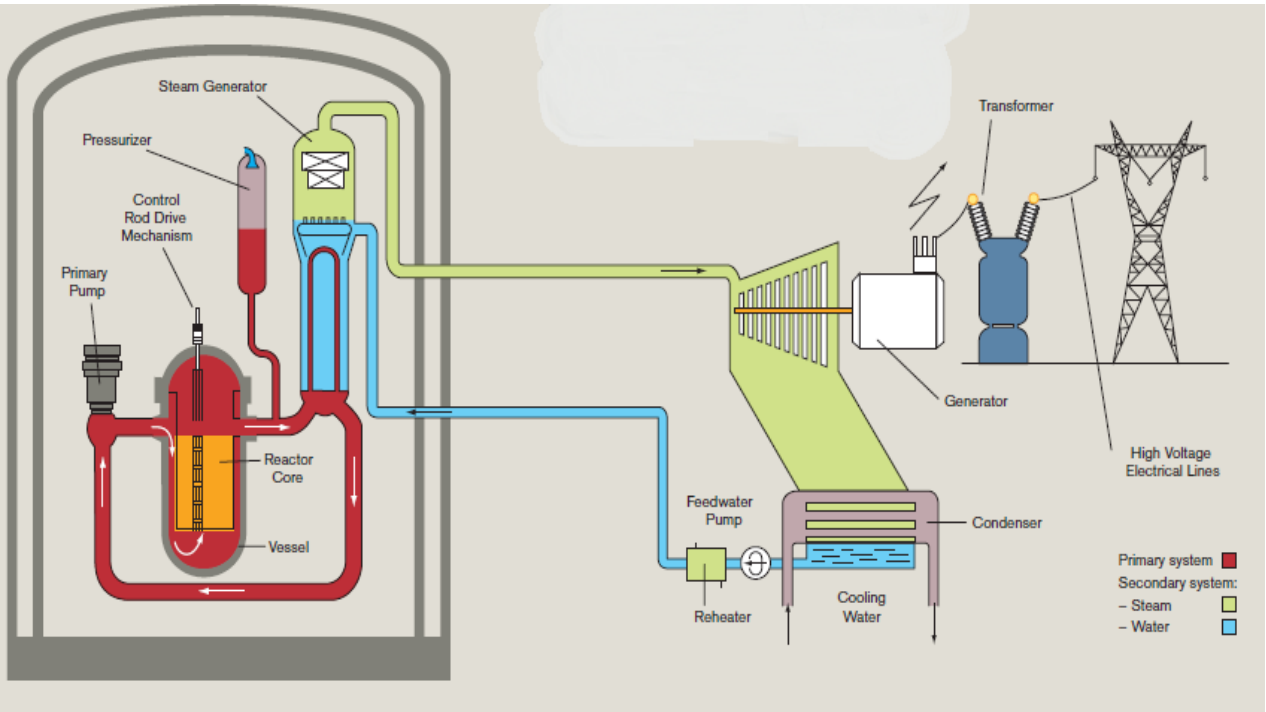

Figure 2:1 Simplified EPR plant layout (AREVA, 2012)

The US-EPR has new features, like the redundant emergency core cooling trains, a shielding and containment building and a core melt catcher for severe accidents. The US EPR design is based on objectives that ensure improved safety and the safety design is rooted on deterministic analysis based on a defence-in-depth concept as explained in (AREVA, 2012).

2.7.3 Key design parameters

The reactor has a core with an active height of 420 cm and a reactor pressure vessel with a 438.5 cm outer diameter. The thick walled RPV withstands the high operating pressure. The RPV is made of low carbon alloy steel with internals made of NiCrFe alloy cladding for increased resistance to corrosion, the RPV provides the volume required for containing the reactor core, heavy reflector, flow directing and supporting internals and the control rods. The

RPV consists of four outlet nozzles and four inlet nozzles that provide connections to the four loops circulating the reactor coolant. The RPV general design is described in the (AREVA, 2012).Below is Figure 2:2 showing the US-EPR RPV.

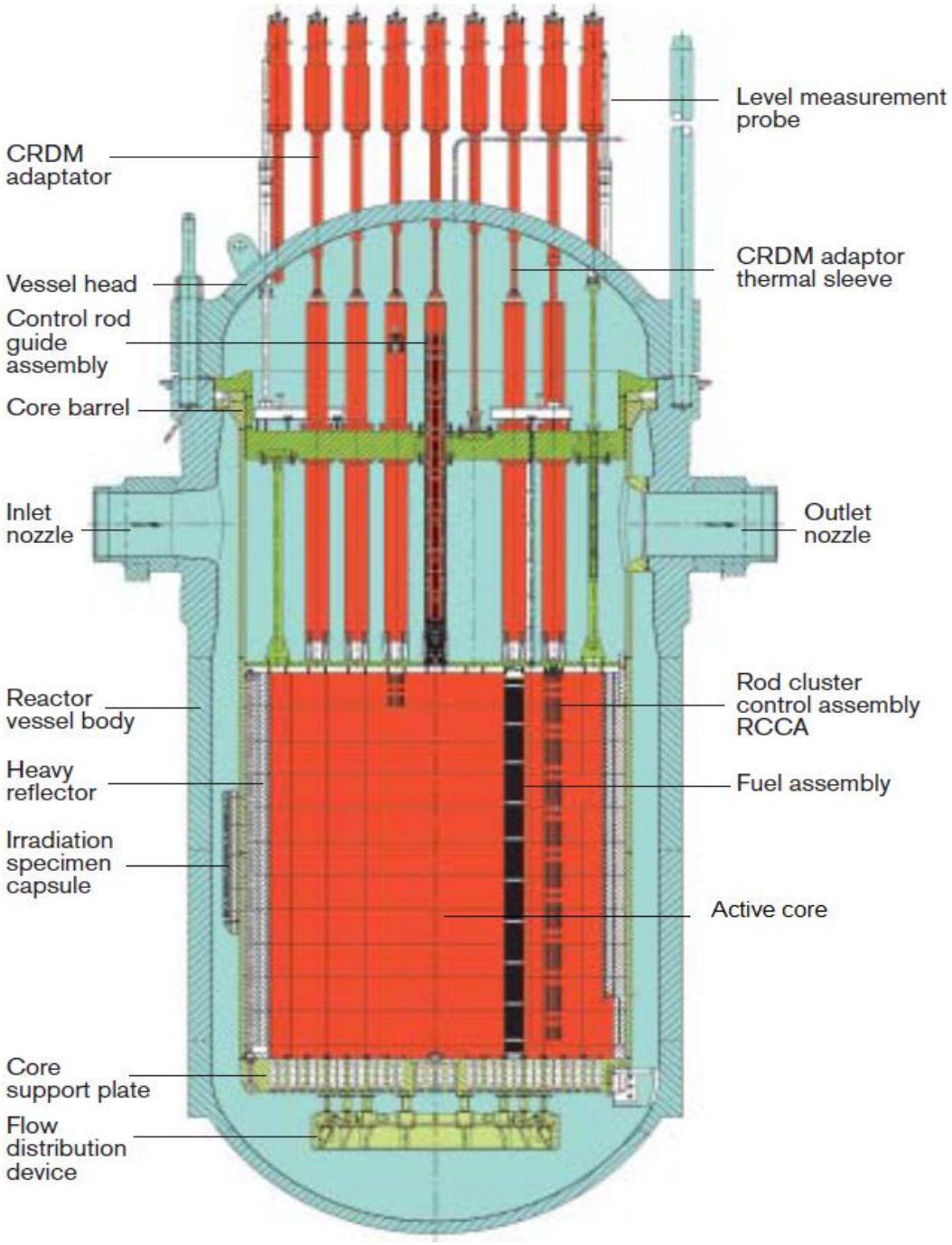

Figure 2:2 EPR reactor pressure vessel (AREVA, 2012)

2.8 Core design

2.8.1 Overall features

The EPR core has a thermal power of 4500 MWt. The core is designed in such a way that it would have a high thermal efficiency, low fuel cycle cost, and flexibility for extended fuel cycle lengths. Below is the core layout at the beginning of life.

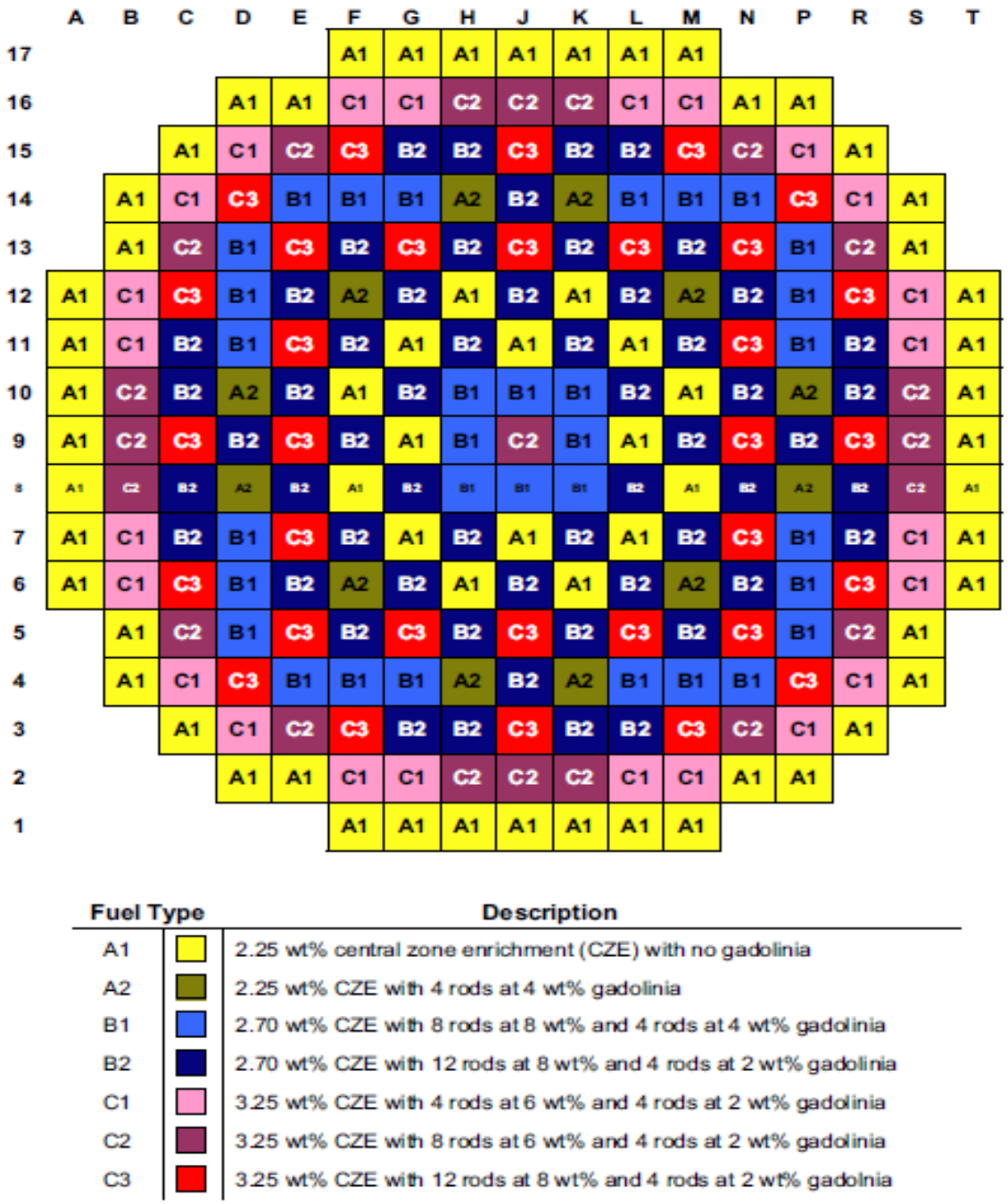

Figure 2:3 EPR core beginning of life layout

The core design cycle length is determined by the energy output required. The life time can differ from 12 to 24 months depending on energy requirements. The End-of-life (EOL) is defined as the point in life where the fuel no longer contains enough reactivity to maintain 100% thermal power.

The reactor core consists of a 241 fuel assembly arrays with the following characteristics:

- A 17 x 17 lattice composed of 265 fuel rods mechanically joined in a square array
- Optimized and proven fuel rod design parameters
- Enrichment of up to 5 wt% 235U
- Gadolinium Oxide Gd2O3 integral burnable poison with Gd concentration of 2 wt% to 8 wt%
- Highly corrosion-resistant and low-growth M5^{TM} cladding and tubing
- Monobloc^{TM} guide thimbles to increase structural strength
- Low growth M5^{TM} intermediate spacers
- Alloy 718 end spacers providing improved fuel rod support and flow-induced fretting resistance
- Debris-resistant robust FUELGUARD^{TM} bottom nozzle
- Removable top nozzle for ease of assembly repair

The core is put together by arrangement of 241 fuel assemblies into a pattern that is approximately like a right circular cylinder. The edge of the active core is surrounded by a heavy reflector, which is a large steel structure of 10.2 to 20.3 cm width that reduces fast neutron leakage and flattens the core power distribution. The heavy reflector also reduces fast neutron fluence on the reactor pressure vessel (RPV).

The initial core loading at beginning of life (BOL) consists of seven different fuel assembly neutronic designs with three rod types. Each fuel assembly's neutronic design for initial core loading contains a uniform distribution of gadolinia and uranium fuel rods. The core fuel assemblies are loaded such that the fuel assemblies with low enrichment are located at the outer boundary of the core to enhance fuel economy, while the reminder of the fuel assemblies are distributed in the interior of the core to establish a more favourable radial power distribution.

Note that this core loading arrangement is not the usual expected loading, where the higher enriched fuel assemblies are located at the outer boundaries of the core.

2.8.2 Fuel assembly design

The EPR core is made of seven different types of fuel assemblies A1, A2, B1, B2, C1, C2, and C3 as seen in Figure 2:3 above but only fuel assembly type C1 and C2 will be discussed in this section. Design drawings of rest of the fuel assemblies can be found in Appendix B.

Fuel Assembly Design C1

Rod Type	# of Rods	Rod Description
	23	Guide Tube
	1	Instrument Tube
	257	3.25 wt% U-235 in the Central Zone
	4	3.08 wt% U-235 with 2 wt% Gd_2O_3 in the Central Zone
	4	2.76 wt% U-235 with 6 wt% Gd_2O_3 in the Central Zone

Fuel Assembly Design C2

Rod Type	# of Rods	Rod Description
	23	Guide Tube
	1	Instrument Tube
	253	3.25 wt% U-235 in the Central Zone
	4	3.08 wt% U-235 with 2 wt% Gd_2O_3 in the Central Zone
	8	2.76 wt% U-235 with 6 wt% Gd_2O_3 in the Central Zone

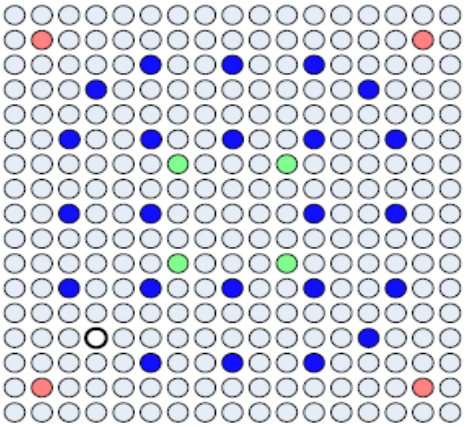

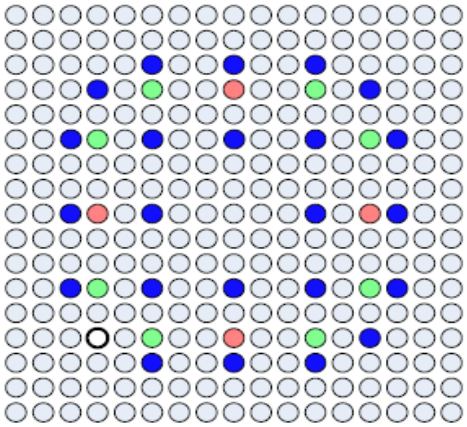

Fuel Assembly Design C1

Axial Height (cm)	Zone	Zone Enrichment (wt% U-235)		
419.999				
	Blanket	2.00	2.00	2.00
399.733				
	Cutback	3.25	3.25	3.25
384.439				
	Central		2.76 with 6 wt% Gd_2O_3	3.08 with 2 wt% Gd_2O_3
30.48				
	Cutback		3.25	3.25
15.24				
	Blanket	2.00	2.00	2.00
0.000				

Fuel Assembly Design C2

Zone	Zone Enrichment (wt% U-235)		
Blanket	2.00	2.00	2.00
Cutback		3.25	3.25
Central		2.76 with 6 wt% Gd_2O_3	3.08 with 2 wt% Gd_2O_3
Cutback		3.25	3.25
Blanket	2.00	2.00	2.00

Figure 2:4 Fuel assembly designs C1 and C2 (AREVA, 2012)

From Figure 2:4 of fuel design of C1 and C2 the following general design features are derived.

- 17x17 lattice design.
- The lattice includes 24 (23 guide + 1 instrumentation) guide tube locations and 265 fuel rods.
- Centre instrumentation tube cell location replaced by a fuel rod and the instrumentation tube is located off centre
- Nominal fuel length is about 420 cm.
- Alloy M5^{TM} cladding.
- M5^{TM} MONOBLOC^{TM} tubes.
- Selected fuel rods have burnable poison rods with up to 8% Gd_2O_3 (from 4 to 8 %).
- No separate burnable poison rod assemblies.
- Axial blankets to reduce axial neutron leakage and improve fuel economy.
- Varying radial and axial fuel enrichments to control power peaking.
- Design is based on a 18 to 24 month fuel cycle

I. Guide tubes description

The guide tubes are made from M5^{TM} alloy. This alloy shows low corrosion and low hydrogen uptake throughout the fuel design burn-up range and low irradiation growth rates (AREVA, 2012).

Each guide tube has two inside diameters and one outside diameter (see Figure 2:5 Guide Tube Assembly below). The bigger inner diameter at the top provides a bigger annular clearance that allows rapid insertion of the Reactor Control Cluster Assembly (RCCA) during reactor trip and also allows coolant flow during normal operation with control rods inserted. The reduced inner diameter section allows a close fit with control rods to decelerate the rods so that the impact of RCCA on the assembly top is minimised.

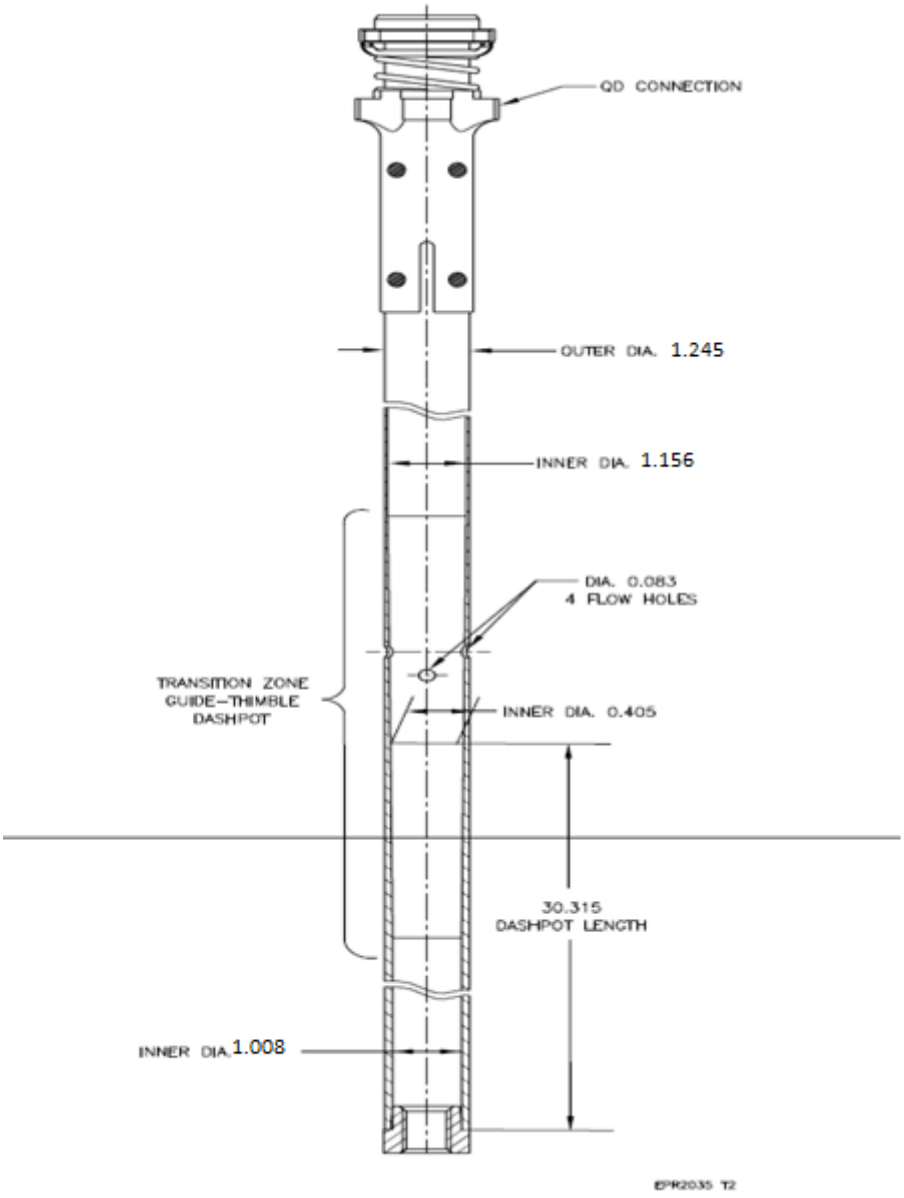

Figure 2:5 Guide Tube Assembly (AREVA, 2012)

II. Fuel rod description

The fuel rod consists of uranium oxide (UO_2) pellets encapsulated in a seamless M5^{TM} Zirconium alloy tube with M5^{TM} plugs welded at each end. The M5^{TM} cladding offers significant resistance to corrosion associated with long fuel cycles, high operating temperatures and high burn-up. The fuel rod gap volume and length offers an acceptable margin for failure due to pressure build-up.

The fuel pellets are cylindrical and sintered, with a high density ceramic dish at each end and chamfers on the edges of the pellet to ease loading of the pellets into the fuel rod. The

ceramic dish and chamfers help reduce the pellet's tendency to change shape into an hour-glass shape during operation. The pellets' enrichment can be of a maximum value of 4.95 weight percent U-235 with a tolerance of about 0.05%.

The fuel rod design also uses an axial blanket and gadolinium fuel configurations as in Figure 2:4 Fuel assembly designs C1 and C2 . The fuel rods may contain a maximum of seven axial zones. The top and bottom of the fuel rods are made of a zone called the blanket and the blanket contains low enriched UO_2 (2.0 wt %) pellets. The zone above and below the central zone is called the cutback zone and is made of higher enriched (3.25%) UO_2 pellets. The central zone is made of UO_2 or UO_2 + Gd_2O_3 pellets with various enrichment levels. The gadolinia in the central region serves as a burnable poison to control power peaking and or core reactivity.

2.8.3 Rod Cluster Control Assemblies description

Each Rod Cluster Control Assembly (RCCA) consists of 24 individual rods fastened to a spider assembly (see Figure 2:7 below). Each of the individual rods consists of an absorber rod of 80 weight percent silver (Ag), 15 weight percent indium (In), and 5 weight percent cadmium (Cd) sealed in a 316L stainless steel cladding tube to protect the absorber against the coolant (see Figure 2:6 below). Note that the units in the figure are centimetres (cm).

ITEM	DESCRIPTION
1	CONTROL ROD
2	UPPER END PLUG
3	PLENUM SPRING
4	ABSORBER
5	LOWER END PLUG

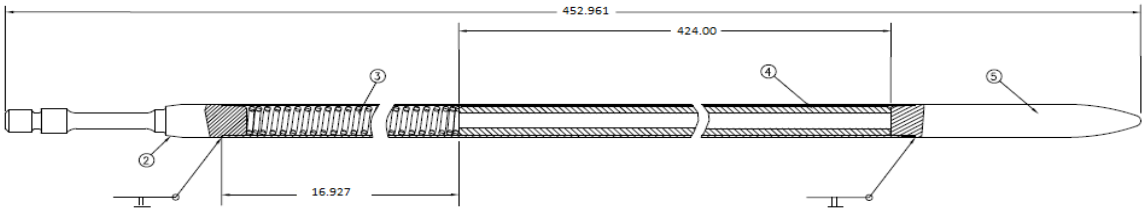

Figure 2:6 RCCA rod (AREVA, 2012)

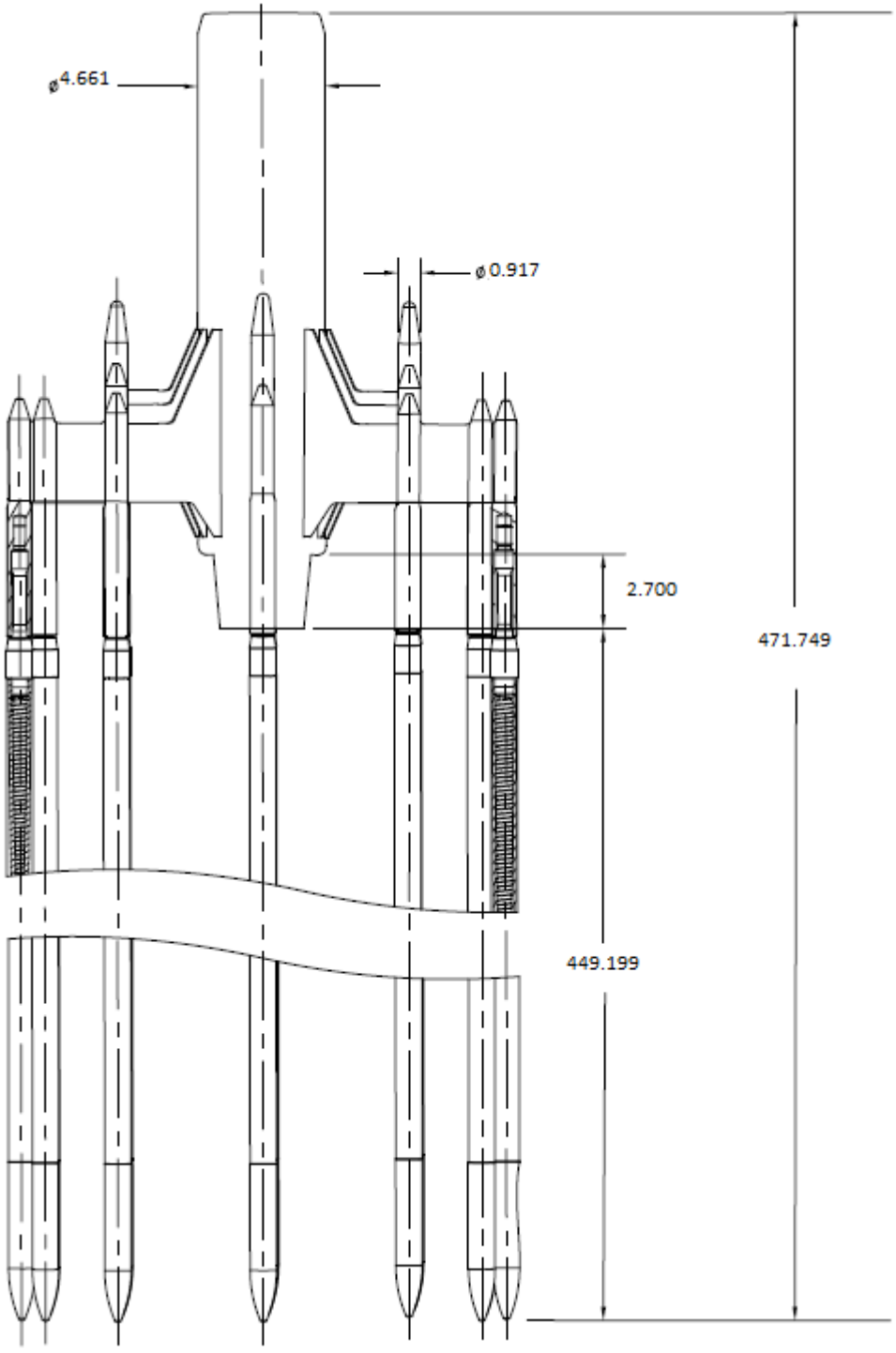

Figure 2:7 Rod Cluster Control Assemblies (AREVA, 2012)

The RCCA are used for shut down and control reasons to compensate for the fast reactivity changes associated with:

- The required shutdown margin in hot zero power, all rods inserted condition with the most reactive rod stuck out.
- The reactivity compensation as resulting from power increase above hot zero power (power defect, Doppler and moderator reactivity changes).
- Unplanned boron concentration, xenon concentration or coolant temperature fluctuation.
- Reactivity ramp rates due to load changes.

There is a limit in control rod bank insertion at full power to maintain shutdown capacity. The limit is such that as the power level is reduced, control rod reactivity limits are also reduced, and this allows for more rod insertion. The control bank position is monitored and if the insertion limit is approached an alarm notifies the operator. The insertion limit of the control rods is strongly dependent on the xenon distributions and the axial power profiles. The RCCA withdrawal patterns are determined from analysis of the xenon distributions and axial power profiles.

The power distribution, rod insertion and rod alignment are based on the arrangement of control and shutdown banks of the RCCAs as shown in Figure 2:8. All shut-down rods cluster assemblies are moved out of the core before moving the control banks. When raising power from zero to 100 percent, control banks A, B, C and D are moved out of the core sequentially in overlap. The control rods movement description is not available in the EPR SAR making it a challenge to determine exactly how the control banks are positioned at beginning of life.

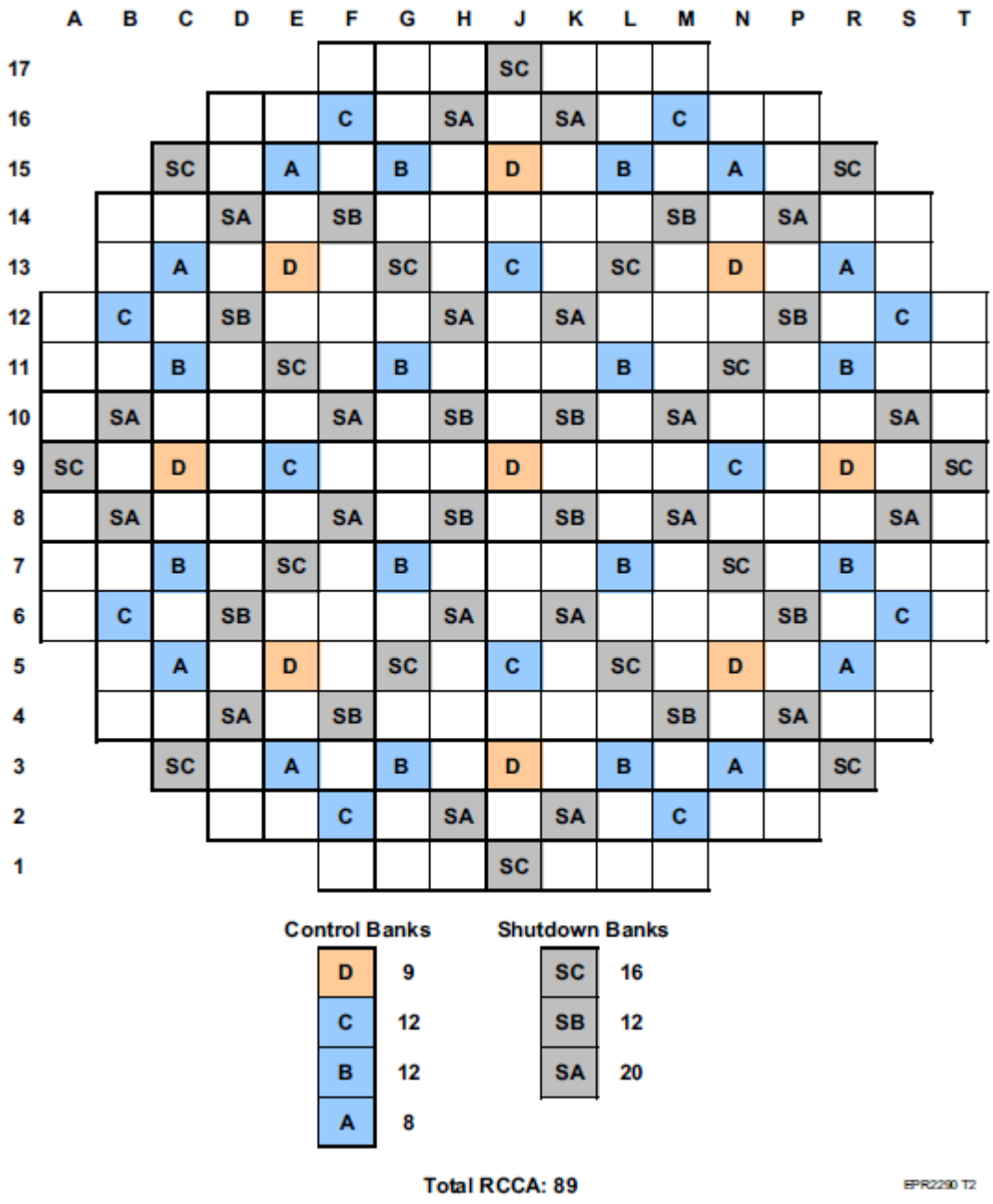

Figure 2:8 Rod Cluster Control Assembly Pattern

I. Control Rods Patterns and Reactivity worths

As explained in section 2.8.3 the above the rod cluster control assemblies are divided into two groups, namely the control groups and the shutdown groups. Control banks are labelled A, B, C and D and the shut-down banks are labelled SA, SB and SC. The position of control banks for criticality under all reactor conditions is determined by the boron concentration in the coolant.

Reactivity worth versus rod position is calculated by a series of steady state calculations at various control rods position. In the EPR-SAR reactivity worth calculations it is assumed that the rods are initially at a power dependent insertion limit to aid in minimisation of the initial reactivity insertion rate.

2.8.4 Chemical absorber

Boron is diluted in water as boric acid. The maximum boron (B-10) content is limited by the moderator temperature coefficient (MTC). PWRs are designed to have a negative MTC as too much B-10 will make MYC positive. B-10 and its concentration is varied to control relatively slow reactivity changes in connection to:

- The moderator temperature defect in going from cold shut down to hot operating temperature at zero power.
- Transients due to change in xenon and samarium concentrations following power changes or control rod cluster poison change.
- Effects due to reactivity of fissile material following depletion and resulting in build-up of long-life fission products.
- The Integral burnable absorber depletion.
- Very important for the depletion of U235

Boron concentrations for various core conditions are presented in table 4.3-5 of the EPR-SAR (AREVA, 2012).

2.9 Main EPR core design description

Active core	Detail
Equivalent diameter	376.682 cm
Active Fuel Height Coe (cold)	419.999 cm
Height–to-diameter ratio	1.115
Total cross-section area	304.673 cm^2
H_2O/Molecular ratio, lattice (cold)	2.78
Reflector thickness and composition used in neutronic design Top – water plus steel Bottom – water plus steel Side – water plus steel	 29.997 cm 29.997 cm ≈10 minimum: ≈20 maximum
Fuel assemblies Number	 241
Rod array	17 X 17
Rods per assembly	265
Rod pitch	1.260 cm
Overall transverse dimensions	21.402 X 21.402 cm
Nominal fuel weight (per assembly)	536.086 kg U
M5 weight in core	34.222 kg
Number of grids per assembly	10
Composition of grids	Alloy 718 (top and bottom grids) M5 (intermediate mixing grids)
Diameter of guide thimbles Upper region above dashpot	1.146 cm ID 1.245 cm OD
Diameter of guide thimbles Lower (dashpot) region	1.008 cm ID 1.245 cm OD
Fuel rods Number	 63.865
Outside diameter	0.950 cm
Diametral gap [($ID_{cladding} - OD_{pellet}$)/2]	0.008 cm
Cladding thickness	0.057 cm
Cladding material	M5

Table 2-1 Reactor core descriptions 1 of 2 (BOL)

Active core	Detail
Fuel pellets Material	UO_2 (sintered)
Diameter	0.08119 cm
Length	1.349 cm (enriched UO_2)
	1.349 cm ($UO_2Gd_2O_3$)
	1.349 cm (blanket UO_2)
Mass of UO_2 per foot of fuel rod	4.824 kg/cm

Table 2:1 Reactor core description 2 of 2 at BOL (AREVA, 2012)

Fuel Assembly Type	Number of assemblies	Average enrichment wt% U-235	Density (Percentage of theoretical density)	For detailed fuel assembly design, see Listed Appendix
A1	64	2.23	96%	APPENDIX B
A2	12	2.23	96%	
B1	32	2.62	96%	APPENDIX B
B2	56	2.61	96%	
C1	24	3.14	96%	APPENDIX B
C2	24	3.13	96%	
C3	32	3.12	96%	

Table 2-2 Fuel assembly summary

3. Methodology and model development

3.1 Introduction

A completed input model would comprise a completed neutronic-thermal hydraulic calculation as discussed in section 2.6.

However, it should be noted that in this study only neutronic calculations were performed. Since the thermal hydraulic calculations were not performed, the temperatures of all the material were taken to be 300 ^{0}C and the density of water was taken to be 1.0gcm^{3}

3.2 MCNP5

MCNP as explained in chapter 2 is a general-purpose Monte Carlo N-particle code that can be used to simulate transport of various particle types (such as neutron, photon, electron or coupled neutron/photon/electron) while treating an arbitrary three-dimensional configuration of material in a geometry of a system, taking into account point wise continuous energy cross section libraries that represent nuclear reactions in the 10^{-11} to 20 MeV energy range. MCNP5 is based on Monte Carlo methodology that simulates particle events and tracking of these events, with all the physics contained in the probability distribution functions. The results specified to be calculated by the user are made available by the use of tallies.

For this study MCNP, Version 5, release 1.40 and with ENDF/B VII release 8 cross-section data (X-5 Monte Carlo team, 2003) were used.

3.2.1 MCNP5 input file description

In order to build a representative MCNP model of the EPR an input file has to be developed, where the 3-D geometry is modelled and surfaces making up the geometry are described together with the material contained in the geometry (X-5 Monte Carlo team, 2003).

The MCNP input file is divided into three basic sections (excluding the message block).

Message block} optional	Section 0
Blank line delimiter Title card Cell cards	Section 1
Blank line delimiter Surface cards	Section 2
Blank line delimiter Data cards Blank line delimiter recommended Anything else optional	Section 3

I. Section 1/Title card

The first card after the optional entry in an MCNP input file is the title card where the user can specify the title of the input file (e.g. kcode EPR V Naicker/ OE Montwedi).

II. Section1/Cell cards

Cell cards contain information about material (e.g. number/mass density) contained in a cell and a 3D (i, j, k) description of the geometry volume containing the material.

The general format for cell cards specification is as follows

j m d geo parmet

Where j denotes the cell number, 'j' should be a positive integer of value$\leq$ 99999.

The entry 'm' denotes the material number that specifies the material contained in a cell and the entry should also be a positive integer of value $\leq$ 99999. The entry "d" denotes either the mass density or number density of the material contained in a cell. A positive entry for the density is interpreted as the atomic density in units of 10^{24} atoms per barn-centimetres, while a negative entry is interpreted as a mass density in units of grams per cubic centimetres. The entry "geo" denotes geometry specification; it uses Boolean operators together with allocated surface numbers to describe how surfaces bind regions of space to form a cell. The "parmet" entry may be used to denote cell parameters on the cell card line rather than in the data card section. For example the cell card importance "imp:n" which specifies the relative cell importance for neutrons.

Example

```
c universe    16  B1  grey
35    11 0.07342 (-90 -19 3)                    imp:n=1 u=   16
```

35 is a cell number, 11 is material number of the material contained in cell 35, 0.07342 is the atomic density of the material 11 contained in cell 35 and (-90 -19 3) describes the cell geometry as three surfaces defining a cell. -90 means material 11 is inside surface 90 which has a height defined to be below a plane surface -19 and on top of a plane surface 3. imp:n=1 u= 16 defines that the importance of neutrons in cell 35 is 1 and cell 35 is contained in universe 16.

III. Section2/Surface cards

Surface cards contain information about the surface making up the geometry of the problem of interest. A surface is defined in Cartesian co-ordinates as $f(x, y, z) = 0$. The MCNP input line defining a cylindrical surface is represented as CZ or (cz, MCNP is not case sensitive)

```
12 px       10.708640   $ plane perpendicular to the x axis
90 cz       0.410000    $ cylinder parallel to the z axis
```

Surface 12 is a plane intersecting the X axis at the origin. Surface 90 is an infinitely long cylinder parallel to the z axis, centred at the origin. Every surface has a "positive" and a "negative" side. The direction of the surface is defined mathematically as $f(x, y, z) > 0$, which represents the positive side of the surface and $f(x, y, z) < 0$, represents the negative side of the surface. For example a region inside a cylindrical surface is negative with respect to the surface and a region outside the cylinder is positive with respect to the surface.

IV. Section3/Data cards

Data cards contain information about the mode of calculation of interest, material specification, source specification and tally types.

The specification of materials filling the cells in an MCNP model involves the following

a) Assigning a material number to each cell.
b) Defining the material isotopic composition.
c) Cross section compilations to be used.

The isotope number ZAID (Z A IDentification) consists of six digits ZZZAAA where ZZZ is the atomic number Z and AAA is the atomic mass number A. U-235 has a ZAID number 092235 or just 92235.

```
c m11 u235 enrichment 2.00
m11    92235.71c   0.006750   $ atomic fraction of U-235
       92238.71c   0.326584   $ atomic fraction of U-238
        8016.71c   0.666666   $ atomic fraction of O-16
```

Material 11 defines UO_2 with an enrichment of 2 % and ZAID numbers of 92235, 92238 and 8016. The .71c entry represents a particular cross-section compilation. The positive entry on the atomic fraction represents atomic fractions instead of mass fractions

More details on the construction of an input file for an MCNP calculation are found in the MCNP5 user guide (X-5 Monte Carlo team, 2003).

V. Section3/Source specification

The criticality source type in MCNP is specified by the SDEF and or kcode command. For this study a general criticality source was used in the KCODE command. The KCODE command has several variables or parameters that are used to define the source characteristics. The KSRC is also used to define source position in Cartesian coordinates.

```
KCODE 100000 1.0 85 150
KSRC 0.0 0.0 -205.71 0.0 0.0 -182.85  0.0 0.0 -160.00  0.0 0.0 -137.14
     0.0 0.0 -114.28  0.0 0.0  -91.43   0.0 0.0   -68.57  0.0 0.0  -45.71
     0.0 0.0   -22.86  0.0 0.0       0.0    0.0 0.0    22.86  0.0 0.0   45.71
     0.0 0.0    68.57  0.0 0.0     91.43  0.0 0.0  114.28  0.0 0.0 137.14
     0.0 0.0  160.00  0.0 0.0  182.85  0.0 0.0  205.71
```

The first entry in the KCODE command is the number of neutron histories per cycle (10000 neurons per cycle), the second entry defines the initial guess value for k_{eff} ($k_{eff} = 1$), the third entry is the number of cycles to be skipped before beginning tally accumulation (85 cycles skipped), and the last entry is the number of cycles to be done (150 cycles done).

The first entry in the KSRC card is the source position in Cartesian coordinates (0.0 cm in the x plane, 0.0 cm in the y direction and -205.71 cm in the z direction). In this example there is a total of 20 source points distributed using the KSRC card.

VI. Section3/Tally specification

The tally cards are used to specify the type of tally the user is interested in investigating. Fission energy deposition averaged over a cell, neutron flux averaged over a cell, etc. Tallies are defined by a tally type and particles type. Tallies are numbered as 1, 2, 4, 5, 6, 7, 8, or increments of 10 thereof and are given particle designator: P,:N, or :E. Only tally type F7 and F4 are investigated in this study and therefore only they are described in this section.

Example f17:n ((14)<13 < 11 < 10[0 0 0])

f144:n ((14 15 16 17 18 19 20 21 22 23 24 25 26)<13 < 11 < 10[0 0 0])

F17 refers to a tally type 7 which is the fission energy averaged over cell (14), cell 14 is the cell containing fissile material and it is within cell 13 which is a fuel assembly that is a 17 x 17 matrix and this fuel assembly is in cell 11 which is the border of a fuel assembly, and cell 11 is in cell 10 which in turn is in a lattice at the centre of the lattice [x= 0, y=0 and z=0].

Similarly f144 refers to the 14nth f4 tally type, because more than one tally is counted. (14-26) are cells making up fuel assembly - they describe the UO_2 pellet, the helium gap, M5^{TM} cladding, guide tube and instrumentation tube, unlike the F7 tally where only the fissile material containing cell is (14) mentioned. The F4 tally type mentions all the cells making up a fuel assembly. The remaining cells 13, 11, 10[0 0 0] refer to the same description as in the F7 tally. In both tallies the designation: N refers to neutrons, F17:n is the fission energy deposited by neutrons and F:144:n refers to the neutron flux averaged over a cell.

3.3 MCNP flow chart for neutron flux and power distribution

Power distribution in MCNP is defined by the fission energy deposition as described in section 2.4 and the neutron flux is also defined in section 2.4.2. The procedure performed by MCNP for analysis of fission energy is described in the flow chart shown below. Furthermore the V, m, p_a refer to volume, mass and atomic density in this order.

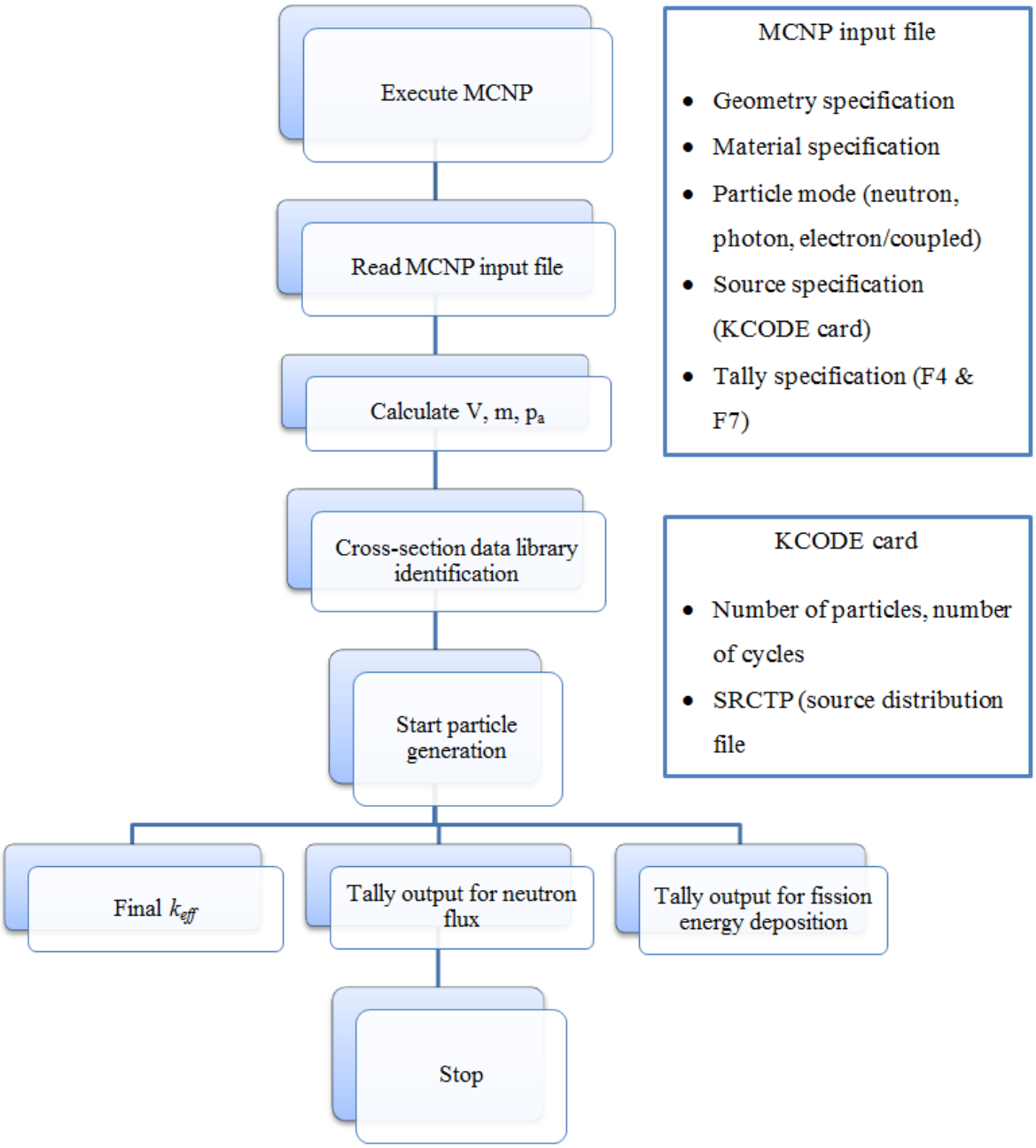

Figure 3:1 Flow chart of the MCNP code for neutron flux and power distribution (Waata, 2006)

The input file for MCNP simulation describes the physical model: geometry specification, material filling the geometry volume, cross-section data library for the isotopes of the materials, the type of source used and the type of output needed (tally specification). A temperature card (TMP card) is included in the input file to activate the free-gas model for treating thermal neutrons.

Upon initiating an MCNP calculation, an input file is read and the data interpreted to obtain information on the type of MCNP calculation to be done, for example, a criticality calculation for a k_{eff} output, a tally for neutron flux, a tally for power distribution or all of the three. In this study the MCNP calculation is performed using a general criticality source in the source specification card and a tally specification card to obtain neutron flux and power distribution from fission. For a fission power profile, MCNP calculates the volume of the cells describing the geometry, the atomic density and mass density of material, as shown in equation 2.6. The number density is given in the input file. The cross-section data libraries specified for all the material isotopes of the fuel, cladding, structural material and water are read from the MCNP data libraries. The types of particles to be simulated are specified in the input file. In this study neutrons are simulated.

The particle generation in MCNP is initiated with a criticality source specified by the KCODE card as discussed in section 3.2.1 V. For the first cycle source sites, the fission sites for neutrons are specified in the KSRC card as discussed in section 3.2.1V.

MCNP uses iteration methods for particle generation for the total number of cycles specified and when the total numbers of cycles are reached the particles generation is terminated. The final value of k_{eff} defined in (X-5 Monte Carlo team, 2003) and the neutron flux and fission energy deposition or power from F4 and F7 tallies are recorded and produced as output. The precision of the MCNP results is discussed in the last section of chapter 3. Note that fission energy deposition in volume cells as a function of axial height gives information about the axial power distribution in the fuel rod and fuel assemblies in the reactor core.

3.4 MCNP5 model of the EPR

In order to build a representative MCNP model of the EPR reactor, all the design details discussed in section 2.9 were used. The MCNP models of the EPR described below cover all important details with the new heavy reflector included. The model was built as precisely to the design specifications as possible, with inherent MCNP geometric modelling inadequacies

introduced in the process. The model description and assumptions are discussed in the ensuing sections.

3.4.1 EPR model development overview

The model development was divided into a number of steps. The first step was to develop a representative MCNP5 EPR homogeneous fuel assembly model, after which the homogeneous fuel assembly model underwent various tests as a form of verification. The second step was to develop a representative MCNP5 EPR heterogeneous assembly model, after which the model was tested as a form of verification and also compared to the results in the US EPR SAR nuclear design (AREVA, 2012). The third step was to develop a representative MCNP5 EPR core, heavy reflector, core barrel, reactor pressure vessel (RPV) and rod cluster control assembly (RCCA).

The following assumptions were made in developing the model:

- Steady state
- No temperature feedback
- No burn up/fresh fuel core
- Beginning of life
- No xenon
- Boron concentration 1383 ppm
- The assembly side boundaries are periodic for infinite assembly models

3.4.2 MCNP5 EPR infinite homogeneous assembly model description

Two MCNP5 models of the US EPR fuel assembly were developed with different lattices for discretisation of the fuel assembly volumes as seen in Figure 3:2 below. This was done to investigate the effect of discretisation on the power profile and neutron flux. The fuel assembly has a total active axial height of 420 cm, assembly pitch 10.71 cm, and a top reflector with a height 30 cm at the top and bottom of the assembly making the total height of active plus inactive equal to 480 cm. It should be noted this section was included for the verification purposes.

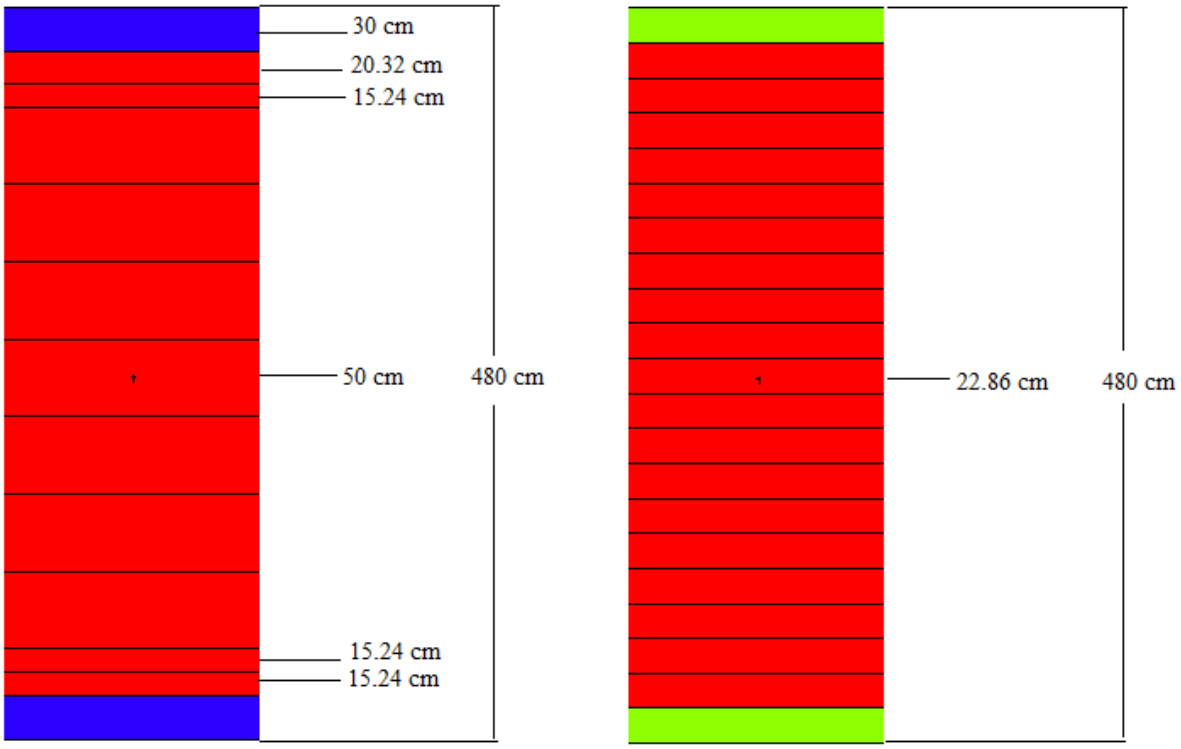

Figure 3:2 homogeneous infinite fuel assembly (a) & (b)

Figure 3:2 (a) and (b) above show the infinite homogeneous assembly model of the US EPR fuel assembly.

a) Has the same dimensions as those used in the EPR fuel assembly in Figure 2:4 Fuel assembly designs C1 and C2 except that the central region/zone has been discretised into seven equal axial regions of 50 cm each. The blue region on top and at the bottom contains the heavy reflector which is a homogeneous mixture of 5% water and 95% stainless steel, while the all red the axial regions contain homogeneous mixture of H_2O +UO_2 (0.5-0.5 ratio).
b) The infinite fuel assembly is discretised into 21 equal axial regions. The top and bottom green regions are filled with the heavy reflector which is a homogeneous mixture of 5% water and 95% stainless steel, while the red the axial regions contain homogeneous mixture of H_2O +UO_2 (0.5-0.5 ratio).

After development of these models the following tests were done, viz. a convergence test, a geometry test and material tests. These tests were done to evaluate the functionality of the model to check whether the model was working as expected.

I. Convergence test

A convergence test was done using the Shannon entropy computing capabilities built into MCNP 5, where a mesh for source entropy assessment was built around both the assemblies as described in section 2.5.2. The mesh is a 17 x 17 x 17 = 4913 mesh cells with the following origin:

Xmin= -1.4994E+01 Xmax= 1.4993E+01

Ymin= -1.4994E+01 Ymax= 1.4994E+01

Zmin= -2.9400E+02 Zmax= 2.9399E+02

Note all the coordinates units are in cm

Convergence of the multiplication factor was also monitored by post-processing, while convergence of the tally was done by use of statistical checks and varying the total number of cycles to be done from 800 to 3000 cycles for complete convergence.

II. Geometry test

A geometry test was done on the fuel assembly (a) to test whether the geometry was correct and had no errors. This test was done using the knowledge gained from nuclear reactor theory and nuclear reactor physics that a solution of the flux profile of a critical slab is $cos\left(\frac{\pi x}{ae_{ex}}\right)$ where $\left(\frac{\pi x}{ae_{ex}}\right)^2$ is the geometric buckling (Stacey, 2007). The test is to see whether the solution of the flux of the infinite homogeneous assembly is the expected solution.

III. Material test

A material test was done on the fuel assembly model. The material test was divided into two tests, (1) to test whether the effect of varying the amount of fuel in the homogeneous mixture of fuel and coolant on the multiplication factor (k_∞) gave expected results, (2) to test whether the effect of varying the enrichment on (amount of U-235 in UO_2) multiplication factor would yield expected results.

For test (1) the fraction of UO_2 in UO_2+H_2O was varied from 10 to 100 % in increments of 10. The value of k_∞ was recoded at each run and plotted against the fraction of UO_2 in UO_2+H_2O

For test (2) the fraction of U-235 in UO_2 was varied from 0.65 to 3.25 wt% U-235 and plotted against k_∞. The value 3.25 wt% was chosen as maximum because it is the highest enrichment

level in the EPR core. The test was done to check whether the model was working properly, i.e. whether the model was behaving as expected (that the value of k_∞ should increase with an increase in enrichment).

IV. Test for Gd_2O_3 + UO_2

A test was performed to investigate the effect of adding burnable absorber Gd_2O_3 in the central region of the homogeneous fuel assembly on the axial power profile. If the assembly model is behaving as expected the addition of a burnable absorber should flatten the axial power profile as discussed in (AREVA, 2012).

3.4.3 MCNP5 heterogeneous assembly models

After studying the homogeneous models (a) and (b) above; the assembly volume was filled with heterogeneous fuel rods as described in the nuclear design document of the EPR SAR, see (AREVA, 2012). The fuel assembly type C2 model was developed first because it resides at the centre of the EPR core. Modelling of this assembly type allowed for making assumptions such as assuming that the side boundaries of the fuel assembly are periodic. Periodic boundaries are discussed in section 3.5.2.

The infinite heterogeneous assembly was discretised like the homogeneous assembly type (a) in Figure 3:2 above, but filled with fuel rods instead of a homogeneous mixture of fuel and water. It should be noted that this section was developed to study the assembly power profile. This allowed for understanding of the way the power profile of each assembly behaves and to compare to the power profiles given in the EPR SAR.

The following parameters were used to develop the infinite heterogeneous assembly and the finite heterogeneous assemblies in the full core model.

Parameter	**Detail**
Assembly pitch	21.42 cm
Rods per assembly	265
Rod pitch	1.26 cm
Guide tube OR Guide tube IR	0.56 cm 0.49 cm
Fuel rods diameter	0.82 cm
He gap thickness	0.008 cm
Cladding thickness	0.023 cm
Cladding material	M5™

Table 3: 1 Fuel assembly design parameters used in MCNP5 model of fuel assemblies

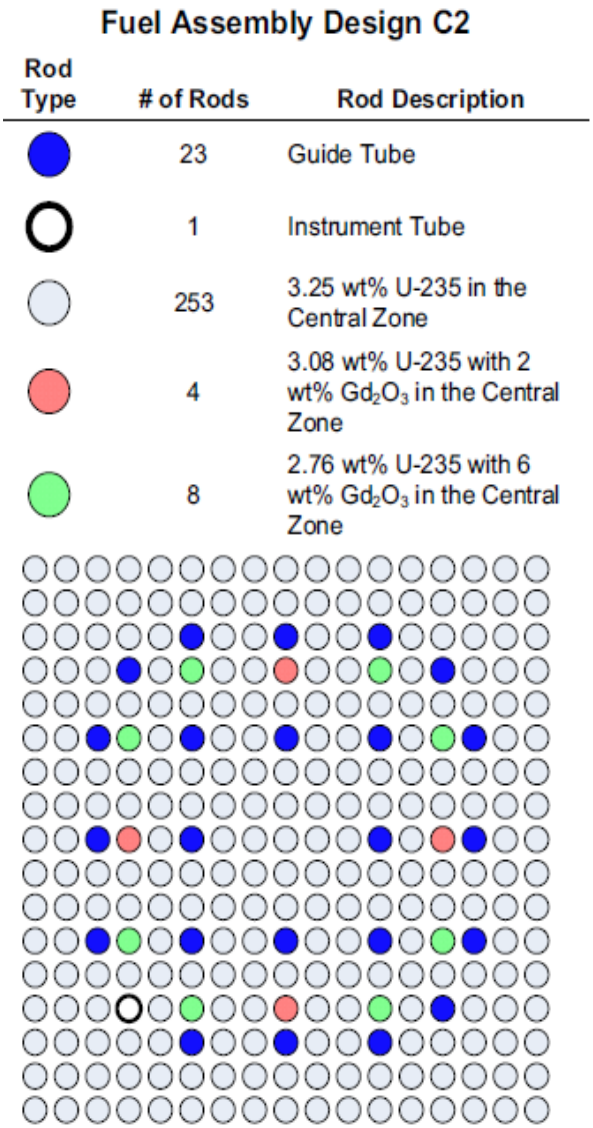

Figure 3:3 Fuel assembly design C2 (AREVA, 2012)

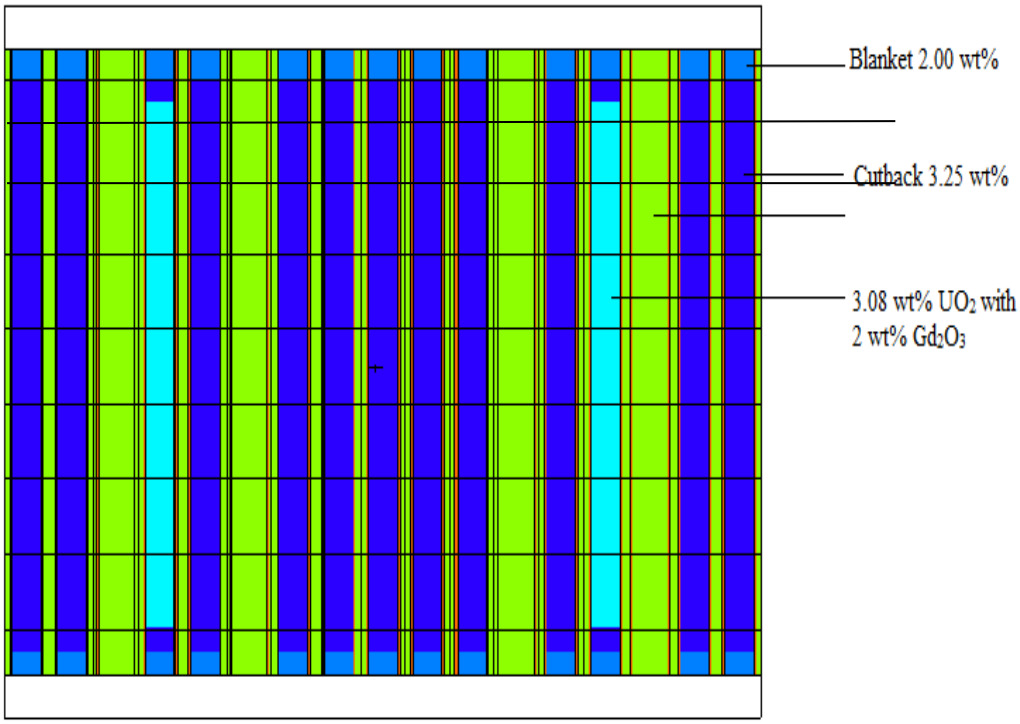

Figure 3:4 MCNP5 representative fuel assembly design C2 sectional side view

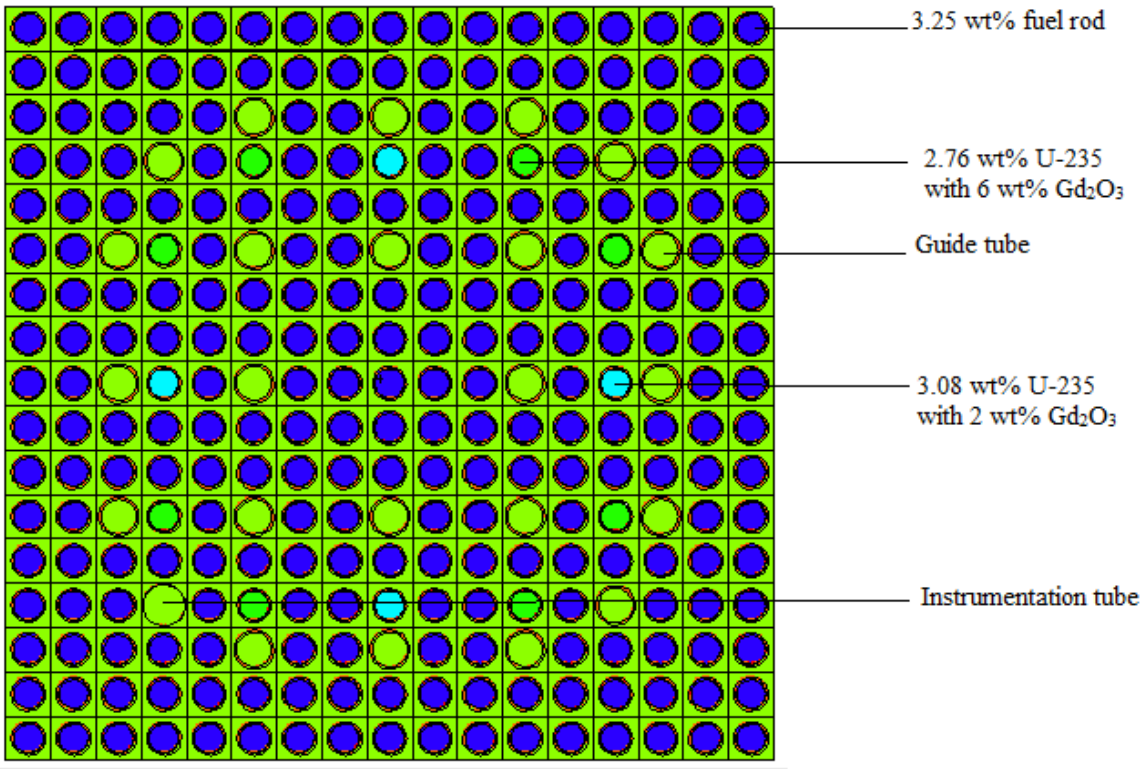

Figure 3:5 MCNP5 representative fuel assembly design C2 sectional top view

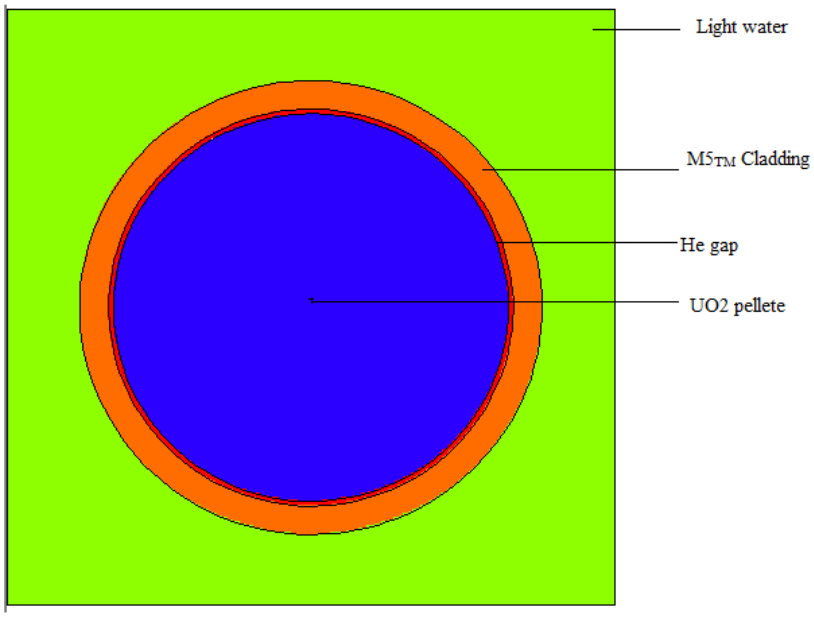

Figure 3:6 MCNP5 representative fuel rod

The MCNP5 representative of the EPR fuel assembly type was developed by discretising it into eleven axial regions see (Figure 3:4) where the blanket, cutback and central regions were also modelled similar to (Figure 3:2). Figure 3:5 represents the top view of the MCNP 5 representative of the EPR fuel assembly according to the fuel design obtained in (AREVA, 2012). Figure 3:6 is the MCNP 5 representative of the EPR fuel rod with the fuel pellet, He gap, M5^{TM} cladding and water around the fuel rod. The fuel assembly is filled with 265 fuel rods, 1 instrumentation tube and 23 guide tubes. See section 2.9 for dimensions of the fuel assemblies, fuel rods, gap fuel pellet, guide tubes and the instrumentation tube. After modelling the infinite fuel assembly C2 the rest of the fuel assemblies were developed using the same modelling approaches used for modelling C2, because the geometry of all the assemblies is the same. The difference between the assemblies is the fuel enrichment and the burnable absorber content. The different types of assemblies can be found in appendix B.

I. Convergence

Convergence of k_{∞} and fission source distribution was monitored using the Shannon entropy methods as specified in sections 3.4.2 I & 2.5.2.

II. Fission energy deposition

The fission power profile was calculated using the F7 tally as described in section 3.3 and compared to results from the US EPR SAR typical axial power shape found in the nuclear design of the EPR (AREVA, 2012). The F7 tally gives the amount of energy deposited by neutrons from fission per cell volume. It should be noted that the fission energy deposition is axially averaged.

III. Neutron flux

The neutron flux was calculated using the F4 tally as described in section 3.3 and the neutron flux was calculated over a range of three energy groups (0-0.41 eV), (0-0.1 MeV) and (0- 1 MeV). The chosen energy groups were used because they correspond to the same energy groups used in the safety analysis report (AREVA, 2012). The F4 tally gives the distribution of a number of neutrons per cell volume.

3.4.4 Local profile for C2 fuel assembly

After modelling the fuel assembly type C2 it was realised that developing an input file for the MCNP5 representative model of the US-EPR full core would be a very big challenge, because there were too many cells and too many elements so human error associated with manually writing the full core input would be great and the number of hours required would also be a lot. For this reason, a FORTRAN program was developed to produce the input of the for the MCNP5 representative EPR core model. The input file has 223491 lines and 60404 cells.

The input generating program was written such that it can form 1x1 assembly configurations to a 19 x 19 core.

3.4.5 MCNP5 representative EPR core model description

The MCNP5 EPR full core model was developed based on the findings from the infinite fuel assembly models after comparison of the assembly results to those in the US-EPR SAR, see Figure 2:3. Each fuel assembly was allocated a position in the core according the EPR SAR's initial core loading map.

The MCNP5 EPR full-core model includes modelling of the reactor pressure vessel, moderator (water), core barrel, heavy reflector, and 17 x17 fuel core configurations. Spacer grids were excluded from this model since it will be part of a later study to investigate the effects of the spacer grids on the calculations.

The core layout modelled is at the beginning of life with all fresh fuel. Below are properties used to model the full core:

Property	**Detail**
RPV_{IR} RPV_{OR}	244.2 cm 269.2 cm
Core barrel $_{IR}$ Core barrel $_{OR}$	202.4 cm 211.3 cm
Heavy reflector	10 cm – 20 cm
Top reflector	30 cm
Bottom reflector	30 cm

Table 3:6 Full core design description

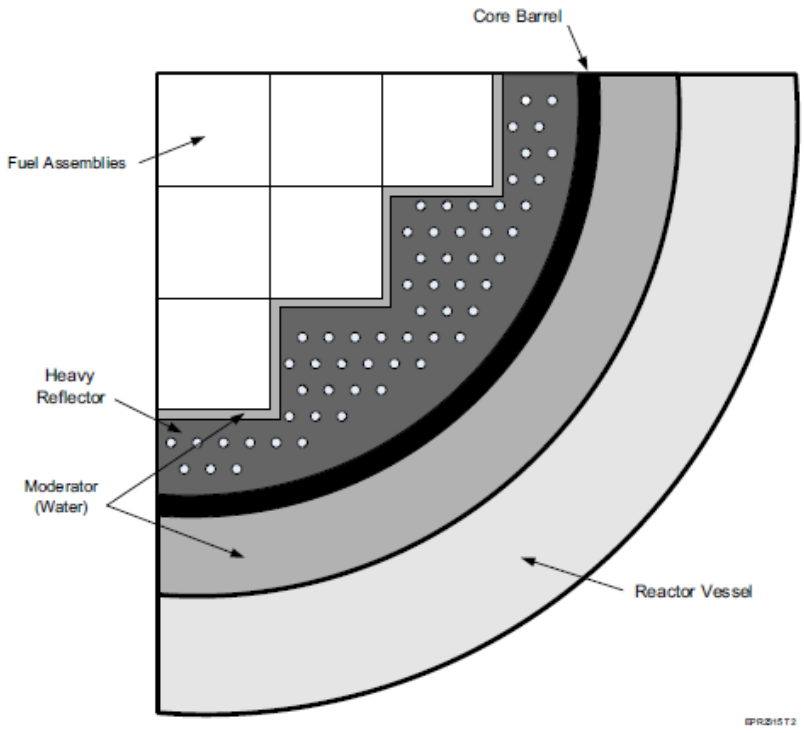

Figure 3:7 reflector layout (AREVA, 2012)

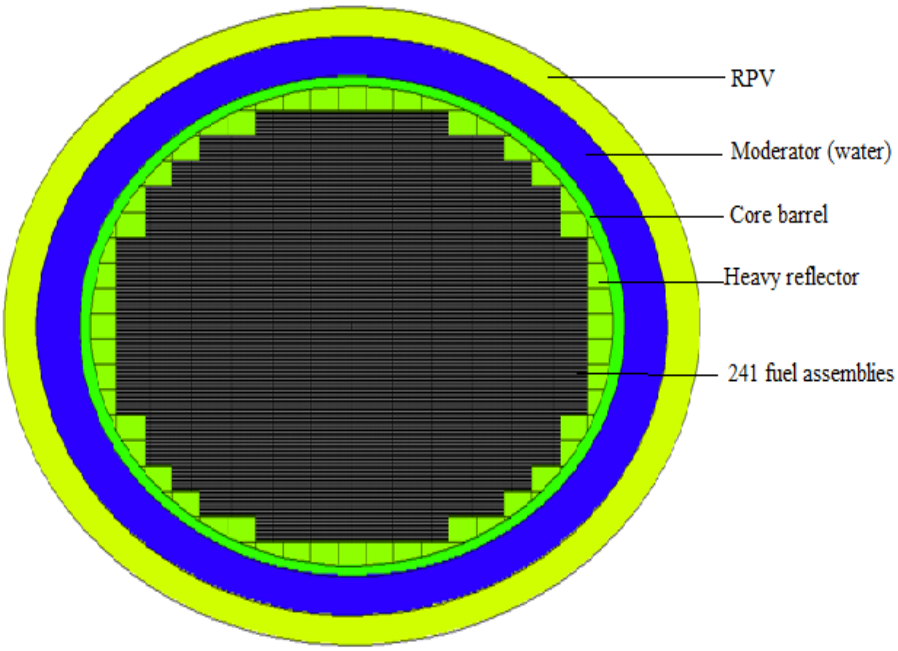

Figure 3:8 MCNP5 repetitive EPR core top view

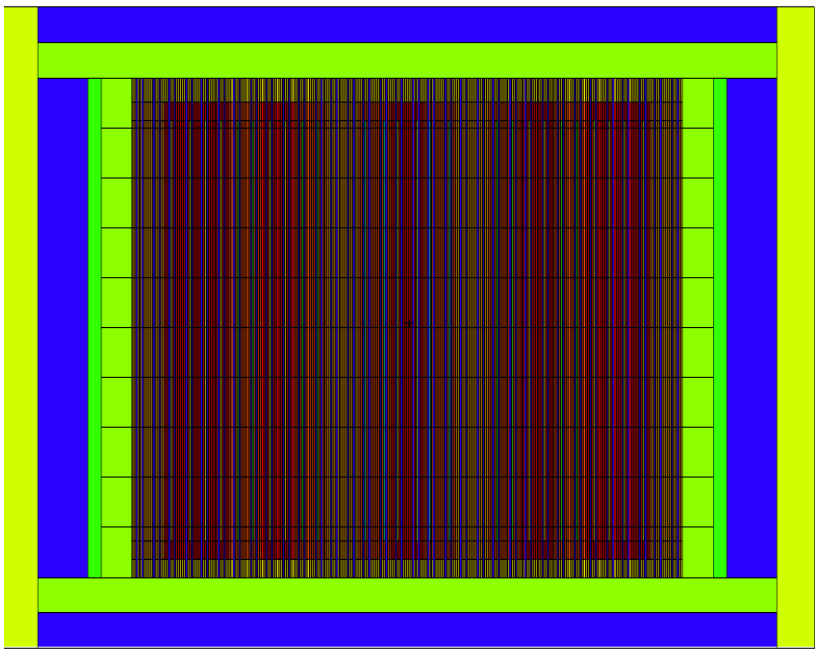

Figure 3:9 MCNP5 repetitive EPR core side sectional view

From Figure 3:8 the reactor pressure vessel was modelled in MCNP5 with dimensions specified in Table 3:2, the RPV is modelled as a homogeneous cylinder made of low alloy steel, with its internal surface cladded with NiCrFe alloy (AREVA, 2012) for resistance against corrosion.

The region between the RPV and Core barrel was modelled in MCNP5 as the moderator or water. The core barrel was modelled as in MCNP5 as a cylinder made of low carbon chromium stainless steel 304L (18Cr-8Ni) (AREVA, 2012). The heavy reflector contained by the core barrel was modelled in MCNP5 as homogeneous mixture of water and stainless steel with 95% stainless steel and 5 %. This was done to reduce the complexity of the model, and will be studied in a later study. The active core layout was modelled in MCNP5 as a 17 x17 array with each fuel assembly in its respective position as seen in Figure 2:3 describing EPR core layout at beginning of life.

Control rods were also modelled in MCNP5 as B_4C which are not the same rods used in the EPR because of the limited time for this work.

Convergence of k_{eff} and fission source distribution was monitored using Shannon entropy methods as specified in sections 3.4.2 I & 2.5.2.

I. Fission energy deposition

The fission power profile was calculated using the F7 tally as described in section 3.3 The F7 tally gives the amount of energy deposited by neutrons from fission per cell volume.

The neutron flux was calculated using the F4 tally as described in section 3.3. The F4 tally gives the distribution of a number of neutrons per cell volume.

II. Reactivity worth/ Reactivity against RCCA position

Using the definition of reactivity as stated in the US EPR submission (Areava, 2012) the control rods worth is calculated as follows and the units are in pcm where 1 pcm = 10^5 and $\Delta\rho$ is calculated from two state-point values of k_{eff} by

$$\Delta\rho = \frac{(k_2 - k_1)}{(k_2 \cdot k_1)}$$

$k_1 = 1.000$ and k_2 is calculated at every rod position (AREVA, 2012)

However, because of the time scope of the project and the amount of time MCNP takes to run a full core calculation, boron dilution into the water was not done to get the reactor exactly critical ($k_{eff} = 1.00$). It was assumed that for the rod worth calculation the value of k_1= 1.09 and k_2 is calculated per rod position.

The RCCA was inserted at various levels from level one to level ten, where level one represents the top axial discretised lattice position of the core and level ten represents the bottom.

The reactivity worth against RCCA position was used to calculate the control rod's worth. Reactivity worth versus rod position is calculated by series of steady calculations at various control rod position. In these calculations it is assumed that no changes in xenon or boron concentration take place (see results in section 4.5-II).

3.4.6 Model limitations

- RCCA: in this study it was assumed that the control rods are B_4C rods and not the (80-Ag15- In 5- Cd) control rods and every assembly contains control rods unlike in the US-EPR that contains only 89 control rods. These assumptions were made because of the limited time available to complete the project.
- Temperature: all the calculations were performed at an average temperature of 300^0C. This assumption was made because the temperature distribution of the US-EPR was out of the scope of the project. Determining the temperature profile of the reactor core would require development of a thermo-hydraulic model and this model would then be coupled to a neutronic model. The reason why this could not be done was because it would be done by another masters' student as Coupled neutronic and thermal hydraulic analysis of the EPR.

3.4.7 MCNP accuracy and precision

It is important to note that the errors or uncertainty estimates for MCNP calculations refer to the precision of the results, not the accuracy. This makes it very possible to calculate a highly precise result that is far from the physical truth because nature has not been modelled properly.

I. Factors affecting MCNP accuracy

From the MCNP manual (X-5 Monte Carlo team, 2003) the three factors that affect an MCNP result are discussed below.

- The code this includes: the physics features in the calculation, as well as the mathematical models used and uncertainties in data like the transport and reaction cross-sections in energy. Because MCNP is a widely used product with increasing users over the years, the likelihood of serious coding errors continues to decrease.
- Problem modelling: this can contribute to a reduction in the accuracy of MCNP calculations. Most calculations produce poor results because of the model of the energy and angular distribution of the source is not adequate. In this study, a continuous energy model was used, which is reported to produce more accurate results compared to the multi-group or few group energy models (X-5 Monte Carlo team, 2003).
- The user: through input problems and misuse of variance reduction techniques. Errors in geometry can be detected earlier when neutrons leak out of the geometry. The MCNP full-core model was created automatically using a FORTRAN script to eliminate the input problem error. Factors affecting MCNP precision
- Tally type

An efficient tally is averaged over a region in phase space as practically as possible. Because of this connection the tally dimensionality is very important. For example, a one-dimensional tally is 10 to 100 times easier to estimate than a two or three dimensional tally.

- Variance reduction techniques

Variance reduction techniques may be used to improve the precision of a given tally by increasing the non-zero tallying and by decreasing the spread of non-zero history score.

- Number of histories

  The number of histories ran can be increased to improve precision, this is due to the fact that precision is proportional to $\frac{1}{\sqrt{N}}$, where N is the total number of histories. However, running a large number of histories is very expensive in computation time and should therefore be done using parallel computing, super computers etc for complex problems.

3.5 Boundary conditions

In this study three model types are discussed and each one has different boundary conditions. This section gives a theoretical description of the boundary conditions and explains why each condition is used.

3.5.1 Reflective boundaries

In MCNP, reflective boundary conditions assume that there are no neutrons crossing the boundary of the volume of interest. Such an assumption can be made for the infinite homogeneous assembly, assuming every neutron that reaches the side of the fuel assembly is reflected back into the assembly volume (X-5 Monte Carlo team, 2003). These boundaries are used when mirror symmetry exists in the system.

3.5.2 Periodic boundaries

Periodic boundaries are applied to pairs of planes to simulate an infinite lattice. This can be used if you have a fuel assembly that is not perfectly symmetrical. This is the case with the EPR fuel assembly which unlike the ordinary PWRs has an instrumentation tube off centre replacing one of the fuel rods while in a PWR assembly the instrumentation tube is at the centre of the assembly making it perfectly symmetrical (mirror symmetry). For example.

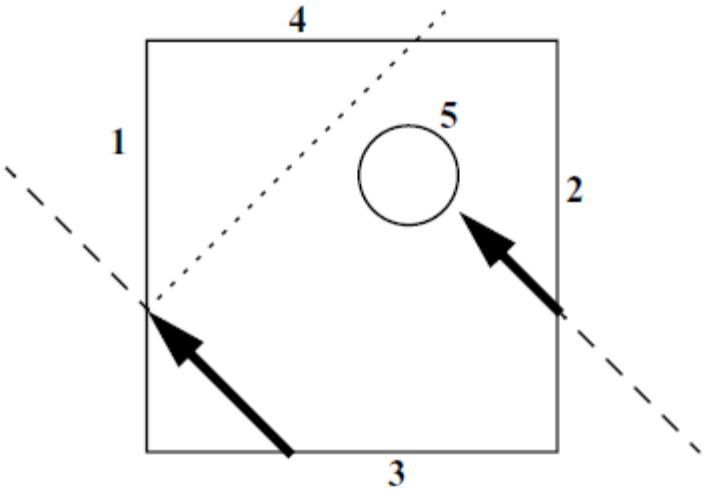

Figure 3:10 Illustration of periodic boundaries

Figure 3:10 above consists of a square reactor lattice infinite in the z direction. Surface 1 is periodic with respect to surface 2 and is in a px plane. Surface 2 is periodic with surface 1 and is in the px plane. Surface 3 is periodic with surface 4 and surface 3 is periodic with respect to surface 4. This implies that a particle leaving surface 1 re-enter on surface 2 and not reflected as shown by the dashed line reflected by surface 1 (X-5 Monte Carlo team, 2003).

The full core model uses actual boundaries specified in the SAR and no boundary conditions are assumed for this case.

3.6 Discretisation

It should be noted that a discretisation study was not done, because discretisation becomes important in a burn-up calculation due to varying of material concentration per region of the core. Similarly discretisation becomes important in a temperature-dependent calculation, for example if temperature varies both axially and radially. Since in this study there is no burn-up and temperature dependence, discretisation is not important. If this was a coupled study or burn-up was carried out, then a test of the level of discretisation should have been done.

3.7 Verification

There is no chapter dedicated to verification due to reasons stated below.

Because of the stochastic nature of MCNP calculation verification was done parallel with the actual model development. The verification of the infinite homogeneous assembly model in section 3.4.2 was done by making use of a convergence test, a geometry test and a material test. Verification of the infinite heterogeneous assembly manually developed model in section 3.4.3 was done by using a comparison of results with the EPR SAR results and similarly the full core model verification was done by comparing the results with those of the EPR SAR.

4. Results and discussions

4.4 Introduction

In this chapter results from all the models are presented and discussed. Results from the infinite homogenous assembly and infinite heterogeneous assembly model are presented and the full core results are presented as well.

4.2 Homogeneous assembly type C2 results

The results below were obtained using methods discussed in chapter 3 on the methodology and model development.

I. Convergence

The results below show the convergence of the infinite homogenous assembly results and were obtained using a method specified in section 3.2 to assess the convergence behaviour of both k_{eff} and the fission source distribution H_{src}. It should be noted that the H_{src} measures the disorder in fission source distribution and its variation should be constant for it to converge.

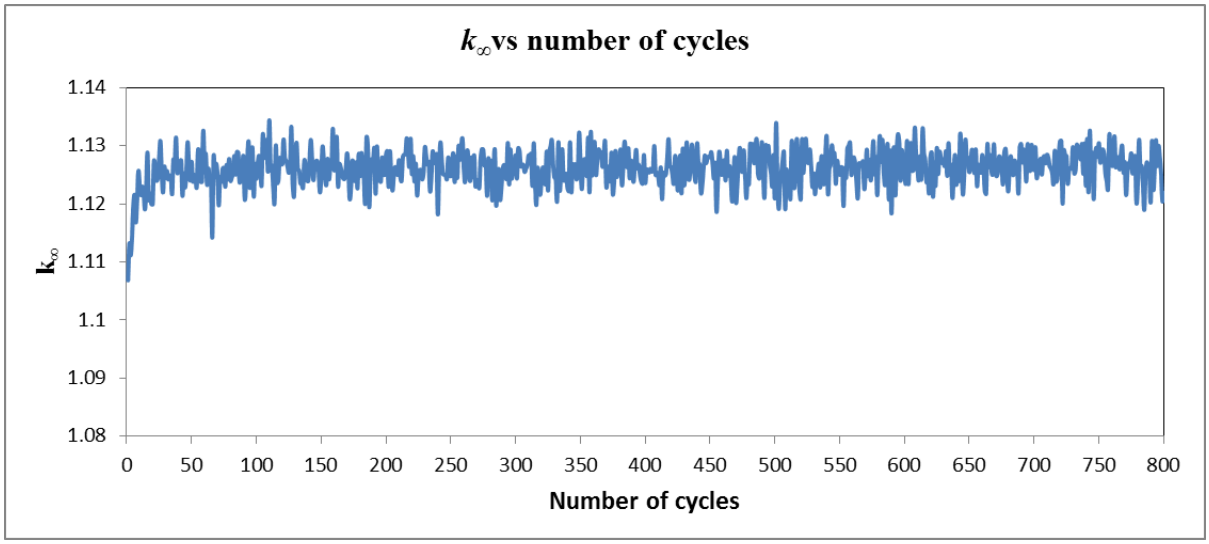

Figure 4:1 k_∞ vs number of cycles

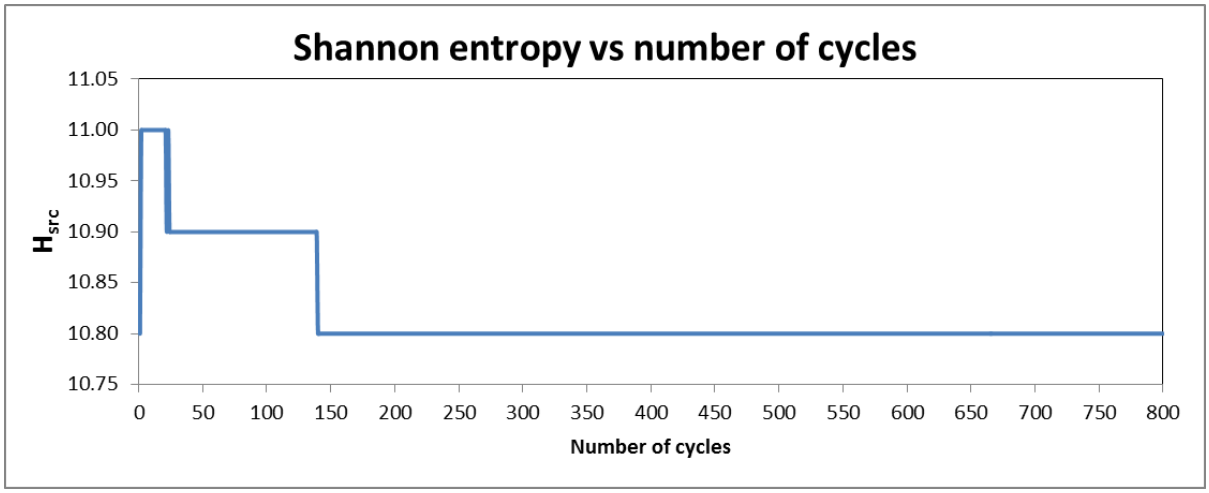

Figure 4:2 H_{src} vs number of cycles

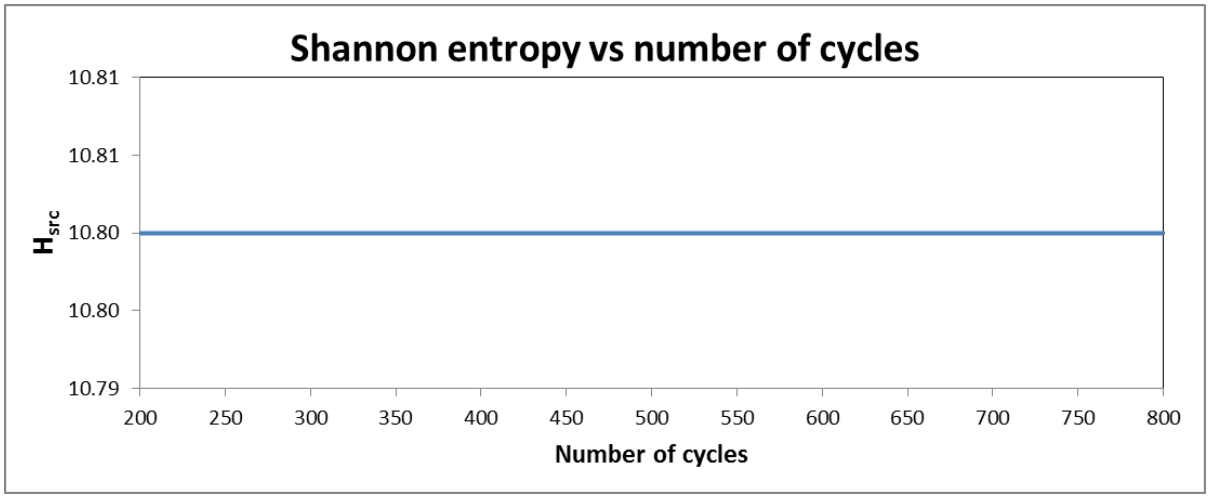

Figure 4:3 H_{src} vs number of cycles

From Figure 4:1 it is seen that the value of k_∞ increases from 1.1 to about 1.13 after cycle 75, while the amplitude of the distribution of k_∞ remains the same. It is difficult to determine precisely from which point k_∞ has converged due to the statistical noise in the k_∞ plot; a conservative estimative would be at about cycle 80.

However from examination of H_{src} in Figure 4:2 it can be seen that the Shannon entropy of the fission source distribution increases to 11 and then becomes constant for a few cycles, then drops to 10.9 and remains constant till about the 149^{th} cycle, then the entropy drops to 10.8 and then remains constant from cycle 150 to 800. This is because MCNP expands the Shannon entropy mesh cells encompassing the geometry of the fuel assembly volume if necessary until the geometry volume has been covered with the mesh over which the Shannon entropy is determined.

The entropy therefore increases from 10.8 to 11.0 seen in the 1st cycle and remains constant until the 25th cycle. The initial source is defined at specific points. After the first cycle, the initial source gets replaced by sources at fission sites. The source entropy will therefore increase (it gets more spread out). The mesh cells are expanded in cycle 25 which means the volume over which the entropy is determined increases, resulting in the decrease in entropy from 11.0 to 10.90. The mesh cells further expand to encompass all fissile material and this means a further increase in volume and a further decrease in the entropy from 10.90 to 10.80 in the 149th cycle after which the entropy remains constant.

From examination of the plot Figure 4:2 it can be seen that about 150 cycles are required for the fission source to fully converge. This therefore implies that at least 150 cycles should be skipped before tallying any results to avoid bias in results. For this study 200 cycles were skipped before tallying of results was done. 200 cycles were chosen because it was recommended in literature as a more conservative approach, but it should be noted that 150 cycles can also be skipped to save time if required.

II. Statistical tests and their effect on precision

In this section the results for determining the paths for convergence of the tallies are presented together with their effect on the precision of the result (refer to section 2.4.3).
Note the acronyms that follow:

Acronyms	**Definition**
Mean B	Mean Behaviour
RE V	Relative Error Value
RE D	Relative Error Decrease
RE DR	Relative Error Decrease Rate
VOV V	Variance of Variance Value
VOV D	Variance of Variance Decrease
VOV DR	Variance of Variance Decrease Rate
FM V	Figure of Merit Value
FM B	Figure of Merit Behaviour
PDF slope	Probability Density Function slope
F	Fail
P	Pass

Table 4-1 Acronyms used in statistical checks

600	Cyles	4.96	Hr									
Statistical test	Tally no	17	27	37	47	57	67	77	87	97	107	117
Mean B	1	P	F	F	P	P	P	P	P	F	F	F
RE V	2	P	P	P	P	P	P	P	P	P	P	P
RE D	3	P	P	P	P	P	P	P	P	P	P	P
RE DR	4	P	P	P	P	P	P	P	P	P	P	P
VOV V	5	P	P	P	P	P	P	P	P	P	P	P
VOV D	6	P	P	P	P	P	P	P	P	P	P	P
VOV DR	7	P	P	P	P	P	P	P	P	P	P	P
FM V	8	F	F	P	F	F	F	F	F	F	P	P
FM B	9	F	F	P	F	F	F	F	F	F	P	P
PDF Slope	10	P	P	P	P	P	P	P	P	P	P	P

Table 4-2Statistical checks 1 of 4

800	Cyles	6.35	Hr									
Statistical test	Tally no	17	27	37	47	57	67	77	87	97	107	117
Mean B	1	P	P	P	P	P	P	P	P	P	P	F
RE V	2	P	P	P	P	P	P	P	P	P	P	P
RE D	3	P	P	P	P	P	P	P	P	P	P	P
RE DR	4	P	P	P	P	P	P	P	P	P	P	P
VOV V	5	P	P	P	P	P	P	P	P	P	P	P
VOV D	6	P	P	P	P	P	P	P	P	P	P	P
VOV DR	7	P	P	P	P	P	P	P	P	P	P	P
FM V	8	P	P	P	P	P	P	P	P	P	F	F
FM B	9	P	P	P	P	P	P	P	P	P	P	F
PDF Slope	10	P	P	P	P	P	P	P	P	P	P	P

Table 4-3 Statistical checks 2 of 4

1600	Cyles	16.91	Hr									
Statistical test	Tally no	17	27	37	47	57	67	77	87	97	107	117
Mean B	1	P	P	P	P	P	P	P	P	P	P	F
RE V	2	P	P	P	P	P	P	P	P	P	P	P
RE D	3	P	P	P	P	P	P	P	P	P	P	P
RE DR	4	P	P	P	P	P	P	P	P	P	P	P
VOV V	5	P	P	P	P	P	P	P	P	P	P	P
VOV D	6	P	P	P	P	P	P	P	P	P	P	P
VOV DR	7	P	P	P	P	P	P	P	P	P	P	P
FM V	8	P	P	P	P	P	P	P	P	P	F	F
FM B	9	P	P	P	P	P	P	P	P	P	P	P
PDF Slope	10	P	P	P	P	P	P	P	P	P	P	P

Table 4-4 Statistical checks 3 of 4

3000	Cyles	27.87	hr									
Statistical test	Tally no	17	27	37	47	57	67	77	87	97	107	117
Mean B	1	P	P	P	P	P	P	P	P	P	P	P
RE V	2	P	P	P	P	P	P	P	P	P	P	P
RE D	3	P	P	P	P	P	P	P	P	P	P	P
RE DR	4	P	P	P	P	P	P	P	P	P	P	P
VOV V	5	P	P	P	P	P	P	P	P	P	P	P
VOV D	6	P	P	P	P	P	P	P	P	P	P	P
VOV DR	7	P	P	P	P	P	P	P	P	P	P	P
FM V	8	P	P	p	P	P	P	P	P	P	P	P
FM B	9	P	P	P	P	P	P	P	P	P	P	P
PDF Slope	10	P	P	P	P	P	P	P	P	P	P	P

Table 4-5 Statistical checks 4 of 4

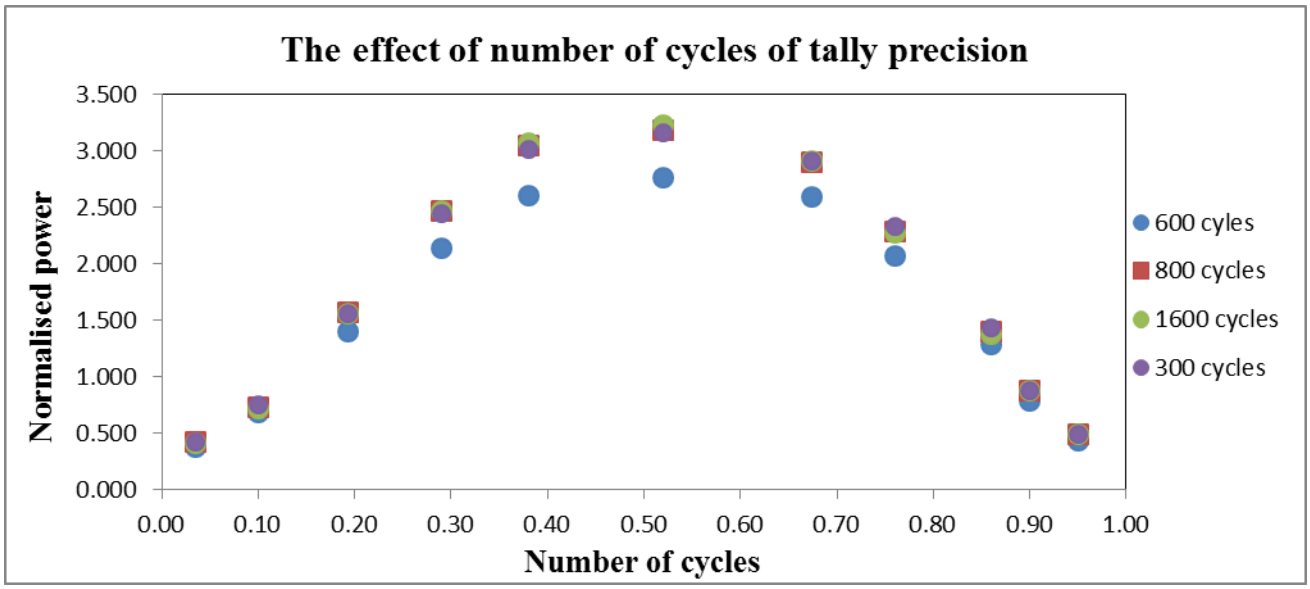

Figure 4:4 The effect of the number of cycles on tally precision

Note that for the tally convergence study the number of neutron histories per cycle is 100000 and the statistical checks are done for 600, 800, 1600 and 3000 cycles.

It can be seen that from Table 4-2 that tally number 1 fails 5 of the 10 statistical tests, tally number 8 fails 8 of the 10 statistical tests and tally number 9 also fails 8 of the 10 statistical tests. From Table 4-3 it can be seen that when the number of cycles is increased from 600 to 800, tally number 8 fails 2 of the 10 statistical tests and tally number 9 fails 1 of the 10 statistical tests. From Table 4-4 it can be seen that when the number of cycles is further increased to 1600 tally only tally number 9 fails 2 of the 10 statistical tests. From Table 4-5 it can be seen that all the tallies pass the ten statistical tests if the number of cycles further increases to 3000; however, this takes 27 hours to run the calculation and might not be the most effective number of cycles to run. One should therefore decide whether the time taken

for the calculation to complete convergence is more important, for example in a preliminary calculation it might not be necessary to achieve complete convergence.

From Figure 4:4 The effect of the number of cycles on tally precisionit can be seen that the power profile with 600 cycles is not in agreement with the power profile run with 800, 1600 and 3000 cycles. However, it can be seen that the power profile from 800, 1600 and 3000 cycles are in very good agreement, which implies that the statistical checks affect the precision of the tally not the accuracy. Depending on the required precision of the result the calculation can be done with a minimum of 800 cycles.

III. Geometry Test

The results below in Figure 4:5 are for the geometry test of the infinite homogeneous fuel assembly as described in section 3.4.2-II. The fuel assembly volume was filled with a homogeneous mixture of UO_2 and H_2O (40% UO_2 and 60% H_2O) and an F4 tally was used to determine the neutron flux of the infinite critical slab (assembly), which from literature is expected to be

$\emptyset(x) = AcosB_1x = Acos(\frac{\pi x}{\tilde{a}})$ (Lamash & Baratta, 2012)

The results in Figure 4:6 are intended to show comparison between two modelling approaches, where one fuel assembly is discretised in to a 1:1:21 lattice and another assembly into a 1:1:11 (x: y: z) lattice. The lattice describing assembly with 21 axial regions is made of equal spaces in all 21 axial regions and the assembly with 11 is divided into 1 1 7 1 1 where only the 7 regions have equal spacing. See Figure 3:2 for the model geometry dimensions. These results indicate that the syntax used in the input model is correct. For example, tally volumes and surface definitions have been interpreted and entered correctly.

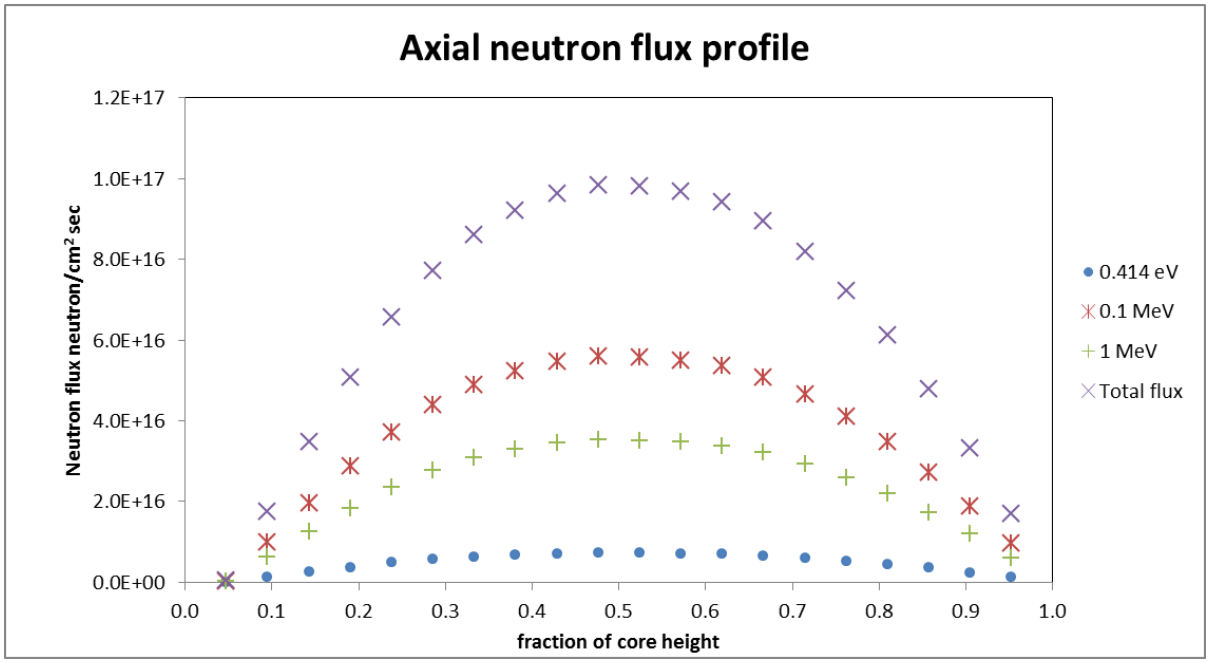

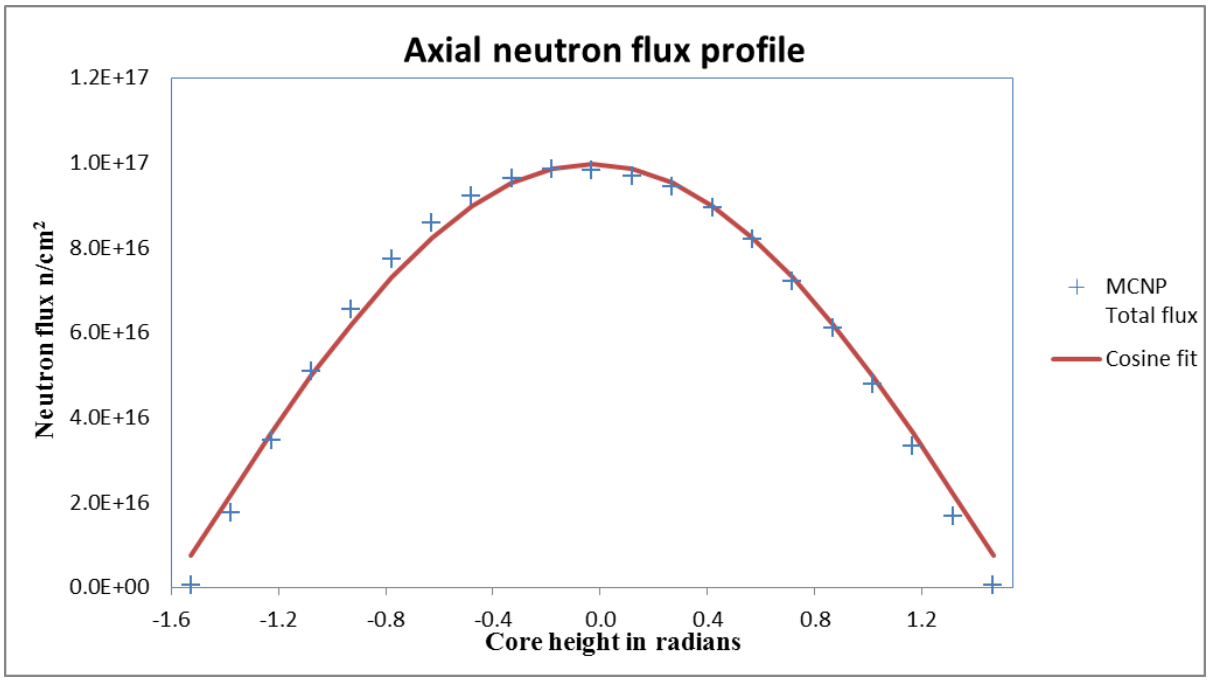

Figure 4:5 Four group neutron flux

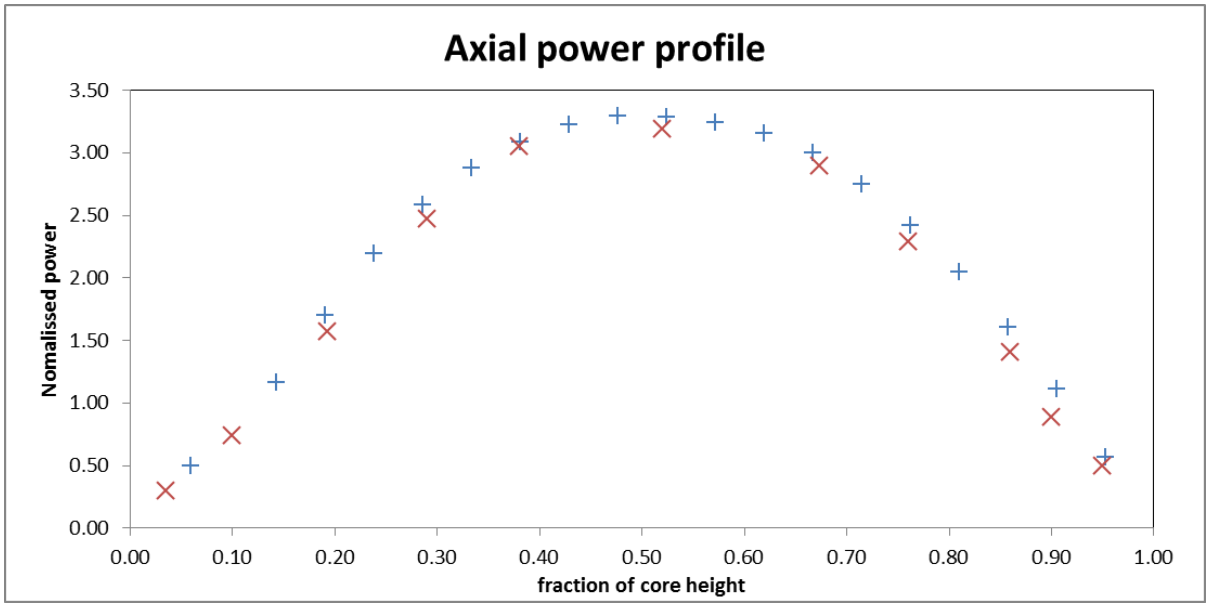

Figure 4:6 Power profile of a 21 equal space grid and 11 non-equal space grid assembly

From Figure 4:5 it is seen the axial neutron flux distribution gives expected results, these being the cosine solutions as explained in section 3.4.2 II, it can further be seen that the MCNP total flux and the cosine fit are in good agreement. There is a deviation on the left side of the plot just after the peak. This difference may be because of the different methods used. The cosine fit was calculated using the diffusion equation while the total flux solution was obtained using MCNP methods. The further difference between the MCNP total flux and the cosine fit on the edges may also be attributed to the nature of the diffusion equation, i.e. the diffusion equation is not expected to be accurate at boundaries. Because of the good agreement between the MCNP and cosine fit further assurance in the correctness of the input model can be assumed.

It is also seen that the axial neutron flux contribution from the (0 - 0.1 MeV) energy range is the largest because it includes both thermal and epithermal neutrons and since the EPR is a thermal reactor it is expected that more neutrons will be present in this region. Contributions from the (0.1 - 1 MeV) range have the second largest contribution to the neutron flux; this is because the neutrons in this region belong to the fast energy region of the neutron spectrum. The least contribution is from the (0 - 0.414 eV) range. This should be so since it is the sub-set of the (0-0.1 MeV) range. The above neutron energy ranges were chosen as they are the ranges presented in the EPR SAR.

From Figure 4:6 it can be seen that the power profiles from two modelling approaches described in section 3.4.2 are in very good agreement. This implies that the interpretation of the MCNP manual on geometry specification was done correctly

.

IV. Material test

As discussed in section 3.4.2 III a material test was done on the infinite homogeneous fuel assembly. This test was divided into three tests. The first test was intended to investigate the effect of the fraction of UO_2 in the fuel water mixture on the multiplication factor. The second test was done to determine the effect of over and under-moderation on the multiplication factor. A more detailed discussion of the over and under moderation test can be found in the Nuclear physics and Reactor Theory Hand book (DOE, 1993). The Third test was intended to determine the effect of enrichment on the multiplication factor.

The results from Figure 4:7 below are from testing of the effect of varying the amount of UO_2 in the homogeneous mixture of UO_2 + H_2O filling the fuel assembly volume, this is done to test if the model behaves as expected.

The results from Figure 4:8 are from testing the effect of over and under-moderation on the multiplication factor.

The results from Figure 4:9 are from testing the variation of U-235 in UO_2 or in other words testing the effect of varying fuel enrichment on the multiplication factor as explained in section 3.4.2- III

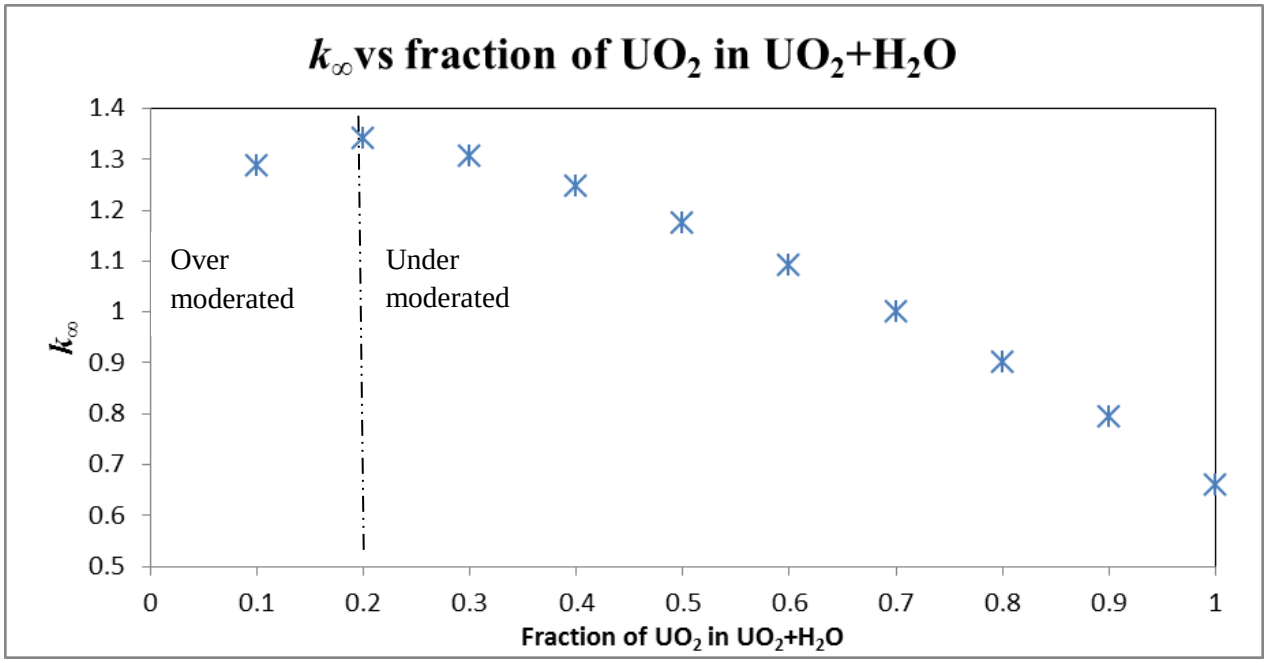

Figure 4:7 k_∞ vs fraction of UO_2 in UO_2+H_2O

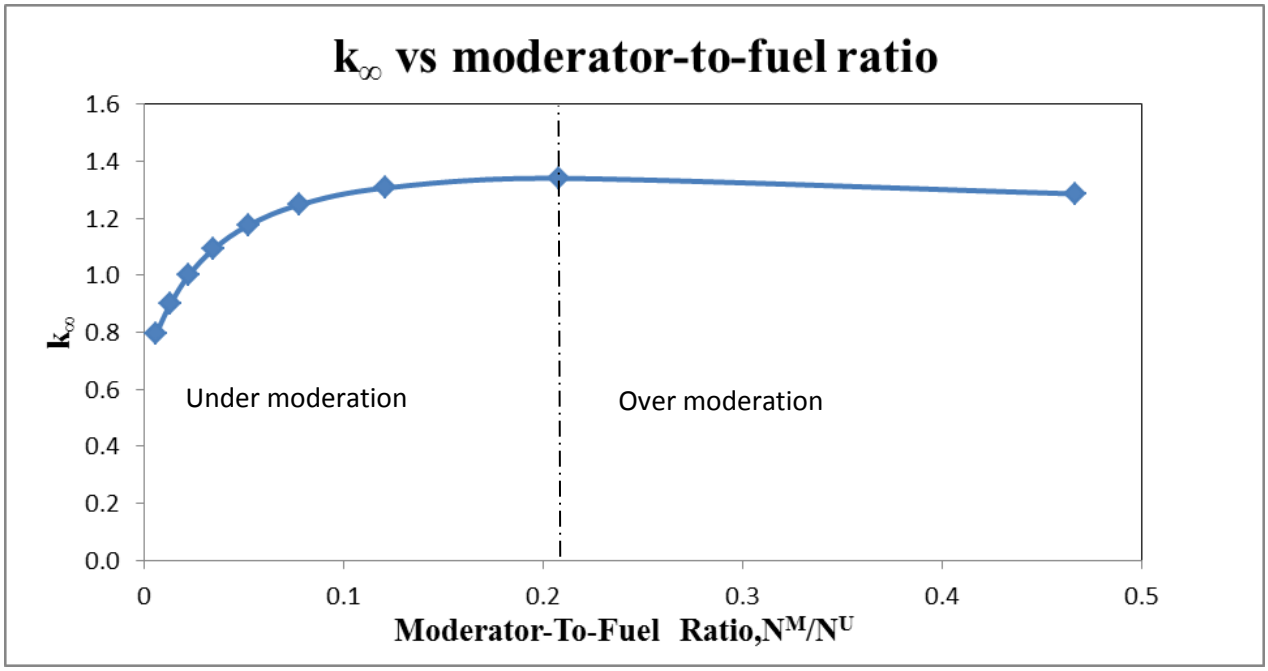

Figure 4:8 Effects of over and under moderation on k_{eff}

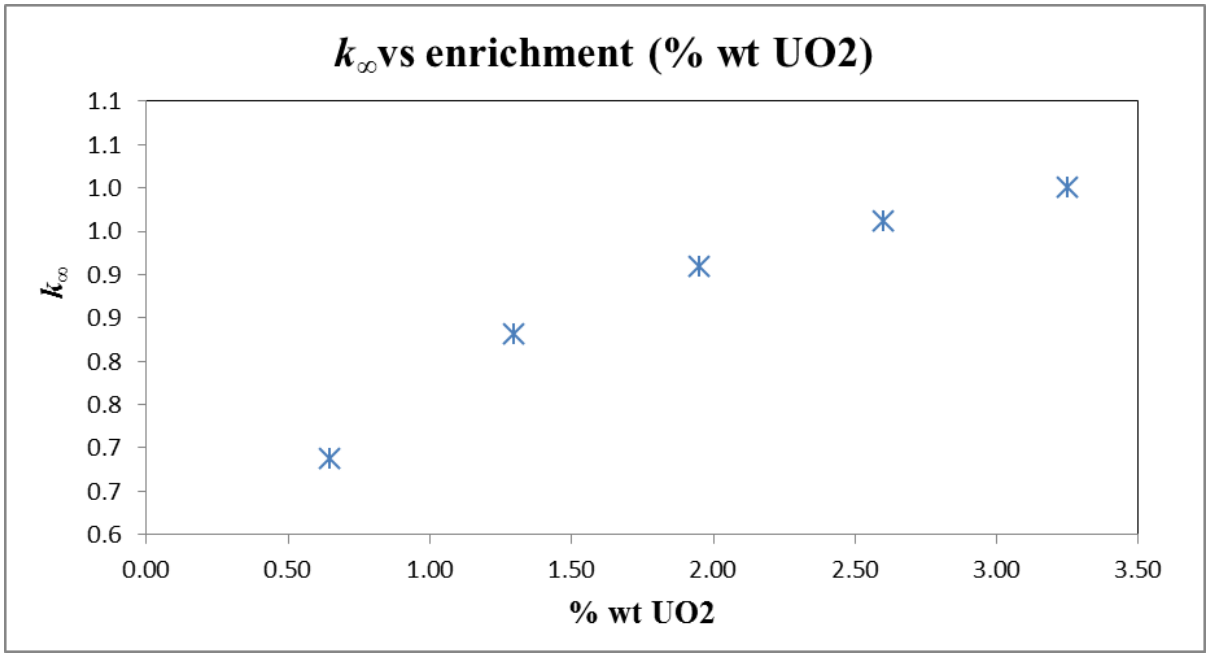

Figure 4:9 k_∞ vs enrichment of UO

From Figure 4:7 it is seen that when the fraction of UO_2 is varied from 10 to 100%, the assembly system is super-critical and peaks at 20 % UO_2, the multiplication factor k_∞ decreases after this point with an increase in UO_2 and the corresponding decrease in H_2O content. This is because the moderation of the fast neutrons to thermal neutrons decreases. It is seen from the graph that at about 70% UO_2 and 30% H_2O the assembly system is critical. This is optimal for reactivity control for this scenario. When the fraction of UO_2 reaches a 100% the assembly system becomes subcritical because there is no water moderating the system or the system is under-moderated.

From Figure 4:8 it can be seen that the multiplication factor increases with the moderator-to-fuel ratio until the ratio reaches 0.21 after which it decreases steadily until a ratio of about 0.47. This behaviour of the fuel assembly aligns itself with a LWR, because LWRs are designed to operate with the moderator-to-fuel ratio such that the reactor is under moderated conditions (DOE, 1993). This is done so that should the system temperature increase there will be a decrease in N^M/M^U because of the expansion of water as its density becomes lower resulting in the addition of negative reactivity and a more self-regulating reactor.

Results in Figure 4:9 are from a test that was done to investigate the effect of enrichment on the multiplication factor k_∞ as discussed in section 3.4.2 III. The enrichment was varied from 0.65 to 3.25%wt UO_2.

From Figure 4:9 it is seen that when the enrichment of the fuel or the fraction of U-235 is varied in UO_2 from 0.65 to 3.25% wt UO_2, the multiplication factor k_∞ increases from 0.7 (subcritical) to about 1.00023 at 3.25% wt of UO_2. This is because at lower enrichment there is not sufficient fissile material to sustain the fission processes.

Two conclusions are realised form the above discussion. Firstly, since the effect of under and over-moderation on k_∞ is as expected from literature (DOE, 1993) the understanding of material specification in the MCNP input can be assumed to be correct. Secondly, from varying the enrichment as discussed above it can be concluded that the material specification was done correctly.

V. Test Gd_2O_3+ UO_2

The results below are for testing the effect of adding burnable absorber in the central region of the fuel assembly. If the model works properly there should be a decrease in the peak of the axial power profile and a corresponding flattening of the profile should be observed.

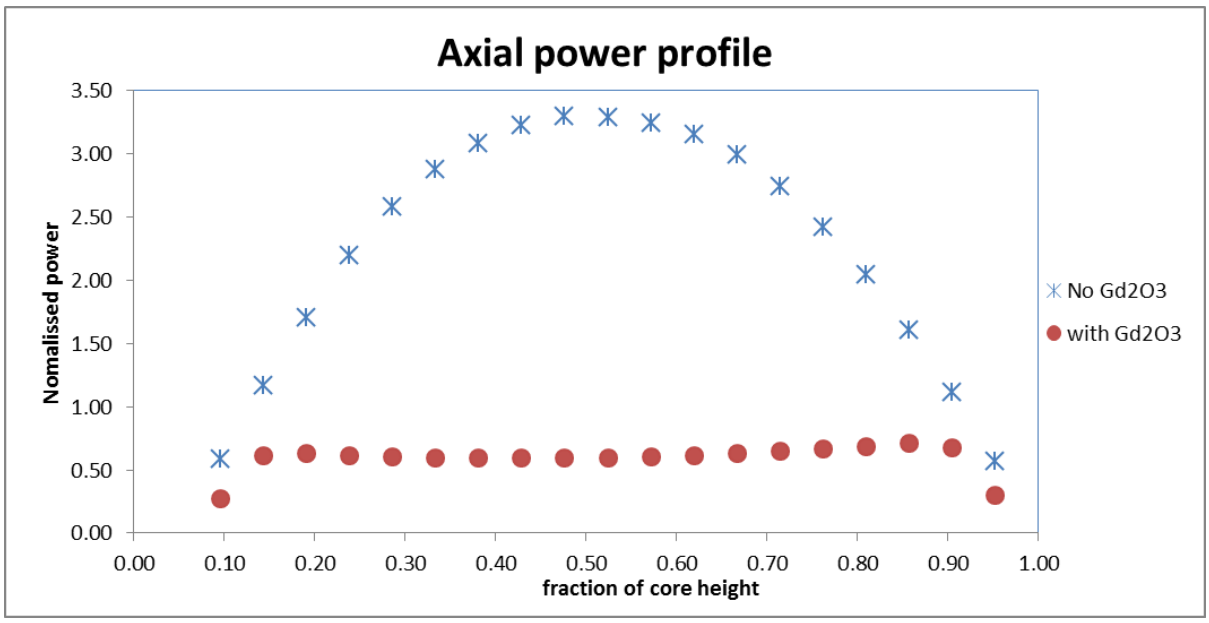

Figure 4:10 Axial power profile with incorporation of Gd_2O_3

From Figure 4:10 the effect of adding the burnable absorber Gd_2O_3 in the central region of the EPR fuel assembly is observed. It is seen that the profile is flattened by addition of 2 wt % Gd_2O_3 which reduces the reactivity and parasitically absorbing neutrons in the regions; as a result the power profile is flattened in the central region of the assembly as expected to occur with addition of the absorber.

4.3 Heterogeneous assembly type C2 manual input results

The results below were obtained using the methods discussed in chapter 3. The assembly type C2 modelled is in the centre of the EPR core, the fuel assembly boundaries are assumed to be periodic. See section 3.5 which discusses different boundary conditions and why they are where they are used in the study. These results were compared to those found in the US-EPR SAR as a form of verification of the results.

4.3.1 Convergence

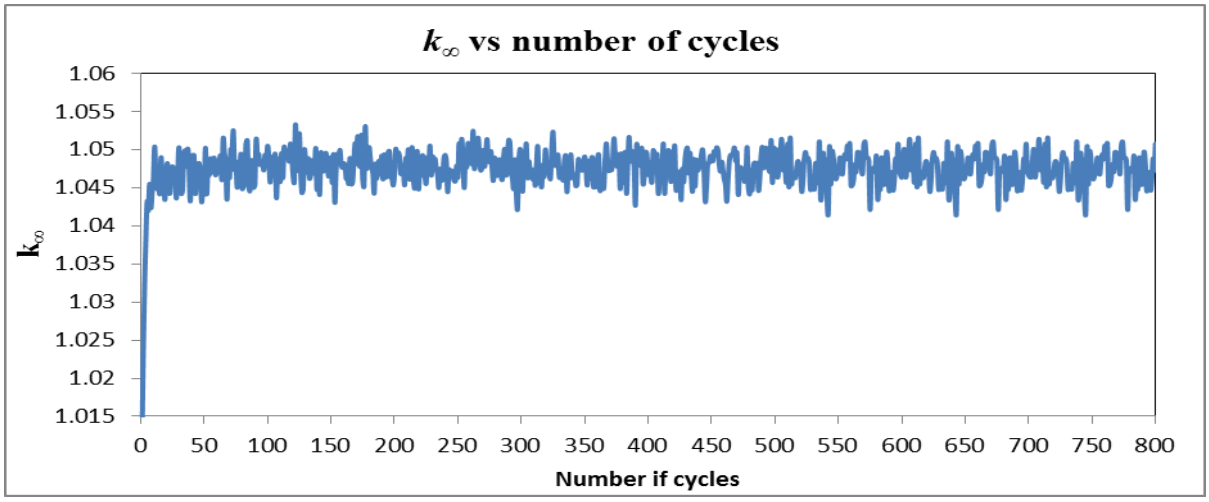

Figure 4:11 k_∞ vs number of cycles

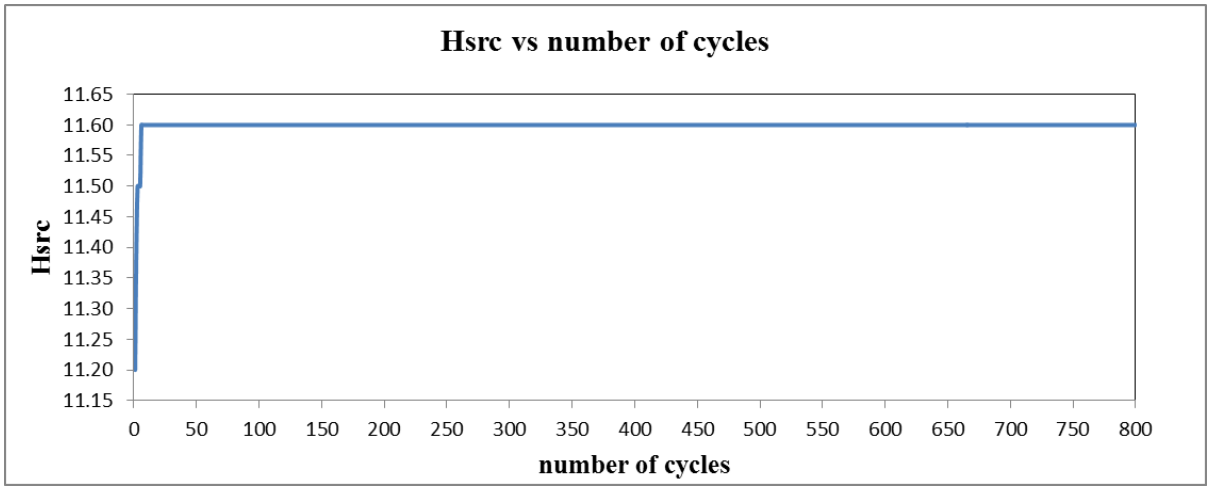

Figure 4:12 Fission source distribution (H_{src}) vs number of cycles

From Figure 4:11 it can be seen that value of k_∞ rises from 1.015 to a maximum of about 1.052 at cycle number 73. The amplitude of the distribution of k_∞ remains constant from cycle 100. It is not clear from which point k_∞ converges due to the high statistical noise in the k_∞ plot - a conservative estimate would be at 73.

However, from examination of the distribution of the Shannon entropy of fission source distribution in Figure 4:12 it can be seen clearly that the H_{src} rises from 11.20 to a maximum of 11.60 and remains constant at this value.

From examination of both the k_{∞} and H_{src} plots it can be concluded that at least 100 cycles need to be discarded before tally accumulation. For this study 200 cycles were discarded. It should be noted that choosing 200 cycles was a conservative choice because from literature it was recommended that 200 cycles be skipped (Waata, 2006). However about 100 cycles can also be skipped if required.

4.3.2 Axial power profile

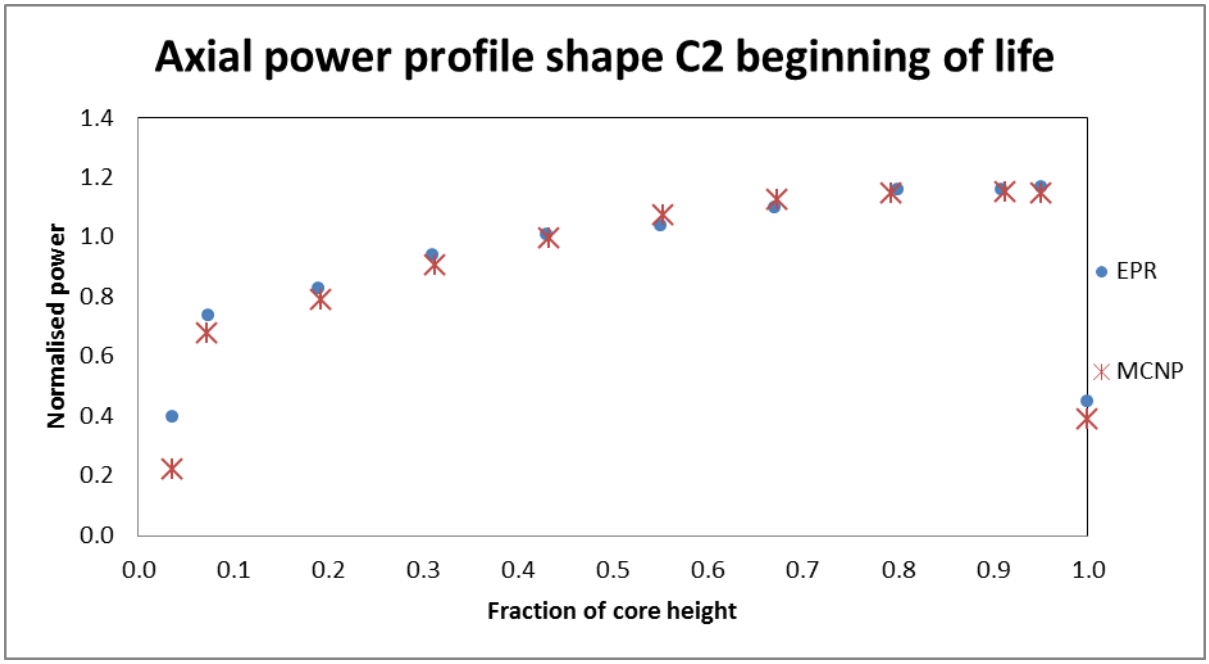

Figure 4:13 Axial fission power profile EPR vs MCNP

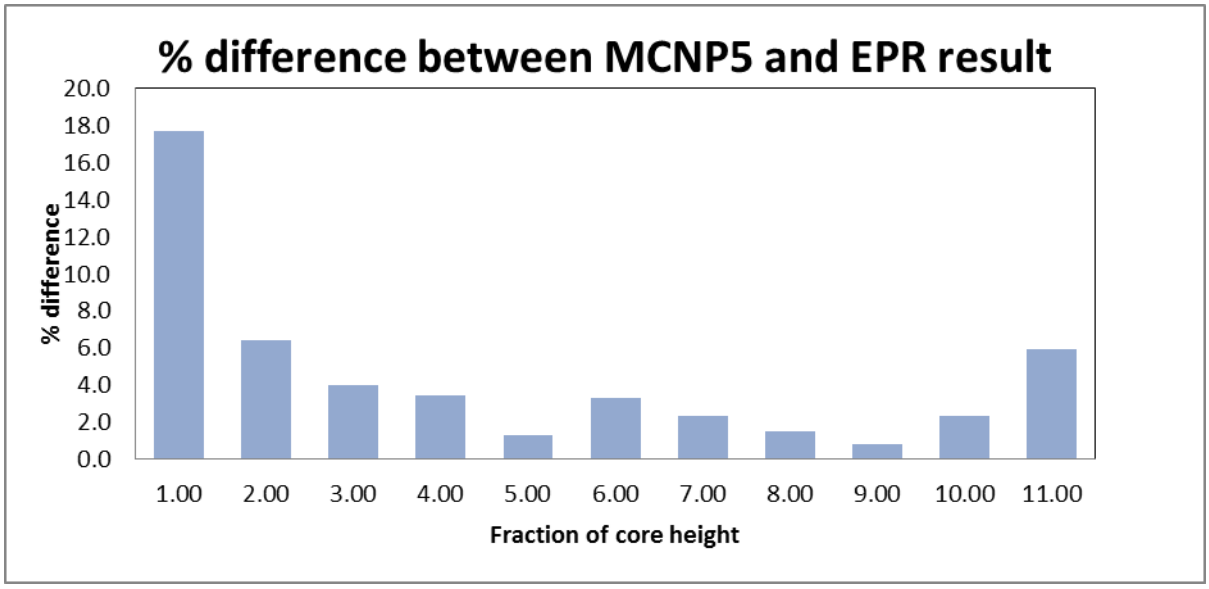

Figure 4:14 Percentage difference between MCNP and US-EPR SAR result

From the axial fission energy distribution in Figure 4:13 the energy deposited by fission neutrons in MCNP5 model can be seen to compare very well with that of the EPR from the US-EPR SAR. From Figure 4:14 it can be seen that 91% of the data points are in very good agreement with less than 6.4% difference .Only one point at the bottom of the core has a % difference higher than 10%, and the large difference may be because the calculation was done at an average temperature of 300^0C and this affects moderation because the water enters the core at a temperature of 295^0C and not 300^0C.

4.3.3 Axial neutron Flux profile

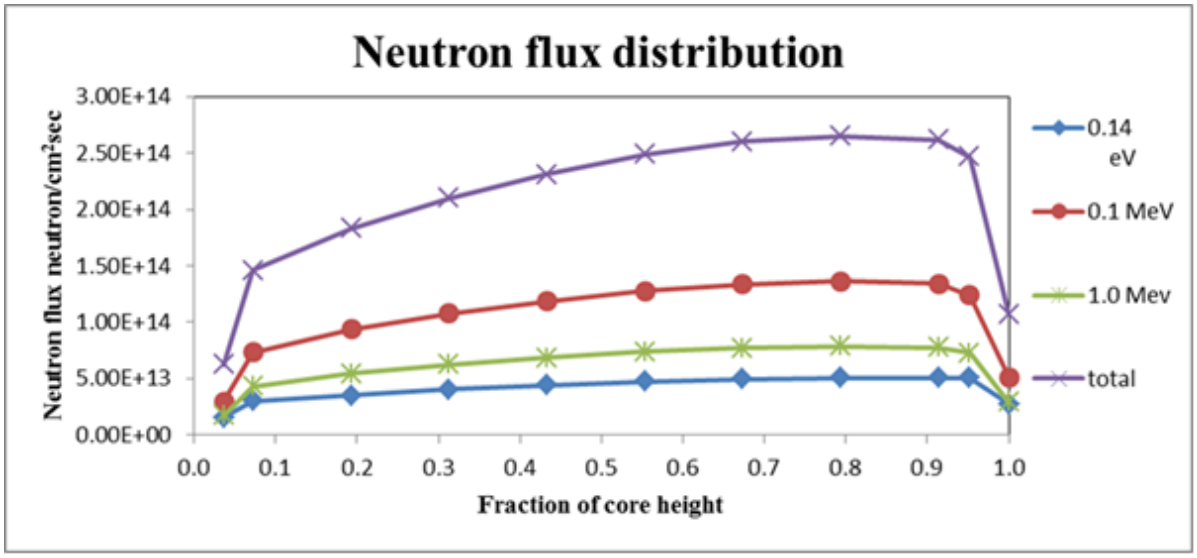

Figure 4:15 Three neutron energy group fluxes tallied from the continuous MCNP5 energy distribution and the total flux over all energies.

Location	Total[1]	E ≥ 1.0 MeV[1]	E ≥ 0.1 MeV[1]	E ≤ 0.414 eV[1]
Core center	$4.43x10^{14}$	$1.11x10^{14}$	$2.34x10^{14}$	$3.84x10^{13}$
Core outer radius at mid-height	$4.96x10^{13}$	$6.03x10^{12}$	$2.54x10^{13}$	$7.36x10^{11}$
Core top	$3.33x10^{13}$	$6.10x10^{12}$	$1.32x10^{13}$	$6.88x10^{12}$
Core bottom	$8.91x10^{13}$	$1.85x10^{13}$	$3.86x10^{13}$	$1.76x10^{13}$
Pressure vessel wetted ID azimuthal peak	$7.64x10^{10}$	$7.74x10^{9}$	$1.89x10^{10}$	$3.92x10^{10}$

Notes:

1. All values have units of n/cm^2-s.

Table 4:6 Typical neutron flux levels in the Reactor core and RPV from US-EPR SAR. Counting from fast to thermal, the SAR listed only the total for all four groups and then the results for Groups 1, 2 and 4 respectively.

From Figure 4:15 it can be seen the neutron flux distribution follows the same trend as the axial power distribution in Figure 4:13 It is also be seen that the axial neutron flux in the $E \geq 0.1$ MeV (i.e. 1 MeV $> E \geq 0.1$ MeV) energy group is larger than in the $E \geq 0.1$MeV group. This is probably because the ^1H in water is such an effective moderator that neutrons loose on average about 50% of their energy per elastic scattering collision with a ^1H nucleus. This means that neutrons with E < 2 MeV will on average need only one such collision to be scattered out of the $E \geq 1$ MeV group into the 1 MeV $> E \geq 0.1$ MeV group. However four such scattering collisions will on average be required to slow neutrons down from the top of the 1 MeV $> E \geq 0.1$ MeV group to the next group below 0.1 MeV. Neutrons will thus be scattered down quickly out of the $E \geq 0.1$MeV group into the 1 MeV $> E \geq 0.1$ MeV group, while they will then linger longer in this group, which explains the higher flux in this group. It can be seen that the flux in the thermal ($E \leq 0.414$ eV) group is much smaller than in the two higher energy groups. This is probably because the macroscopic absorption cross section (mainly for absorption for fission) is much higher in the thermal energy range than at higher energies. Therefore the thermal neutrons are absorbed much faster than fast neutrons. On the other hand the intermediate energy groups (e.g. 1 MeV $> E \geq 0.1$ MeV) gain neutrons from down scattering out of the higher energy group just above it, but simultaneously also loose neutrons through down scattering out of itself to the lower energy group just below 0.1 MeV. This is different from the thermal group that only gains neutrons from down scattering out of the group just above it, while it cannot loose neutrons to a lower group as there is no group below it. Therefore the most important factor that explains the lower flux in the thermal group is probably the following: the flux at any energy is defined as the number density of

the neutrons multiplied with the speed at that energy. As the neutrons slow down to lower energies, their speeds will by definition decrease dramatically. Therefore a given number density of thermal neutrons will produce a much lower neutron flux than the same neutron density at higher energies.

The above neutron energy ranges were chosen since they are the ranges presented in the EPR SAR. However it should be noted that the energy ranges used in the SAR is not self-evident from the column headings of Table 4:6 above: As opposed to MCNP5's continuous energy calculations used for this study, the SAR used a diffusion code which fundamentally works with energy groups, which together must cover the complete energy range under investigation. From the headings in Table 4:6 it is clear that there is a gap between the top of the thermal energy group at 0.414 MeV and the lower limit of the next reported group at 0.1 MeV. There thus clearly was an epithermal group with 0.414 eV > E ≥ 0.1 MeV. Counting from fast to thermal, as is the convention in reactor physics, the ranges of the four neutron energy groups used in the SAR can thus be seen in the following table.

Energy group number and name	**Energy (E) range**
1 (Fast)	E ≥ 1 MeV
2 (Intermediate)	1 MeV > E ≥ 0.1 MeV
3 (Epithermal)	0.1 MeV > E ≥ 0.414 eV
4 (Thermal)	E ≤ 0.414 eV

From the addition of the three group fluxes at each position in Table 4:6 above, it is clear that the listed flux totals are larger than the sum of the three listed group fluxes, i.e. the sum of Groups 1, 2 and 4. It is thus clear that Group 3 is included in each total and that the flux for Group 3 can thus be obtained by subtracting the listed fluxes for Groups 1, 2 and 4 from the Total flux at each position.

It can also be seen from comparison of the neutron flux from MCNP5 calculation in Figure 4:15 and the EPR neutron flux in Table 4:6 above that the results are of the same order of magnitude even though quantitatively the values are not the same. This is because the flux has not been scaled to the required power input. This was not done, because it was decided that the coupling with thermal hydraulic calculation be done before scaling the power of the reactor. This coupling will be done in a later study.

4.4 Verification of fuel assembly FORTRAN script generated input (C2)

The FORTRAN program that generates the MCNP input was developed by the NWU School of Mechanical and Nuclear Engineering. The program was developed to generate an MCNP EPR model of the reactor core and any of the seven fuel assembly models (A1, A2, B1, B2, C1, C2 and C3). This was done because the MCNP input for the fuel assembly model has about 1149 lines and the Full MCNP model has about 248353. An attempt to manually write these inputs will introduce human error and it would take a very long time.

This test was done to verify whether the FORTRAN program was generating the correct input representing the EPR 3D MCNP5 representative input. This was done by comparing results obtained from testing the FORTRAN program generated input versus the manually written MCNP5 EPR input file. The results presented passed k_{∞} and H_{src} convergence tests and the tallies have been accumulated over 800 cycles to minimise statistical errors. Note that this is a fuel assembly level calculation.

4.4.1 Axial power profile

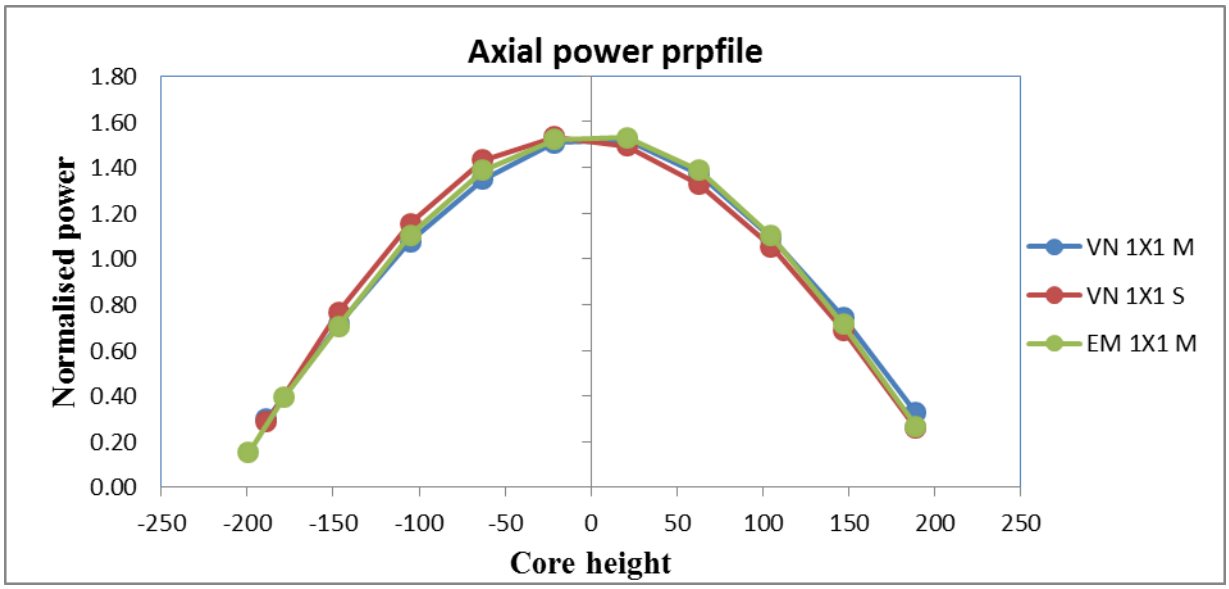

Figure 4:16 Axial power for verification of FOTRAN program generated EPR assembly input

Note that all the fuel assemblies have fuel with an enrichment of 2 %wt and no burnable absorber. It should also be noted that the reason why Figure 4:16 Axial power for verification of FOTRAN program generated EPR assembly input is different from Figure 4:13 is because for Figure 4:16 the fuel assemblies are filled with fuel with enrichment of 2 %wt and no burnable absorber, hence there is no flattening of the curve.

From figure 4:16 above the blue plot VN 1x1 M represents results from an independently manually rewritten MCNP input file for fuel assembly type C2. The red plot represents results of a FORTRAN program generated input file of fuel assembly type C2 from the program developed by the department and the green plot represents results from a manually written MCNP input of fuel assembly type C2 developed as part of this work to test the fuel assembly geometry similar to the way it was done in section 4.2 III.

The three plots are seen to be in good agreement and as expected are producing a cosine shape. The reason the green plot seems to not be the same as red and purple at axial height-199.5 and -178.5 is because the power is taken at positions different to that on the blue and red plot; however it can be realised that the average of the power at this point will give the same result as both the blue and red plot. The above shows that the methodology used in developing the EPR input producing program is correct.

4.5 Full core results

The FORTRAN program generating the MCNP5 representation of the EPR reactor core includes all the details such as fuel assemblies, heavy reflector, core barrel, moderator and the reactor pressure vessel. See section 3.4.5 for a detailed discussion of the full core model and geometry. A full core model was developed rather than a 1/8 core model, because modelling a 1/8 of the EPR core implies that reflecting boundaries will have to be used. Reflecting boundaries would make the geometry setup simpler; however, using them could make it difficult to get the correct answers. The MCNP manual cautions against the use of reflecting surfaces (X-5 Monte Carlo team, 2003).

Note that the results presented below are for testing of the FORTRAN generated MCNP5 representative of the EPR reactor core model as seen in Figure 3:8 and Figure 3:9 .The main objective of the section was to test whether the FORTRAN input-generated model is working properly. It is important to also note the results calculations below are for calculations done with all control rods inserted fully in the core.

I. Power profiles

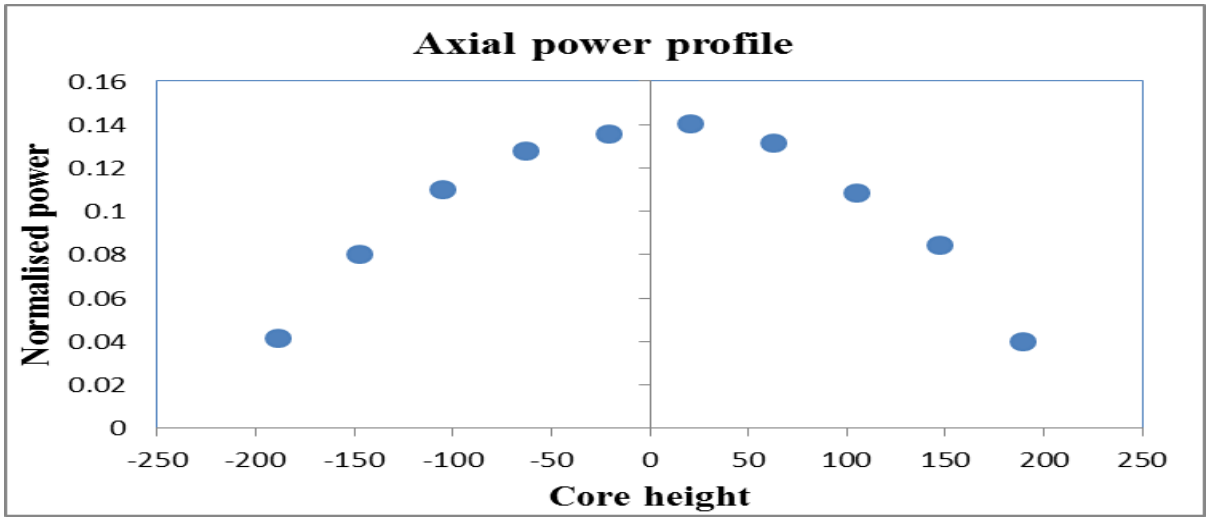

Figure 4:17 Axial power profile full core all RCCA in at BOL

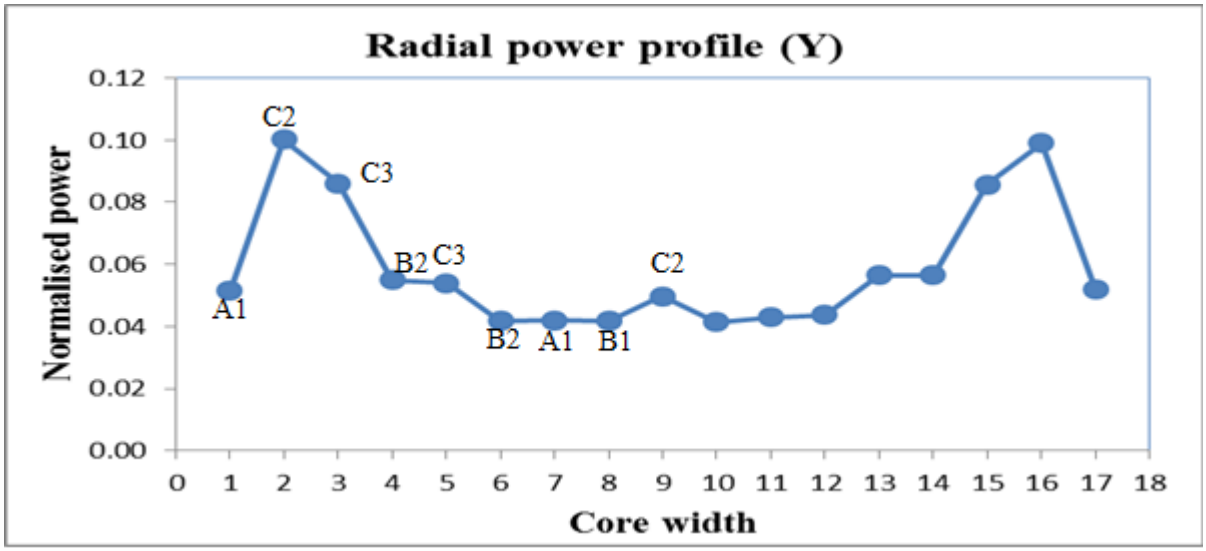

Figure 4:18 Radial power profile full core all RCCA in at BOL

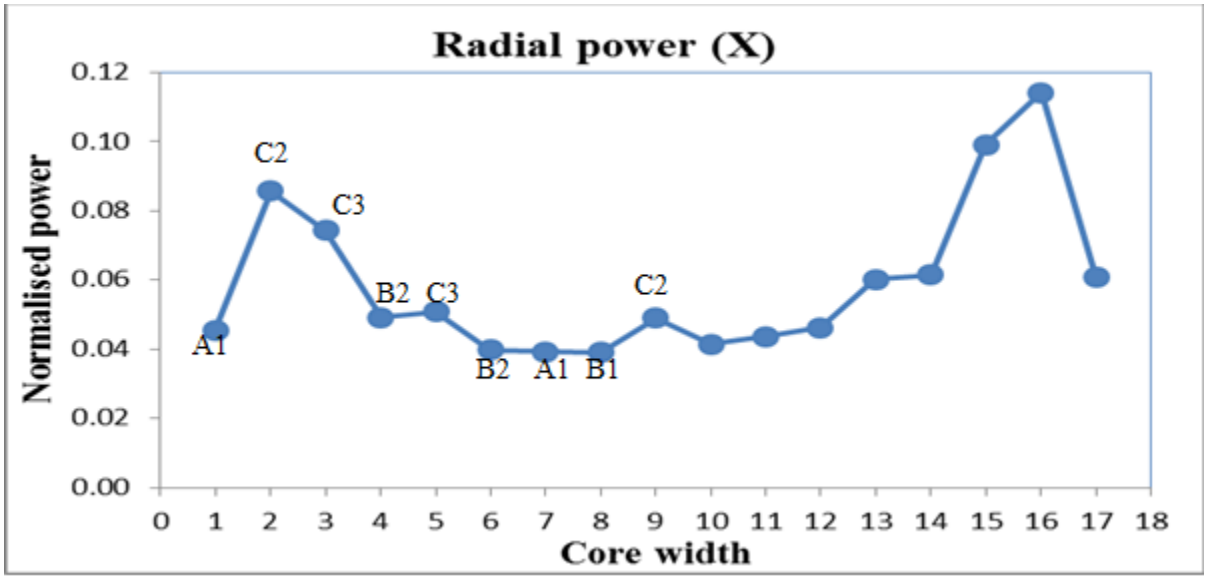

Figure 4:19 Radial power profile full core all RCCA in at BOL

It should be noted that the power profile above is axially averaged. Furthermore, the plots above are labelled only on the left due to the symmetry of the core.

From Figure 4:17 it can be seen that the plot gives a shape similar to a PWR power profile. The shape is not flat as expected because flattening of the shape is done by the burnable absorber Gd_2O_3 in the central region of the core. In this case all control rods are fully inserted into the core and since the control rods are boron rods and boron is a better absorber than gadolinium the neutron absorption is dominated by boron in all regions of core resulting in the above shape. If one is to flatten the power profile boron concentration will have to be adjusted such that gadolinium will dominate the neutron absorption.

However, the profile above is not symmetrical as it might be expected. This might be because of mixing of materials in the materials allocation subroutine of the full core FORTRAN program and it is recommended that the program should be rechecked and corrected in this regard. Another reason might be because the full core tally convergence was not fully reached due to the amount of time required to for all the statistical tests to be passed since each calculation takes ± 3 days.

Note that the analysis of the full core results in Figure 4:18 and Figure 4:19 was done with reference to Figure 2:3 EPR core beginning of life layout which is the EPR core layout at BOL.

It should be further noted that there are many parameters that are used to determine the reactor power profile (and flux). This is most clearly seen when the deterministic transport equation is used to solve the problem (Stacey, 2007).

Important parameters to consider are isotopic concentrations and the geometry of the reactor and fuel assemblies.

In the following paragraph, an attempt has been made to correlate the isotopic content of each fuel assembly as a function of the power profile. The location of the core boundary is also considered.

From Figure 4:18 it can be seen that the power shape is nearly symmetrical and follows a certain pattern. Because the fuel assembly with the lowest enrichment (A1) is at the edges of the core as seen in Figure 2:3 position 1 and 17 have the lowest power output but not zero because the heavy reflector reflects the neutrons back into the core raising the flux and the power at the edges. Positions 2 and 16 show the highest power because the fuel assembly type C2 has the highest enrichment and lower amount of burnable absorber. Assembly C3 at positions 15 and 3 has a lower power than 2 and 16. Positions 4 and 14 have lower power than positions 3 and 15 because its fuel assembly type B2 which has lower enrichment than its neighbours 3 and 15 (C3). Positions 5 and 13 have lower power output than its neighbours even though they represent fuel assembly type C3, this is because the neighbours represent assembly type B2 which has lower enrichment which implies there is a smaller influx of neutrons into positions 5 and 13 causing fission than in 4 and 14. Positions 6 and 12 represent fuel assembly type B2 and have lower power output than its neighbours 5 and 13, after this

point the power profile stabilises until positions 8 and 10 and rises at position 9 because it represents assembly type C2 which has a higher enrichment than positions 8 and10.

From Figure 4:19 Radial power profile full core all RCCA in at BOL the power profile is nearly symmetrical and follows a similar behaviour as the profile in Figure 4:18 Radial power profile full core all RCCA in at BOL. The reason for the shape to not be perfectly symmetrical might be because of some mixing up for material allocation in the program while the full core MCNP is being generated and it is recommended that the program should be checked.

II. Reactivity worth/Control rods worth

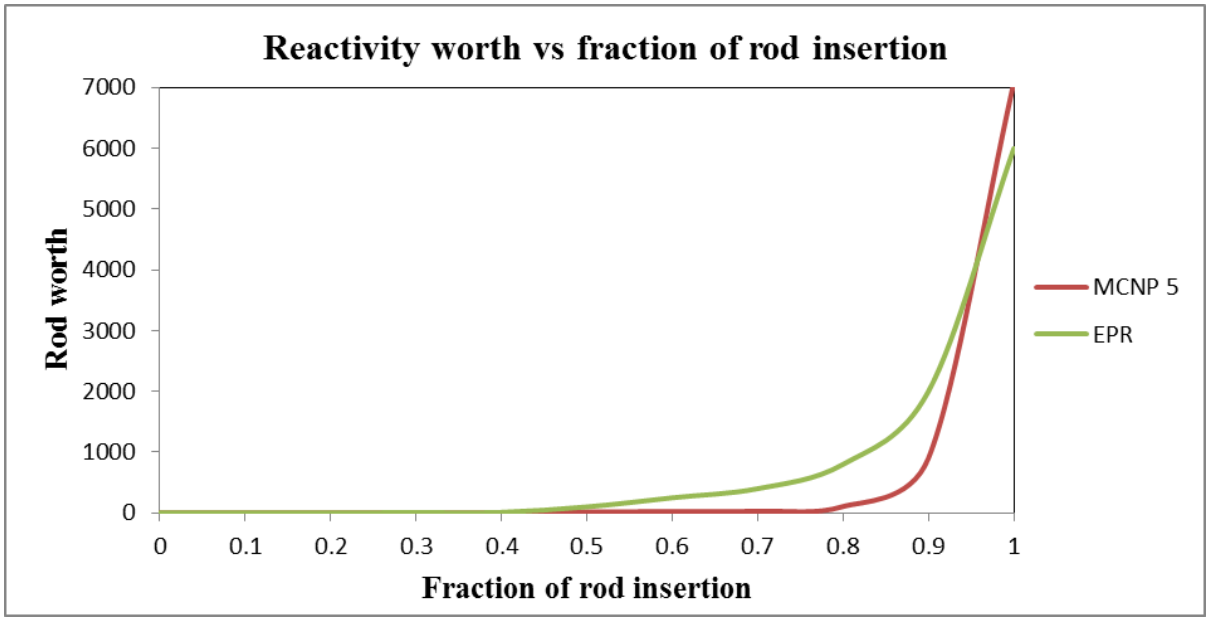

Figure 4:20 Reactivity worth vs fraction of rod insertion

The reactivity worth was investigated using a method discussed in section 3.4.5-II. The multiplication factor was calculated at each of the 10 control rod positions and then the rod worth was calculated externally at each position and plotted against axial height

From the figure above it can be seen that the MCNP5 calculation agrees with the EPR results from insertion point 0 to 0.46 and after that there EPR rod worth is higher than the than the MCNP5 worth and intersects at about insertion 0.95. The difference might be because for this study the initial value of k_1 is not equal to 1.00 as in the case in the EPR results; this implies that the MCNP5 calculation will on average have lower rod worth that the EPR result. Another reason might be because only the RCCA is absorbing the neutrons and there is no boron in the system and this makes it difficult to ramp down the reactor.

4.5 MCNP calculation economy

For this section the time taken to run each MCNP simulation was analysed to in order to determine how economical it is to use MCNP for core analysis.

The calculations were done on a windows-based Acer computer with the following properties

Computer: Acer OS : Windows 7

Processor: i3 2.4 GHz RAM: 4.00 GB

MCNP calculation	**Time (min)**
Infinite homogeneous fuel assembly complete convergence	1672.42
Heterogeneous assembly C2 manual input	1907.16
Full core model	3017.48

Table 4-1 Economical study of MCNP core calculations

From Table 4-1 it can be seen that it took 1672.42 minutes (1.2 days) for the infinite homogeneous assembly calculation to run to complete convergence. The heterogeneous assembly manual input calculation took 1907.16 minutes (1.3 days) and the full core calculation took 3017.48 minutes (2.1 days). From literature it is evident that the calculation time can be significantly reduced by using parallel computers or super computers. D Kotlyar did a coupled neutronic thermo-hydraulic analysis of a 1/8 PWR on 2.9 GHz Xeon 550 series processors and a 24GB of RAM in parallel mode and the execution time for each MCNP run was 4 hours. Bernnat also did a study on "*Application of coupled Monte Carlo and burn-up method for detailed neutronic analysis for the FRJ-2 research reactor on a high performance computer*" and found that it took an MCNP calculation with 10^6 neutrons/ cycle about 40 to 60 minutes for each run (W. Bernnat, etal, 2005).

From the above discussion it can be concluded that if the neutronic calculations are done on a super-computer or in parallel mode the CPU time can be reduced significantly. Because it would take three days to run a calculation before one can analyse the output and do necessary corrections.

5. Conclusions and recommendations

5.1 Introduction

In this chapter conclusions and recommendations derived from evidence and the results in above chapters are presented to show how the objectives of the study were met.

5.2 Conclusion

Development of a MCNP5 representative model of the US EPR fresh fuel assembly model and the full core model was done. Various aspects of the model have been investigated as part of verification and testing of the model.

The first step was to develop a fresh fuel assembly model and this was done as explained in section 3.4.3 and the results are in very good agreement with the EPR results implying that the fresh fuel assembly model had been successfully developed.

The second step was to test the input program used to create the input for both fresh fuel assembly calculation and fresh full core calculations. This was done and it was found that the program might be mixing up material contents of both the core and assembly model. It is recommended that the program should be re-checked.

The third step was to determine the path to convergence of the multiplication factor, Shannon entropy and the tally convergence. It was found that at least 200 cycles have to be set as inactive with 100 000n/s and up to 3000 cycles have to be done for complete convergence of the multiplication factor, Shannon entropy and tally convergence.

The fourth step was to determine the control rods' worth in section 4.4-II and it was found that the shape followed the same trend as the control rod worth shape of the EPR and it was also found that MCNP and EPR results agreed from a point of total insertion of the rods until the control rods are withdrawn halfway from the bottom. After this point the rods' worth varies. This may because burn-up was not incorporated into the calculation and the control rods used in this study are not the same as those in the US EPR SAR.

An analysis was also done to see how economical it is to use MCNP for full core calculation and it is found that it is only economical if the full core calculations are done on a parallel computer or a super-computer so that more cycles can be done at a shorter time.

5.2 Recommendations

The first recommendation is that the MCNP full core calculations be done in parallel mode on a super computer or a high performance computer in order to reduce the CPU time significantly. This is recommended because if thermal hydraulic, neutronic and burn-up calculations are incorporated the calculation time will be increases significantly.

The second recommendation is that the code package EPR_input5 that generates the full core input file be re-done and tested.

The third recommendation is that a thermal-hydraulic model of the EPR be developed and coupled to the neutronic model to form a coupled neutronic and thermal-hydraulic analysis of the EPR to get more accurate results.

The forth recommendation is that burn-up should be investigated, which may have a much greater influence on the results than the small uncertainties in temperatures that occur throughout the fuel core.

The fifth study recommendation is that the heavy reflector be studied in more detail because of its importance to flattening on the flux.

Bibliography

AREVA, 2012. *US EPR Brochure,* Paris-La Defense cedex France: FRamatome ANP.

AREVA, 2012. *US EPR Final Safety Analysis Report,* Washington D.C: AREVA.

Bell, G. I. & Glasstone, S., 1958. *Nuclear Reactor Theory.* 3rd ed. Malaba Florida: Robert E. Krieger Publishing CO., INC.

Blomquist, R. N. et al., 2006. *Source convergence in criticality safety analyses,* Paris, France: Nuclear Energy Agency.

Brown , B. F., 2005. *Fundamentals of Monte Carlo particle transport LA-UR-05-4983.* Los Alamos, Los Alamos National Laboratory.

Brown, F. B., 2006. *On the use of Shannon Entropy of the Fission Distribution for Assessing Convergence of Monte Carlo Criticality Calculations,* Los Alamos: Los Alamos National Laboratory.

Brown, F., Nease, B. & Cheatham, J., 2007. *Convergence Testing for MCNP5 Monte Carlo Eigenvalue Calculation LA-UR-07-1123.* Monterey, Califonia, Los Alamos National Laboratory (Joint International Topical Meeting on mathematical & computation and supercomputing in Nuclear Applications).

Crissue, 2004. *Neutronic/Thermal-Hydraulic coupling in LWR technology,* Grands_Augustins Paris: European Nuclear Energy Agency.

DOE, 1999. *NUCLEAR PHYSICS AND REACTOR THEORY Handbook,* Washington: US-DOE.

DOE, 2011. *INTEGRATED RESOURCE PLAN FOR 2010-2030.* Pretoria South Africa, Department of Energy.

DOE, 2011. *INTEGRATED RESOURCE PLAN FOR 2010-2030.* Pretoria South Africa, Department of Energy.

Duderstadt, J. J. & Hamilton, L. J., 1974. *Nuclear Reactor Analysis.* 1st ed. Michigian: John Wiley & Sons.

Framatome ANP, Inc, 2005. *EPR Design description,* Lynchburg, Virginia: Framatome ANP, Inc.

Glasstone, S. & Sesonske, 1994. *Nuclear Reactor Engineering.* 4th ed. New York: Chapman & Hall.

IAEA, 2013. *Nuclear power today and tomorrow,* Vienna, Austria: IAEA Bulletin.

Ivanov, A., Sanchesz, V. & Imke, U., 2011. *Development of a coupling scheme between MCNP5 and SUBCHANFLOW for the pin and fuel assembly-wise simulation of LWR and innovative reactors.* Brazil, American Nuclear Society (ANS).

Knief, R. A., 2008. *Nuclear Engineering theory and technology of commercial Nuclear Power.* 2nd ed. Washington DC: Taylor & Francis.

Kotlyar, D., shaposhinik, Y., Frindman, E. & Shwageraus, E., 2011. Coupled neutronic thermo-hydraulic analysis of a full PWR core with Monte-Carlo based BGCore system. *ELSEVIER,* 18 july.pp. 3778 - 3786.

Lamash, J. R. & Baratta, A. J., 2012. *Introduction to Nuclear Engineering.* Firth ed. New Jersey: Prentice Hall.

Los Alamos National laboratory ,US department of Energy, 2003. MCNP A General Monte Crlo N-Particle Transport Code, Version5. *Los Alamos National Laboratory,* pp. 1-19.

Los Alamos National Security for ,US department of Energy, 2003. MCNP A General Monte Carlo N-Particle Transport Code, Version 5. *Los Alamos National Laboratory,* pp. 1-19.

Mattes, M. & Keinert, J., 2005. *Thermal Neutron Scattering Data for the Moderator Materials H20, D2O and Zrx in the ENDF-6 format and ACE library for MCNP(X) codes,* Vienna: INTERNATIONAL ATOMIC ENERGY AGENCY.

MCNP5, X.-5. M. C., 2003. MCNP- A general Monte Carlo N-Particle Transport code. *Los Alamos National Laboratorty,* 24 April, Volume I, pp. 1-19.

Miller, W. F. & Lewis, E. E., 1993. *Computational methods of Neutron Transport.* 1st ed. Illinois USA: American Nuclear Society, INC..

Mohammad, M. A., 2011. *Transmutation Rates in the Annulus Gas of Pressure Tube Water,* Ontario, Canada: Faculty of Energy Systems and Nuclear Science, University of Ontario Institute of Technology.

Pautz, A., Hasse, U. & Zwermann, W., 2005. Fuel assembly calculations using the method of discrete ordinates. *Nuclear Science and Engineering,* 149(2), pp. 197-210.

Reisis, T., 2011. *Coupled Neutronics – Thermal hydraulics analysis of SCWRs,* Budapest, Hungary: Budapest University of Technology and Economics Institute of Nuclear Techniques.

Roger, N. B. et al., 2006. *Source Convergence in Criticality Safety Analyses,* Paris: Nuclear Energy Agency (NEA); Oganisation For Economic Co-operation and Development(OECD).

Sanchez, V. & Al-Hamry, A., 2009. *Development of a coupling scheme between MCNP and COBRA-TF for the prediction of the pin power of a PWR fuel assembly.* New York, American Nuclear Society.

Sanchez, V. H. & Hering , W., 2002. *Analysis of the OECD/NEA PWR main steam line break (MSLB) benchmark exercise 3 withthe coupled code sysem RELAP5/PANBOX,* Karsruhe: Forschungszentrum Karlsruhe GmbH.

Sanchez, V. H., Hering, W. & Knoll, A., 2002. *Analysis of the OECD/NEA PWR Main steam line break (MSLB) benchmark exercise 3 with the coupled code system Relap5/PANBOX,* s.l.: Framatome ANP Erlangen.

Seker, V., Justin, W., Downar, T. & Downar, T. J., 2007. *Reactor simulation with Coupled Monte Carlo and Computational Fluid Dynamics.* Califonia, American Nuclear Society.

Shan, J., Chen, W. & Leung, L., n.d. *Coupled neutronic/thermal-hydraulics analysis of CANDU-SCWE fuel channel.* s.l., s.n.

Sheffield, S., 2011. *Law of large Numbers lecture notes,* Massachusetts: Massachusetts Institute of Technology.

Stacey, W. M., 2007. *Nuclear Reactor Physics.* 2nd ed. Atlanta USA: Wiley-VCH.

U Grundmann, U. R. S. M., 2004. *DYN3D- Three- dimensional core model for steady-state and transient analysis of thermal reactors,* Dresden: Forschungszentrum Ressendorf.

V.H Sanchez, W. H. A. K., 2002. *Analysis of the OECD/NEA PWR Main steam line break (MSLB) benchmark exercise 3 with the coupled code system Relap5/PANBOX,* s.l.: Framatome ANP Erlangen.

Waata, C. L., 2006. *Coupled Neutronics / Thermal-Hydraulics analysis of a High-Perfomance Light-Water Reactor Fuel Assembly,* Germany: In: FZKA 7233, Forschungszentrum Karlsruhe.

X-5 Monte Carlo team, 2003. MCNP A General Monte Carlo N-Particle Transport Code, Version5 Overview and theory. *Los Alamos National Laboratory,* Volume 1, pp. 1-19.

X-5 Monte Carlo team, 2003. MCNP A General Monte Crlo N-Particle Transport Code, Version5 user guide. *Los Alamos National Laboratory,* Volume II chapter 3, pp. 1-19.

Zibi, Z., 2010. *Benchmarking of MCNP modelling of HTR cores against Experimental data from the ASTRA criticality facility,* Potchefstroom: School of Mechanical and Nuclear engineering North West University.

6.1 Appendix A

In this appendix material specifications used in the MCNP models of this study are presented.

Below is a copy of the material card in each of the models used in the study. The materials are specified as MCNP; hence the data was not tabulated.

6.2 Homogeneous fuel assembly

```
c Heavy reflector  heavy reflector Homo mixture of stainless steel and water (304L or 18 Cr-8Ni )
m34  26054.71c  0.0387736
     26056.71c  0.6086627
     26057.71c  0.0140567
     26058.71c  0.0018707
      6000.71c  0.0013006
     24050.71c  0.0078322
     24052.71c  0.1510363
     24053.71c  0.0171263
     24054.71c  0.0042631
     28058.71c  0.0483165
     28060.71c  0.0186114
     28061.71c  0.0008090
     28062.71c  0.0025795
     28064.71c  0.0006569
     25055.71c  0.0189561
     15031.71c  0.0007565
     16032.71c  0.0004625
     16033.71c  0.0000037
     16034.71c  0.0000209
     16036.71c  0.0000001
     14028.71c  0.0128243
     14029.71c  0.0006512
     14030.71c  0.0004293
      1001.71c  0.0333334
      8016.71c  0.0166667
c  UO2+H2O    3.25 UO2 in UO2+H2O
m35  92235.71c  0.0076772
         92238.71c  0.2256562
          8016.71c  0.4666697
          1001.71c  0.2000001
         8016.71c  0.0999999
```

6.3 Heterogeneous fuel assembly manual input (C2)

```
c  u235 enrichment 3.25 Gd2O3 %: 0
m2   92235.71c   0.010967
     92238.71c   0.322367
      8016.71c   0.666666
c u235 enrichment 2.00 Gd2O3 %: 0
m3   92235.71c   0.006750
     92238.71c   0.326584
      8016.71c   0.666666
c m20 u235 enrichment 3.08 Gd2O3 %: 2
m7   92235.71c     0.010137
     92238.71c     0.314962
     64152.71c     0.000020
     64154.71c     0.000215
     64155.71c     0.001462
     64156.71c     0.002023
     64157.71c     0.001546
     64158.71c     0.002455
     64160.71c     0.002160
      8016.71c     0.665019
c u235 enrichment 2.76 Gd2O3 %: 6
m11   92235.71c    0.008631
      92238.71c    0.300233
      64152.71c    0.000059
      64154.71c    0.000640
      64155.71c    0.004346
      64156.71c    0.006011
      64157.71c    0.004595
      64158.71c    0.007294
      64160.71c    0.006419
       8016.71c    0.661772
c Borated  Water   [0-1500 ppm]
m18     1001.71c   0.666067
        8016.71c   0.333033
        5010.71c   0.000173
        5011.71c   0.000727
c Cladding   MT[5] Zirconium
m27  40090.71c   0.527641
     40091.71c   0.113801
     40092.71c   0.172057
     40094.71c   0.170655
     50112.71c   0.000122
     50114.71c   0.000082
     50115.71c   0.000042
     50116.71c   0.001767
     50117.71c   0.000925
     50118.71c   0.002894
     50119.71c   0.001018
     50120.71c   0.003828
     26054.71c   0.000204
     26056.71c   0.003080
```

```
   26057.71c   0.000070
   26058.71c   0.000009
   24050.71c   0.000082
   24052.71c   0.001514
   24053.71c   0.000168
   24054.71c   0.000041
c Helium  Gap
m32  2004.71c    1.000000
```

6.4 Full core EPR model

```
c  Water
m1    1001.71c  0.666359  8016.71c  0.333180
       5010.71c  0.000092  5011.71c  0.000369
mt1
c  Cladding    MT[5] Zirconium
m2   40090.71c   0.527641
      40092.71c   0.172057
      40094.71c   0.170655
      50112.71c   0.000122
      40091.71c   0.113801
      50114.71c   0.000082
     50115.71c   0.000042
     50116.71c   0.001767
     50117.71c   0.000925
     50118.71c   0.002894
     50119.71c   0.001018
     50120.71c   0.003828
     26054.71c   0.000204
     26056.71c   0.003080
     26057.71c   0.000070
     26058.71c   0.000009
     24050.71c   0.000082
     24052.71c   0.001514
     24053.71c   0.000168
     24054.71c   0.000041
c Helium     Gap
m3   2004.71c    1.000000
c Boron  density = 2.52 g/cm3
m4    5010.71c    0.159200   5011.71c   0.640800
       6000.71c    0.200000
c core barrel Low carbon chromium stainless steel 304l (18Cr-8Ni) Z2 CN 19-10 ARE
m5  26054.71c   0.041584  26056.71c   0.652784
   26057.71c   0.015076  26058.71c   0.002006
    6000.71c   0.000300
   24050.71c   0.007821  24052.71c   0.150820
   24053.71c   0.017102  24054.71c   0.004257
   28058.71c   0.054462  28060.71c   0.020978
   28061.71c   0.000912  28062.71c   0.002908
   28064.71c   0.000740
   25055.71c   0.020000
   15031.71c   0.000450
```

```
    16032.71c   0.000285  16033.71c   0.000002
    16034.71c   0.000013
    14028.71c   0.006917  14029.71c   0.000351
    14030.71c   0.000232

c heavy reflector Homo mixture of stainless steel and water (304L or 18 Cr-8Ni )
m6 26054.71c   0.038774
     26056.71c   0.608663
     26057.71c   0.014057
     26058.71c   0.001871
     6000.71c    0.001301
     24050.71c   0.007832
     24052.71c   0.151036
     24053.71c   0.017126
     24054.71c   0.004263
     28058.71c   0.048316
     28060.71c   0.018611
     28061.71c   0.000809
     28062.71c   0.002580
     28064.71c   0.000657
     25055.71c   0.018956
     15031.71c   0.000756
     16032.71c   0.000462
     16033.71c   0.000004
     16034.71c   0.000021
     16036.71c   0.0000001
     14028.71c   0.012824
     14029.71c   0.000651
     14030.71c   0.000429
     1001.71c    0.033333
     8016.71c    0.016667

c rpv not correct
m7  26054.71c   0.041584  26056.71c   0.652784
      26057.71c   0.015076  26058.71c   0.002006
       6000.71c   0.000300
      24050.71c   0.007821  24052.71c   0.150820
      24053.71c   0.017102  24054.71c   0.004257
      28058.71c   0.054462  28060.71c   0.020978
      28061.71c   0.000912  28062.71c   0.002908
      28064.71c   0.000740
      25055.71c   0.020000
      15031.71c   0.000450
      16032.71c   0.000285  16033.71c   0.000002
     16034.71c   0.000013
     14028.71c   0.006917  14029.71c   0.000351
     14030.71c   0.000232
```

```
c m11 u235 enrichment 2.00 Gd2O3 %: 0
m11    92235.71c  0.006750  92238.71c  0.326584
          8016.71c  0.666666
c
c m12 u235 enrichment 2.25 Gd2O3 %: 0
m12    92235.71c  0.008437  92238.71c  0.324897
          8016.71c  0.666666
c
c m13 u235 enrichment 2.70 Gd2O3 %: 0
m13    92235.71c  0.009112  92238.71c  0.324222
          8016.71c  0.666666
c
c m14 u235 enrichment 3.25 Gd2O3 %: 0
m14    92235.71c  0.010967  92238.71c  0.322367
          8016.71c  0.666666
c
c m15 u235 enrichment 2.13 Gd2O3 %: 4
m15    92235.71c  0.006835  92238.71c  0.310106
      8016.71c  0.663387
     64152.71c  0.000039  64154.71c  0.000429
     64155.71c  0.002911  64156.71c  0.004027
     64157.71c  0.003079  64158.71c  0.004886
     64160.71c  0.004300
c
c m16 u235 enrichment 1.89 Gd2O3 %: 8
m16    92235.71c  0.005758  92238.71c  0.295101
      8016.71c  0.660171
     64152.71c  0.000078  64154.71c  0.000850
     64155.71c  0.005768  64156.71c  0.007977
     64157.71c  0.006099  64158.71c  0.009680
     64160.71c  0.008519
c
c m17 u235 enrichment 2.56 Gd2O3 %: 4
m17    92235.71c  0.008215  92238.71c  0.308728
      8016.71c  0.663387
     64152.71c  0.000039  64154.71c  0.000429
     64155.71c  0.002911  64156.71c  0.004026
     64157.71c  0.003078  64158.71c  0.004886
     64160.71c  0.004300
c
c m18 u235 enrichment 2.56 Gd2O3 %: 2
m18    92235.71c  0.008426  92238.71c  0.316673
      8016.71c  0.665019
     64152.71c  0.000020  64154.71c  0.000215
     64155.71c  0.001463  64156.71c  0.002023
     64157.71c  0.001547  64158.71c  0.002455
     64160.71c  0.002160
```

```
c
c m19 u235 enrichment 2.76 Gd2O3 %: 6
m19    92235.71c  0.008631  92238.71c  0.300233
         8016.71c  0.661772
      64152.71c  0.000059  64154.71c  0.000640
      64155.71c  0.004346  64156.71c  0.006011
      64157.71c  0.004595  64158.71c  0.007294
      64160.71c  0.006419
c
c m20 u235 enrichment 3.08 Gd2O3 %: 2
m20    92235.71c  0.010137  92238.71c  0.314962
       8016.71c  0.665019
      64152.71c  0.000020  64154.71c  0.000215
      64155.71c  0.001462  64156.71c  0.002023
      64157.71c  0.001546  64158.71c  0.002455
      64160.71c  0.002160
c
c m21 u235 enrichment 2.27 Gd2O3 %: 8
m21    92235.71c  0.006915 92238.71c  0.293945
       8016.71c  0.660171
      64152.71c  0.000078 64154.71c  0.000850
      64155.71c  0.005767 64156.71c  0.007977
      64157.71c  0.006099 64158.71c  0.009680
      64160.71c  0.008519
```

7.1 Appendix B

In this section fuel assembly designs are presented. The designs are for the different fuel assembly types as on the US-EPR SAR.

Fuel Assembly Design B1

Rod Type	# of Rods	Rod Description
	23	Guide Tube
	1	Instrument Tube
	253	2.70 wt% U-235 in the Central Zone
	4	2.56 wt% U-235 with 4 wt% Gd_2O_3 in the Central Zone
	8	1.89 wt% U-235 with 8 wt% Gd_2O_3 in the Central Zone

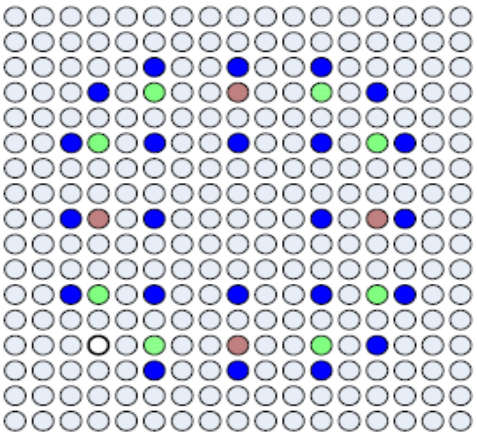

Fuel Assembly Design B2

Rod Type	# of Rods	Rod Description
	23	Guide Tube
	1	Instrument Tube
	249	2.70 wt% U-235 in the Central Zone
	4	2.56 wt% U-235 with 2 wt% Gd_2O_3 in the Central Zone
	12	1.89 wt% U-235 with 8 wt% Gd_2O_3 in the Central Zone

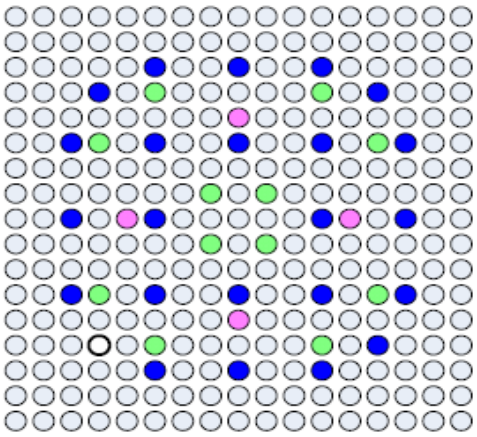

Fuel Assembly Design B1

Axial Height (cm)	Zone	Zone Enrichment (wt% U-235)		
419.99				
	Blanket	2.00	2.00	2.00
399.73				
	Cutback	2.70	2.70	2.70
384.44				
	Central		1.89 with 8 wt% Gd_2O_3	2.56 with 4 wt% Gd_2O_3
30.48				
	Cutback		2.70	2.70
15.24				
	Blanket	2.00	2.00	2.00
0.00				

Fuel Assembly Design B2

Zone	Zone Enrichment (wt% U-235)		
Blanket	2.00	2.00	2.00
Cutback	2.70	2.70	2.70
Central		1.89 with 8 wt% Gd_2O_3	2.56 with 2 wt% Gd_2O_3
Cutback		2.70	2.70
Blanket	2.00	2.00	2.00

Figure 7:1 Fuel assembly design B1 and B2

Fuel Assembly Design C1

Rod Type	# of Rods	Rod Description
	23	Guide Tube
	1	Instrument Tube
	257	3.25 wt% U-235 in the Central Zone
	4	3.08 wt% U-235 with 2 wt% Gd_2O_3 in the Central Zone
	4	2.76 wt% U-235 with 6 wt% Gd_2O_3 in the Central Zone

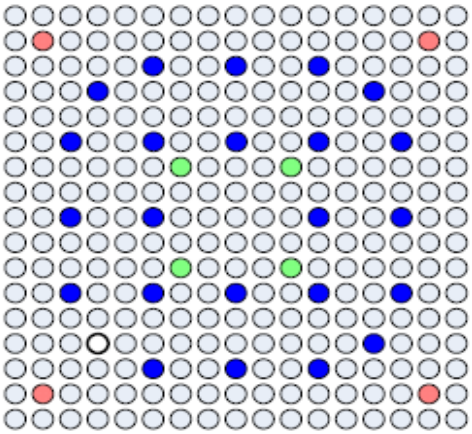

Fuel Assembly Design C2

Rod Type	# of Rods	Rod Description
	23	Guide Tube
	1	Instrument Tube
	253	3.25 wt% U-235 in the Central Zone
	4	3.08 wt% U-235 with 2 wt% Gd_2O_3 in the Central Zone
	8	2.76 wt% U-235 with 6 wt% Gd_2O_3 in the Central Zone

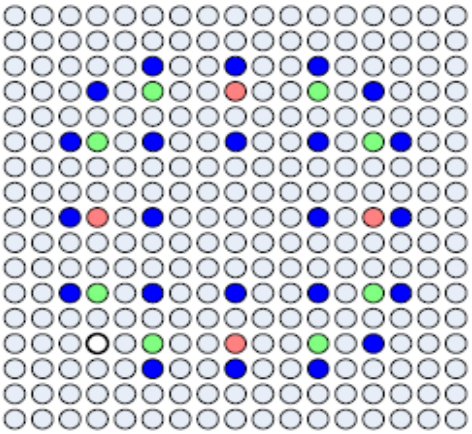

Fuel Assembly Design C1

Axial Height (cm)	Zone	Zone Enrichment (wt% U-235)		
419.99				
	Blanket	2.00	2.00	2.00
399.73				
	Cutback	3.25	3.25	3.25
384.44				
	Central	3.25	2.76 with 6 wt% Gd_2O_3	3.08 with 2 wt% Gd_2O_3
30.48				
	Cutback	3.25	3.25	3.25
15.24				
	Blanket	2.00	2.00	2.00
0.00				

Fuel Assembly Design C2

Zone	Zone Enrichment (wt% U-235)		
Blanket	2.00	2.00	2.00
Cutback	3.25	3.25	3.25
Central	3.25	2.76 with 6 wt% Gd_2O_3	3.08 with 2 wt% Gd_2O_3
Cutback	3.25	3.25	3.25
Blanket	2.00	2.00	2.00

Figure 7:2 Fuel assembly design C1 and C2

Fuel Assembly Design C3

Rod Type	# of Rods	Rod Description
●	23	Guide Tube
○	1	Instrument Tube
○	249	3.25 wt% U-235 in the Central Zone
●	4	3.08 wt% U-235 with 2 wt% Gd_2O_3 in the Central Zone
●	12	2.27 wt% U-235 with 8 wt% Gd_2O_3 in the Central Zone

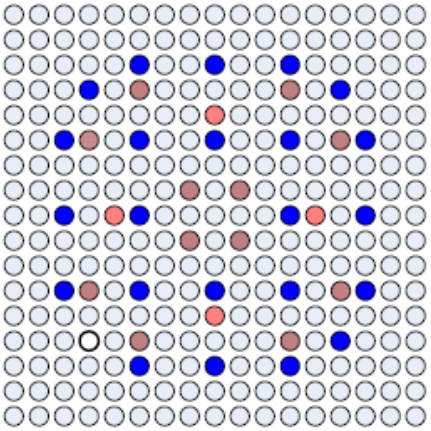

Fuel Assembly Design C3

Axial Height (cm)	Zone	Zone Enrichment (wt% U-235)		
		○	●	●
419.99	Blanket	2.00	2.00	2.00
399.73	Cutback	3.25	3.25	3.25
384.44	Central		2.27 with 8 wt% Gd_2O_3	3.08 with 2 wt% Gd_2O_3
30.48	Cutback		3.25	3.25
15.24	Blanket	2.00	2.00	2.00
0.00				

Figure 7:3 Fuel assembly design C3